UNIVERSITY OF CALIFORNIA
RIVERSIDE

Spatially Controlled Multi-Phenotypic Differentiation of Stem Cells in 3D Via an Engineered Mechanical Gradient

A Dissertation submitted in partial satisfaction
of the requirements for the degree of

Doctor of Philosophy

in

Bioengineering

by

Christopher Bowman Horner

June 2016

Dissertation Committee:
Dr. Jin Nam, Chairperson
Dr. B. Hyle Park
Dr. Victor Rodgers

The Dissertation of Christopher Bowman Horner is approved:

_____

_____

_____
Committee Chairperson

University of California, Riverside

ACKNOWLEDGEMENTS

I would like to begin by expressing my deepest gratitude to my committee chairperson and advisor, Professor Jin Nam. His guidance and mentorship through the entirety of my Ph.D. work has significantly contributed to the achievement of this degree. I owe him greatly for all of the opportunities afforded to me. Furthermore, I would like to extend my sincere appreciation to my other committee members, Professors B. Hyle Park and Victor Rodgers, for their support and criticism over the course of my graduate work.

Next, I would like to thank each of my lab colleagues who have provided invaluable advice and friendship the last few years: Dr. Maricela Maldonado, Dr. Karen Low, Dr. Gerardo Ico, as well as all other members of TREAT Lab. Without sharing their knowledge, expertise, and offering welcomed assistance this work would not have been possible.

The text of this dissertation, in part, is a reprint of the material as is appears in Ch. 10: Electrospun scaffolds for cartilage regeneration, Nanocomposites for Musculoskeletal Tissue Regeneration (1/2016), and Microstructure-dependent mechanical properties of electrospun core-shell scaffolds at multi-scale levels, *Journal of the Mechanical Behavior of Biomedical Materials* (1/2016). The co-author, Professor Jin Nam, listed in these publications directed and supervised the research which forms the basis for this work.

Additionally, I would like to thank Karen Low for her helpful criticism of my writing; Koji Hirota, Junze Liu and B. Hyle Park for their expertise in acquiring, processing and analyzing OCT data; Gerardo Ico for his technical expertise in programming; and finally, Dr. Jed Johnson and Dr. Yi Zhao for their assistance in sample testing and helpful revisions.

DEDICATION

I would like to dedicate this work to my family and friends whose continuous love and support made all of this possible. Their never-ending encouragement has always driven me to push further, both personally and professionally. I would not be where I am today without all of these amazing people in my life.

To my parents Bruce and Julia Horner, I cannot thank you enough for having always provided me with the opportunities to reach for my dreams and goals. Your unconditional love and support throughout my educational career and life have truly made me the person I am today. I can only aspire to be as thoughtful and compassionate as each of you are one day.

To my brother Michael, and his wonderful wife and children, you inspire me to have such a loving and caring family as you do. Thank you for understanding why I missed so many of the children's birthdays, but once everything is said and done I will be there for all of the rest.

Finally, I feel gratefully inclined to thank all of my friends who have always been there for me through thick and thin. The journeys and lifelong memories we have encountered are experiences that I would not trade for the world.

Fly High, Free Bird - BNE

ABSTRACT OF THE DISSERTATION

Spatially Controlled Multi-Phenotypic Differentiation of Stem Cells
in 3D Via an Engineered Mechanical Gradient

by

Christopher Bowman Horner

Doctor of Philosophy, Graduate Program in Bioengineering
University of California, Riverside, June 2016
Dr. Jin Nam, Chairperson

The goal of this research was to engineer a scaffold composed of a mechanical gradient and understand the effects of dynamic stimulation on the morphogenesis of the interfacial tissue via spatially controlled differentiation of a single stem cell source. Osteoarthritis is a degenerative joint disease affecting articular cartilage and the underlying subchondral bone resulting in severe pain and disability of the joints. While current clinical treatments provide limited efficacy in long-term success, tissue engineering strategies prove to be a viable option to address regeneration of the osteochondral gradient interface. To address this challenge spatial patterning of mechanical factors are essential for the development of a gradient tissue structure in three dimensions. Here, the overarching goal of this work was to examine (1) the preferential differentiation capacity of MSCs towards multi-phenotypic lineages when subjected to variations in compressive strain, (2) the control of micro- and macro-scale

scaffold mechanics through utilizing a core-shell microfiber electrospinning technique, and finally (3) the engineering of a dynamic mechanical gradient that can spatially control the local strain that MSCs will sense and differentiate into multi-phenotypic lineages. My findings demonstrate that MSCs differentiate in a magnitude-dependent and phenotype-specific manner in response to different magnitudes of dynamic compressive strain suggesting that MSCs are mechano-responsive and their multi-phenotypic differentiation can be controlled by varying the strain regimens. Furthermore, it was demonstrated that the mechanical properties of core-shell electrospun fibers can be modulated by controlling the composition and the dimension of core, decoupled from the cell-interfacing surface chemistry. More importantly, it was shown that mechanical properties of such fibers/scaffolds at the micro- and macroscale can be independently regulated by modulating micro- and macro-structure. Finally, spatial control of the mechanical properties of individual core-shell fibers in a monolithic scaffold was able to modulate the preferential multi-phenotypic differentiation of MSCs when subjected to dynamic compressive strain. Thus, these findings provide an additional avenue for directing stem cell differentiation in lieu of biochemical cues commonly used for osteochondral tissue regeneration. Addressing the influence of mechanical stimulation on spatially controlled multi-phenotypic MSC differentiation is the basis behind the work presented in the following dissertation.

TABLE OF CONTENTS

LIST OF FIGURES x
LIST OF TABLES xiii

CHAPTER 1 – INTRODUCTION 1

1.1 – Clinical Challenge 1
1.2 – Cell Sources and Scaffold Designs 5
1.3 – Osteochondral Tissue Engineering Strategies 10
1.4 – Aim of Thesis 21

CHAPTER 2 – ELECTROSPUN SCAFFOLDS FOR CARTILAGE REGENERATION 23

2.1 – Abstract 23
2.2 – Introduction 24
2.3 – Synthesis of Electrospun Scaffolds 31
2.4 – Electrospun Scaffolds for Cartilage Regeneration 42
2.5 – Current Limitations of Electrospun Scaffolds in Cartilage Tissue Engineering 59
2.6 – Tables & Figures 61

CHAPTER 3 – MAGNITUDE-DEPENDENT AND INVERSELY-RELATED OSTEOGENIC/CHONDROGENIC DIFFERENTIATION OF HUMAN MESENCHYMAL STEM CELLS UNDER DYNAMIC COMPRESSIVE STRAIN 70

3.1 – Abstract 70
3.2 – Introduction 72
3.3 – Materials and Methods 75
3.4 – Results 81
3.5 – Discussion 87
3.6 – Conclusions 90
3.7 – Figures 92

CHAPTER 4 – MICROSTRUCTURE-DEPENDENT MECHANICAL PROPERTIES OF ELECTROSPUN CORE-SHELL SCAFFOLDS AT MULTI-SCALE LEVELS 99

4.1 – Abstract 99
4.2 – Introduction 101
4.3 – Materials and Methods 105
4.4 – Results 111

4.5 – Discussion 116
4.6 – Conclusions 120
4.7 – Tables & Figures 121

CHAPTER 5 – CONTROL OF MULTI-PHENOTYPIC DIFFERENTIATION OF STEM CELLS IN THREE-DIMENSIONS BY DYNAMICALLY CULTURED ENGINEERED GRADIENTS 137

5.1 – Abstract 137
5.2 – Introduction 139
5.3 – Materials and Methods 143
5.4 – Results 152
5.5 – Discussion 160
5.6 – Conclusions 163
5.7 – Tables & Figures 165

CHAPTER 6 – CONCLUSIONS 179

6.1 – Summary 179
6.2 – Future Directions 180

CHAPTER 7 – REFERENCES 183

LIST OF FIGURES

Figure 2.1. Cross-sectional schematic of articular cartilage. 63

Figure 2.2. Randomly oriented electrospun fiber morphology. 64

Figure 2.3. Co-polymer electrospinning setup. 65

Figure 2.4. Core-shell fiber electrospinning setup. 66

Figure 2.5. Single nozzle polymer blending electrospinning setup. 67

Figure 2.6. Mesenchymal stem cells (MSCs) cultured on various two-dimensional substrates. 68

Figure 2.7. Microstructure morphology of cells cultured in three-dimensions. 69

Figure 3.1. Morphological characterization of electrospun scaffolds. 92

Figure 3.2. The osteogenic or chondrogenic differentiation of hMSCs cultured in 3D electrospun scaffolds for various durations. 93

Figure 3.3. Dynamic mechanical analysis of cell/scaffold constructs cultured under daily mechanical stimulation with various dynamic compressive magnitudes and culture durations. 94

Figure 3.4. The osteogenic or chondrogenic differentiation of hMSCs by sdurations. 95

Figure 3.5. Representative SEM and histology images of cell/scaffold constructs cultured under various conditions exhibiting different ECM compositions from hMSCs. . 96

Figure 3.6. Optical Coherence Tomography (OCT) of acellular and cellular scaffolds cultured with or without dynamic compression. 98

Figure 4.1. A schematic of the core-shell electrospinning setup. 124

Figure 4.2. A representative image of a three point bending test on an individual electrospun core-shell fiber. 125
Figure 4.3. A custom compression device for mechanical testing. 126
Figure 4.4. Representative cross-sectional SEM images of electrospun core-shell fiber with various core-to-shell dimensional ratios. 127
Figure 4.5. Morphological characterization of electrospun core-shell fiber/scaffold with various core/shell dimensional ratios at micro- and macroscales. 128
Figure 4.6. Wettability of electrospun scaffolds. 129
Figure 4.7. Representative SEM images of electrospun fibers before and after soaking in an aqueous solution. 130
Figure 4.8. Mechanical characterization of individual core-shell fibers with different core/shell dimensional ratios by a three point bending test using an AFM. 131
Figure 4.9. Compressive mechanical characterization of the scaffolds composed of core-shell fibers. 132
Figure 4.10. Tensile mechanical characterization of scaffolds composed of core-shell fibers. 134
Figure 4.11. A schematic demonstrating individual fiber and scaffold deformation under various modes of loading. 136
Figure 5.1. Mechanical properties of core-shell microfiber scaffolds with different core/shell diameter ratios resulted from altering core:shell flow rate during electrospinning. 166

Figure 5.2. Generation and characterization of a linear gradient in the hollow core diamter with respect to the thickness of the scaffold under reciprocal core:shell flow rate control. 167

Figure 5.3. Generation and characterization of a biphasic gradient in the hollow core diamter with respect to the thickness of the scaffold under reciprocal core:shell flow rate control. 169

Figure 5.4. A COMSOL modeling of linear and biphasic strain gradients and their experimental validation. 170

Figure 5.5. Maintainance of linear strain gradients during cell culture. 171

Figure 5.6. Maintainance of biphasic strain gradients during cell culture. 172

Figure 5.7. Dynamic mechanical analysis of cell/scaffold constructs with various engineered gradient configurations and culture durations. 173

Figure 5.8. The osteogenic or chondrogenic differentiation of hMSCs in an engineered linear strain gradient scaffold as determined by relative gene expression. 174

Figure 5.9. The osteogenic or chondrogenic differentiation of hMSCs in an engineered biphasic strain gradient scaffold as determined by relative gene expression. .. 176

Figure 5.10. Representative histology images of cell/scaffold constructs cultured under various gradient conditions exhibiting different ECM compositions. 178

LIST OF TABLES

Table 2.1. Common polymers used in electrospinning. 61

Table 2.2. List of common electrospinning parameters. 62

Table 4.1. Electrospun core-shell fiber dimensions. 121

Table 4.2. Morphological and mechanical properties of PEKK-PCL core-shell electrospun fibers. 122

Table 4.3. Morphological and mechanical properties of gelatin-PCL core-shell electrospun fibers. 123

Table 5.1. Custom real-time polymerase chain reaction (PCR) primers. 165

CHAPTER 1 – INTRODUCTION

1.1 – Clinical Challenge

1.1.1 – Development and progression of osteoarthritis, and societal impact

Articular cartilage serves a vital role in the musculoskeletal system acting as a low friction and shock absorbing connective tissue in the joints while preventing direct bone to bone contact [1]. Damage to this tissue, whether by acute trauma or degenerative diseases such as osteoarthritis (OA), often results in severe pain and disability. While OA is a degenerative joint disease affecting cartilage and the subchondral bone, due to the avascular and aneural nature of the tissue, not only has it proven difficult for spontaneous healing and self-regeneration, but recognition of damage to cartilage and resulting pain, often occurs at the point in which surgical intervention is required [2]. Prolonged damage to the articular cartilage often leads to damage of the underlying subchondral bone generating an osteochondral defect. If the cartilage tissue does regenerate in response to the osteochondral defect, it is commonly in the form of fibrocartilage, which serves little protection to the subchondral bone and will further progress the disease.

Osteoarthritis is commonly associated with limited joint mobility, severe pain, and an overall reduction in the quality of life for those impacted. It is estimated that health

care costs in the United States are approximately $95 billion annually [3], while estimates predict total costs of approximately $125 billion annually as a result of lost productivity and reduction in the quality of life for those who suffer from OA. [4, 5]. Due to the ever aging and active population, damage to cartilage and subchondral bone will continue to rise, and hence will require clinical treatment. Therefore, there have been a variety of techniques developed and utilized to repair the tissue to date, and these will be described below.

1.1.2 – Current clinical technologies

The anatomical structure and function of articular cartilage and the underlying subchondral bone are highly organized in osteochondral tissue and provide very distinct relationships in healthy tissue. The interface of these tissues possess a continuous stratification in cellular number and shape, extracellular matrix (ECM) composition, and biochemical gradients. An interruption of the tissue homeostasis will create lesions on the articular surface, and degeneration of the tissues will continue without surgical intervention for repair.

There have been several techniques which have been developed and employed to treat damaged or diseased cartilage. Clinical technologies to treat damaged cartilage tissue will be tailored to the degree of deterioration of the joint ranging from arthroscopic

debridement, microfracture, autologous chondrocyte implantation (ACI), and matrix-assisted autologous chondrocyte implantation (MACI) in more severe cases. While each of these methodologies provide a means by which defects are repaired they vary with the long term success for full scale tissue treatment and regeneration. Commonly they provide short term success of newly generated tissue, and will typically require follow-up treatments or additional surgical interventions.

Arthroscopy is a debridement technique commonly used to treat very small lesions on the surface of cartilage at very early stages of OA. Loose cartilage is removed from the surface of the tissue to alleviate any pain occurring between the articulating joints [6, 7]. Microfracturing of the cartilage is a clinical technique that aims to address defects of only a few square centimeters [8]. In order to initiate the formation of fibrocartilage in these sites of injury or disease, the cartilage is fractured until reaching the subchondral bone, which will enable blood flow to the site and subsequent mesenchymal stem cells from the bone marrow to generate new tissue. Oftentimes this treatment option will require additional surgical interventions as the formation of fibrocartilage further progresses the development of OA, as mentioned previously.

A widely accepted clinical technique for the treatment of large chondral defects is the use of autologous chondrocyte implantation. ACI has been proven to provide a means of relocating healthy hyaline cartilage from non- or low-loadbearing areas of the joints to

those surfaces which have significant deterioration in high loadbearing areas. However, this method does have some drawbacks as mentioned previously including the harvest of limited mature chondrocytes, and decreased success with *in vitro* expansion including cellular apoptosis, dedifferentiation or even hypertrophy [9].

More recently, tissue engineering approaches to assist in enhancing functionality and long-term success in cartilage repair is through the use of matrix-assisted autologous chondrocyte implantation (MACI) [10]. This clinical technique is the first tissue engineering approach to treat and regenerate damaged osteochondral tissue [11]. By combining autologous chondrocytes along with scaffolding it is then subsequently implanted into focal defects for tissue regeneration. Common scaffold materials that have been used in MACI include collagen and hyaluronic acid due to their biocompatibility, reduce immune response as well as their intrinsic biodegradability, but have also proven to have limitations due to their low mechanical properties. Therefore, while each of the aforementioned treatment option have shown varying levels of clinical success tissue engineering strategies have emerged as promising alternatives to regenerating osteochondral defects.

1.2 – Cell Sources and Scaffold Designs

1.2.1 – Cell selection

It is very important to consider the source in which cells are acquired for any sort of tissue engineering strategies. Autologous cells are of great interest for tissue engineering applications due to the minimization of potential for immune rejection, as well as enhancing native tissue integration and overall mechanical function. Primary cells, such as mature chondrocytes or osteoblasts, serve as the most direct cell source for use in osteochondral tissue engineering strategies due to their fully committed cellular phenotype and functionality, despite arising from the same progenitor cell. Following isolation from biopsies of patients these cells may be expanded *in vitro* for subsequent use. The issue when it comes to their use in regenerative medicine techniques, especially chondrocytes, is the low rate of expansion in two dimensional cell culture, as well as the potential for dedifferentiation, degradation of functionality or the generation of fibrocartilage [12]. Therefore, the use of multipotent stem cells may overcome the drawback of using primary cells.

Due to the increased attention and added benefits to using stem cells, there are several sources of acquiring multipotent stem cells for tissue engineering applications. Bone-marrow stromal cells (BMSCs), adipose tissue-derived stem cells (ADSCs), umbilical

cord mesenchymal stem cells (UCMSCs), and amniotic fluid-derived stem cells (AFSCs) have all been proven to differentiate successfully into mesenchymal tissues, including bone and cartilage [13-16]. Though it should be noted that the use of UCMSCs and AFSCs would not be ideal candidates for current focus in the regeneration of osteochondral tissue due to the lack of autologous cell sources available. These cells do provide for an interesting avenue for young and future generations due to the foresight of banking tissues and fluids containing these cells to treat conditions later in life. Though the primary focus of this analysis will be towards the use of BMSCs and ADSCs for osteochondral tissue engineering strategies for autologous use. Benefits to using autologous stem cells include minimal surgery for cell retrieval, large expansion of cells to maintain multipotent abilities *in vitro,* and the ability for multiphenotypic differentiation into numerous phenotypes. Notably, the use of mesenchymal stem cells (MSCs), which include both BMSCs and ADSCs, give rise to the many tissues which compose the mesenchymal lineage including those mentioned previously. Therefore, stem cells are a very attractive and promising option for study and development to treat osteochondral defects using a variety of scaffold designs.

1.2.2 – Scaffold designs

In order to design scaffolds for the regeneration of osteochondral defects consideration for both the mechanical and biochemical properties of the cartilage-bone

interface need to be addressed [17]. In addition to acknowledging the mechano-chemical components of this tissue interface, the scaffolds used for implantable substitutions should also be biodegradable and their rate of degradation should match the rate of the extracellular matrix that is produced from either implanted differentiating cells or incorporation of the surrounding tissue. The scaffolds should be designed in such a fashion that their porosity and pore size allow for cellular attachment, infiltration, and stability under mechanical stresses. This is particularly important for the case of bone formation, which requires notable pore sizes as well as significant mechanical properties.

Many scaffold fabrication techniques have been developed over the years and can be utilized for osteochondral tissue engineering including solvent casting and particulate leaching, phase inversion, fiber bonding, additive manufacturing/3D printing/rapid prototyping, fiber bonding, electrospinning, membrane lamination, high pressure method, and supercritical fluid technologies [18-28]. The large variation in techniques provides an almost unlimited number of combinations to address osteochondral repair, and some of these techniques will be discussed later on for current strategies used for regenerating cartilage and bone. It should be noted though that the combination of such a wide breadth of techniques could complicate production of scaffolds, and thus simplicity of fabrication is always an appealing option. Additionally, the materials used for scaffold fabrication have many important implications when trying to provide a sufficient

physio-chemical template and many of those commonly used for osteochondral tissue engineering will subsequently be described.

1.2.3 – Common scaffold materials

When designing an appropriate scaffold for osteochondral tissue engineering, material selection plays in important role in developing biomimetic constructs. There have been a plethora of materials studied for *in vitro* osteochondral tissue regeneration. Many of these materials include both natural and synthetic polymers, bioceramics, as well as composites of each [13, 29-31]. Each of these categories of materials provide beneficial aspects for regenerating both the chondral and subchondral layers by providing adequate materials which can appropriately integrate with their respective layers.

Firstly, materials used for regeneration of the osteochondral interface should provide a biomimetic environment which enhance cells to adapt similarly to when in the native microenvironment found within the physiological tissue. This is where naturally derived polymers such as collagens, glycosaminoglycans (GAG), polypeptides, or polysaccharides including chitosan, hyaluronic acid or alginates are an attractive option. All of these contain specific domains that can provide important signals to cells at different stages in their tissue development [32-34]. Though it has been shown that the

bioactive materials can cause certain problems with antigenicity [35] and their processing into functional constructs has proven to be difficult.

In order to work around some of the limitations associated with the use of natural polymers, there are several synthetic polymers which have been employed for osteochondral reconstruction. A few of the most popular synthetic polymers include poly (lactic acid) (PLA), poly (glycolic acid) (PGA), their co-polymers (PLGA), and poly (ε-caprolactone) (PCL). These materials have varying mechanical properties which can be tailored to mimic physiological conditions, and are not only biocompatible, but biodegradable. They offer relatively easy processing in a variety of scaffold syntheses and allow for design of constructs that not only recognize or can be recognized by the physiological tissue, but can also adapt to the tissue microenvironment providing an extracellular matrix that guides tissue morphogenesis and repair.

Finally, while the use of polymeric materials typically serves as appropriate platforms for the use in chondral tissue engineering, exploration in the use of bioceramics has proven to be a suitable method for regeneration of the subchondral bone components. Ceramic materials such as hydroxyapatite (HA) or calcium phosphates (tricalcium phosphate, TCP), or bioactive glasses such as Bioglass®, have all been used as biomaterial substrates that enhance biomineralization and the regeneration of bone-like tissue [36, 37]. Each of these components, whether alone or combined with the natural

or synthetic polymers mentioned previously, have all shown great potential for use in the osseous components of osteochondral tissue engineering strategies.

As a continuous stratified tissue, osteochondral tissue is well known to be composed of glycosaminoglycan (GAG) and collagen type II in the cartilage, while the subchondral layer is a highly porous structure that is rich in HA and collagen type I [13]. With an appropriate selection of materials to address both the chondral and subchondral layers for both biological and mechanical functionality, researchers have shown fascinating approaches to regenerate the osteochondral interface. Ultimately, scaffold design should not only address the function of the tissues in question, but should enable real-life clinical application and use to treat arthritic defects. Therefore, the following section will describe previous and current osteochondral tissue engineering strategies which aim to recapitulate the cartilage to bone interface. The basis for the work in this thesis will be then be briefly discussed following a review of the variety of techniques that have been attempted to date.

1.3 – Osteochondral Tissue Engineering Strategies

The importance for the study of osteochondral tissue engineered replacements aim to address both the mechanical and biological requirements of cartilage and bone. Instead of solely focusing efforts on chondral defects, strategies for regenerating full-

thickness constructs for use as osteochondral implants provide a greater change of tissue integration since the bone-to-bone interface typically integrates better than the cartilage-to-cartilage interface [38]. In this regard, several strategies have been attempted to use many scaffold tissue designs, as well as utilize various mechanical stimulation regimens through bioreactor cultivation to regenerate the interfacial tissue.

1.3.1 – OC scaffold designs

Single-layered constructs

A few strategies have been attempted at regenerating osteochondral tissue through the use of a single phase or monolithic scaffold. The concept behind this approach relies on seeding autologous chondrocytes in the upper region of a 3D scaffold for implantation, similar to the clinical approach of MACI described earlier. One example used β-TCP scaffolds seeded with autologous chondrocytes, and implanted into sheep [39]. While the authors did not report any long term success with this method, they did note that the scaffold generated a hyaline-like cartilage structure on the surface after 24-weeks of study. Another group decided to test the effects of cartilage formation in hyaluronan-based scaffolds that possessed different rates of degradation [40]. Their hypothesis was that better cartilage formation would be observed in those scaffolds which had a slower degradation as compared to those which degrade much quicker.

Indeed, they were able to show that a thicker, more robust cartilage layer formed in those slower degrading constructs, emphasizing the importance of matching the rate of degradation to the formation of the ECM by the cells contained within. Other techniques for the formation of a dense chondral layer on the top of singular scaffolds include seeding chondrocytes into fibrin glues [41] or PLLA composites [42], and spatially controlling their density and location to the top of HA scaffolds. In both cases, dense cartilage-like layers were prominently formed and showed superior tissue formation and integration when implanted *in vivo* when compared to constructs which were not treated in similar manners. While many of the single layer scaffolds provide easy fabrication, and can be treated or designed in such a way to treat osteochondral defects, they fail to address the true spatial challenges faced when attempting to regenerate the complicated and structured tissue. The different cell types contained in the diverse tissues will understandably interact with one common material in various fashions. Therefore, the simultaneous regeneration of the cartilage and bone layers should provide adequate support for both types of tissues. This is where an alternative approach to regenerating the osteochondral interface utilizes the construction of biphasic or multiphasic structures. By providing different chemical surroundings, mechanical properties, and pore morphologies guided growth of two heterogeneous tissues can be developed. A mechanically rigid and porous structure is favorable to support bone ingrowth, whereas the development of a viscoelastic material which is much more compliant is preferred for cartilage regeneration. While each layer is proven to be independent in their

functionality, they should also serve to work together for the best success of tissue integration into defect sites.

Stratified constructs – Biphasic or multiphasic scaffolds

Due to the compartmentalized structure of the cartilage to bone interface it is very important to take the structure and function of each of the tissues into consideration. Again, due to the lack of vasculature and innervation of cartilage, chondral tissue has proven difficult for integration and grafting with the native tissue [43-45]. Therefore, by providing a subchondral bone layer, engineered osteochondral tissue has a greater chance for securing long-term stability and incorporation with the surrounding native physiological tissue around the defect site. The subchondral bone should provide significant nutrient supply to the full scale engineered implantation, thus reducing the chance for tissue rejection. Additionally, the engineered tissues should address both the mechanical and biological compositions as found in physiological tissue to mimic the interfacial tissue. There have been numerous strategies for accomplishing the development of robust biphasic constructs including variations in materials, scaffold designs, and the predifferentiation of stem cells through mechanical stimulation and biochemical compositions [13, 46-53].

Given that the osteochondral interface is a stratified tissue, and tissue maturation for bone and cartilage commonly requires different time frames for maturation, one of the more widely accepted methods for osteochondral tissue generation requires culturing of two independent constructs. There are a few methodologies that have been attempted in this regards. Firstly, it is possible to generate two completely independent constructs which are later integrated to form one single macroscopic interfacial tissue. This would be considered the easiest way to construct an osteochondral construct. One such example of this was the formation of a chondral layer using a PLGA scaffold reinforced with PGA fibers, whereas the bone layer used the same scaffold but reinforced with Bioglass® [54]. Upon generation of the independent layers, they were then glued together and were seeded with primary autologous chondrocytes. The scaffolds were then seeded into goats and analyzed for performance. After 16 weeks, it was observed to have a large amount of hyaline cartilage with very good bone integration, but it should be noted that acellular scaffolds used as a control showed similar results indicating no added benefits to the use of cells. Another example of two independent layers being joined together was the use of a hyaluronan-based sponge for the cartilage layer and a calcium phosphate scaffold to support bone growth [48]. The layers were first joined with a fibrin sealant, and then each of these layers were seeded with MSCs that were subcultured in two distinct differentiation media. They confirmed that the scaffolds provided an environment for the formation of bone in the ceramic and fibrocartilage in the sponge. While these attempts exhibit varying levels of promise for potential clinical use, the lack

of a true osteochondral interface with continuous changes in chemical and material properties is achieved. Therefore, due to this limitation this methodology would not be considered the best option due for regeneration of the tissue. Another shortfall to the method of using two separate constructs for tissue development and later adjoining them would be mechanical stability and integrity. It is very likely that these engineered constructs will be subject to delamination due to the mismatch of material properties to the surrounding tissue. To get around this obstacle researchers have tried integrating the layers prior to tissue development by co-culturing the chondral and osseous layers at the same time or providing intermediate/transitional layers in engineered scaffolds.

Many research groups address the importance of developing an intermediate layer in between the cartilage and bone phases to simulate the transition from cartilage, beyond the definitive tidemark, to calcified cartilage, and into the subchondral bone. This is where the development of triphasic scaffolds has come into perspective and would prove to alleviate some of the shortcomings when using biphasic constructs for repair and regeneration of osteochondral defects. One particular group studied the effects of autologous MSCs seeded in triphasic scaffolds composed of a beta-tricalcium phosphate osseous phase, an intermediate activated plasma phase, and a collagen I hydrogel chondral phase in ovine models [55]. The MSCs we predifferentiated towards the chondrogenic lineage and seeded in the chondral layer prior to implantation. Osteochondral defects were created, followed by implantation of their scaffolds after 6

weeks. Their goal was to determine whether the triphasic scaffolds could be used as comparable substitute to osteochondral autografting. They noted that after 6-months post-implantation their triphasic scaffolds had enhanced cartilage bonding to the surrounding native tissue, but after 12-months of analysis the osteochondral autografts had better neo-cartilage morphology as compared to their scaffolds. Overall, they concluded that the triphasic scaffolds showed comparable repair capabilities when compared to osteochondral autografting when assessing the histology and biomechanical response of the tissue after 12-months.

Gradient scaffold techniques

There have been several attempts to date in addressing continuous gradients of biochemical or material composition directing stem cell differentiation. One of these methods involved the use of creating scaffolds composed of gradient growth factors [56]. PLGA microspheres were sequentially loaded with either TGF-β1 or BMP-2 with and without HA for the regeneration of the cartilage and bone layers, respectively. Scaffolds were implanted into the medial condyle of artificial osteochondral defects made in rabbits. After analyzing the biochemical gradient effects on tissue regeneration at 6 and 12 weeks it was observed that the gradient scaffolds had the best enhancement of both bone and cartilage layers as compared to blank scaffold controls. The scaffolds containing the biochemical gradient along with the PLGA and PLGA/HA microspheres showed the

greatest formation of GAG and bone integration with native tissue indicating the promise for the use of continuous gradients for osteochondral tissue engineering. Not only does the method of using a gradient structure provide a means for spatiotemporal development of the tissue interface, but it also seeks to get around the limitations found with using biphasic or multiphasic constructs. In a separate study from the same group, the authors wanted to see the effects of stem cell differentiation in response to the biochemical loading regime [57]. This time the authors used hBMSCs and UCMSCs to compare the cell responses to the gradient scaffold. It was shown that hBMSCs had significant upregulation of gene markers *COLI*, *SOX9,* and *RUNX2,* but did not have noticeable differences in DNA, GAG, ALP and hydroxyproline as compared to UCMSCs. The scaffolds were superior in the development of spatially controlled ECM formation, and showed much greater enhancement of cellular differentiation with regards to the total cell number, GAG production, collagen content, and alkaline phosphatase activity as compared to the blank controls.

To further emphasize the intriguing formation of gradient scaffolds for osteochondral tissue engineering the use of recombinant human BMP (rhBMP) and recombinant human insulin-like growth factor-1 (rhIGF-1) were incorporated in either PLGA or silk microparticles [58]. These growth factors were studied to observe the effects on hBMSC differentiation to either an osteogenic or chondrogenic lineage. The growth factors were incorporated in a gradient fashion in cylindrical alginate gels and salt-leached

silk scaffolds with either a linear of reverse gradient fashion, and cells were either seeded onto the scaffold surface or encapsulated into the gel. The gradients with the silk microparticles proved to be more effective in the alginate gels with rhBMP-2 delivery, and less effective delivering rhIGF-1 that was in the PLGA microparticles. Because of the very shallow gradient structure in the gels the delivery was rather insufficient, but the silk scaffold group had very good chondrogenic and osteogenic differentiation in the linear rhBMP-2 gradient and reverse rhBMP-2/rhIGF-1 gradient.

In another gradient study, Di Luca et al. wanted to analyzed the effects of surface energy and stiffness gradients on the differentiation of hMSCs to skeletal lineages over the course of 28 days [59]. They used an additive manufacturing, also known as 3D printing, technique to create 3D porous scaffolds sequentially composed of poly(lactic acid), polycaprolactone (PCL), and poly(ethylene oxide terephthalate)/poly(butylene terephthalate) (PEOT/PBT) copolymers. It was observed that the PEOT/PBT scaffolds supported greater signs of osteogenesis by alkaline phosphatase expression, whereas the PLA layer generated significantly higher expression of GAG as compared to the other layers. The authors concluded that stiffness gradients through the additive manufacturing technique didn't seem to directly influence hMSCs, but due to the PEOT/PBT copolymer regions used it was noticed that the surface energy gradients resulted in enhanced early osteogenic differentiation as well as noticing improved chondrogenic differentiation in PLA regions. Not only do these gradient studies provide methods developing complex

tissues, but gives promise to the fabrication of the osteochondral tissue interface by spatially controlling the multiphenotypic differentiation of a single stem cell source.

1.3.2 – Mechanical stimulation and bioreactors

It is well known that MSC differentiation is highly influenced though mechanical stimulation such as applications of extrinsic compression, tension, hydrostatic pressure or laminar shear. It has been shown that cyclic tensile strain and fluid shear increase osteogenic differentiation [60-65], whereas dynamic compressive loading has been reported to support both the generation of chondrogenic and osteogenic differentiation [63, 66-72]. While most scaffold design strategies rely on biphasic or multi-phasic constructs, there have been many studies which have used various combinations of custom design bioreactors for inducing multiphenotypic differentiation of a single stem cell source towards with chondrogenic or osteogenic lineages through different type of stimuli. One study in particular utilized a combination of agarose gels and decellularized bone scaffolds for induction of the chondral and osseous layers, respectively [73]. The authors decided to study the spatial control of MSC differentiation by looking at the effects of pre-differentiated cells, the use of media supplementation, and the rate of media perfusion through the scaffold. It was found that through the use of static culture of the agarose gels in chondrogenic differentiation medium provided the best chondrogenic response, whereas the osteogenic layer should the most promising results

when either pre-differentiated or undifferentiated hMSCs were subjected to defined medium perfusion in the bone region. Ultimately, they concluded that by employing a bioreactor that is capable to treating the biphasic constructs in two discrete segments, either with or without medium perfusion or variations in pre-differentiated cell types and media cocktails, that spatial control of MSC differentiation is possible and such a bioreactor system that can support independent culture of the biphasic constructs is necessary.

While many studies primarily focus around the use of media perfusion or stirring bioreactors for segmental construction and regeneration of both the chondral and osseous layer of an osteochondral construct [74-78], there have been a few which have used compressive loading on full thickness constructs. One particular example of this is the use of compressive loading on a biphasic construct composed of photo-polymerized poly (ethylene glycol)-based hydrogels that possessed different mechanical properties [79]. Due to the variation in hydrogel stiffness, the authors produced high magnitudes of strain in the soft chondral layer, whereas the stiffer bone-like layer produced lower magnitudes of strain. Additionally, they provided biochemical cues, in these two distinct layers by providing high chondroitin sulfate in the chondral layer, where the osseous layer had greater RGD concentrations. They concluded that a single hMSC cell source was insufficient in spatially differentiating in response to the local biochemical and matrix stiffness cues alone when cultured in osteochondral differentiation media. Though

importantly it was recognized that when subjected to dynamic stimulation not only did they have spatially oriented distributions in collagen II, collagen X, and collagen I in the chondral, intermediate, and cone layers, respectively, but had localized mineral deposits in the bone layer alone. These results further exacerbate the importance of external mechanical stimuli of hMSC differentiation towards osteochondral phenotypes. Therefore, the basis behind the work in this dissertation will pertain to the use of continuous mechanical gradients subjected to dynamic mechanical stimulation to direct multi-phenotypic stem cell differentiation.

1.4 – Aim of Thesis

The objective of this project is to spatially control, in three-dimensions, the multi-phenotypic differentiation of a single multi-potent stem cell source in depth-dependent manner utilizing dynamic mechanical stimulation on a monolithic scaffold composed of a mechanical gradient. The overarching hypothesis of this work is that human mesenchymal stem cells (hMSCs) respond to mechanical stimulation in a magnitude dependent manner. These mechanosensitive cells can sense variations in their local microenvironment through compressive strain, and in turn regulate their differentiation potential to either osteoblasts or chondrocytes. In literature, it has been well documented that hMSCs are capable of differentiating to various mesenchymal tissues in response to mechanical stimuli, but to date no physiologically suitable tissue replacements mimicking

the true structure and function of osteochondral tissue have been developed. In order to address these limitations, three-dimensional cell culture in core-shell electrospun scaffolds will provide a biomimetic environment which can direct phenotype specific differentiation depending on the mechanical stimulation sensed by the hMSCs.

CHAPTER 2 – ELECTROSPUN SCAFFOLDS FOR CARTILAGE REGENERATION

2.1 – Abstract

Electrospinning is a versatile scaffold synthesis method to produce highly porous structures composed of extracellular matrix-resembling nano- and microfibers from a variety of polymeric materials. This chapter will discuss electrospinning as a suitable method to create biomimetic engineered cartilage tissue. Additionally, it will explore the current techniques, applications, and limitations in electrospun scaffolds for the regeneration of diseased or damaged cartilage.

This chapter has been reproduced from *Horner C.B.,et al., 2016. 10 - Electrospun scaffolds for cartilage regeneration, Nanocomposites for Musculoskeletal Tissue Regeneration. Woodhead Publishing, Oxford, pp. 213-240., with permission from Elsevier Books.

*Adapted from book chapter: Figures: 2.1–2.7 and Tables: 2.1–2.2

2.2 – Introduction

2.2.1 – Cartilage regeneration

Cartilage is an avascular and anervous tissue with minimal intrinsic repair capabilities [80]. Even the slightest damage to the tissue due to disease or injury results in an unrecoverable decline in tissue health and functionality. The societal costs associated with cartilage degeneration total approximately $128 billion, and are attributed to clinical treatments, lost productivity in the workplace, and decline in the quality of life [4, 5]. Therefore, the urgent action for devising engineering tools to restore the functionality of cartilage is necessary for our increasingly aging population.

Due to limited self-healing capability of cartilage, current repair techniques require invasive procedures to restore physiological functions. A significant feature for any type of tissue regeneration requires the presence of blood vessels for progenitor cell migration (*i.e.*, stem cell homing), proper nutrient transport and waste removal. Therefore, the lack of vasculature in cartilage will then impede the native ability for self-regeneration of the tissue due to the limited cell source and metabolic processes within the innate tissue. Additionally, without the presence of nerves, the gradual degeneration of cartilage is typically not noticed until tissue is severely damaged and the patient experiences pain due to friction between the bones of their joints [81]. This ultimately

leads to the formation of bone spurs, to replace injured cartilage, which further progresses the degeneration of the cartilage tissue. Such cartilage degeneration commonly occurs in high load-bearing joints of the body such as the knee or hip.

For current cartilage treatment methods, there are a few clinical techniques other than the use of prostheses, including autologous chondrocyte implantation (ACI) and micro-fracture of the subchondral bone [82]. Limitations to the use of ACI, which harvests chondrocytes from the patient, expand and implant them directly into cartilage defects, include the complexity of the surgical procedure, leakage of transplanted chondrocytes from the defect site, uneven distribution of the mature cells, periosteal hypertrophy, limited availability of autologous chondrocytes, as well as dedifferentiation of the primary chondrocytes in monolayer culture. When considering the treatment of damaged or diseased cartilage via micro-fracturing to initiate mobilization of mesenchymal stems cells from subchondral bone for localized repair of the damaged tissue, the formation of undesired fibrocartilage becomes a clinical concern [83]. In contrast, tissue engineering approaches provide an opportunity to precisely place proper cells into the defect site in a controlled cellular microenvironment to maintain/enhance chondrocyte phenotype and increase cell delivery efficiency for facilitated tissue regeneration.

In order to repair or replace the damaged cartilage, typically in the high load-bearing joints of the body such as the knee and hip, it is important to consider the local

structure of the cartilage for appropriate biomechanical functions [84]. The solution of this complex problem should be based upon a combinatory approach of material selection, cell sources, and biochemical/biophysical cues [85]. All of these components should be carefully considered when deciding on a proper tissue engineering strategy to implement over current clinical treatment methods for cartilage regeneration.

2.2.2 – Structure-function relationship of cartilage

The body is composed of three primary types of cartilage: elastic, fibro-, and hyaline cartilage. Each serves specific functions within the musculoskeletal system. Elastic cartilage is a structural cartilaginous tissue for non-load bearing body parts, such as the ear, nose, and epiglottis [86]. It typically does not experience high mechanical loads for prolonged periods of time. Therefore, the damage of this tissue is not common or chronic, as compared to other types of cartilage found in the body. On the other hand, fibrocartilage acts as a mechanical supporting tissue in the intervertebral discs of the spine, the temporomandibular joint (TMJ) of the jaw, and the meniscus of the knee [87]. This type of cartilage contains a combination of both fibrous and cartilaginous tissue to serve as a tough, yet flexible supporting tissue within the musculoskeletal system. The directional woven structure of collagen type I as well as the more common collagen type II, typically found in hyaline cartilage, provides the greatest mechanical strength among different cartilages [88]. While the regeneration of elastic and fibrocartilage is also of

importance for medicine, this chapter will primarily focus on the most easily injured, thus the most widely studied type of cartilage, hyaline cartilage.

Hyaline cartilage is located along the surface at the ends of long bones in the joints and within the rib cage and the trachea, providing low-frictions surfaces throughout the body [89]. This particular musculoskeletal tissue is highly susceptible to damage from injury or degenerative disease due to its exposure to severe mechanical loadings. While there have been a large number of reported successes for experimental *in vitro* neo-cartilage production, there have been little to no reports for long-term clinical efficacy of the implanted engineered tissues [90-92].

The articular cartilage (AC) composed of hyaline cartilage tissue, plays an important role for joint functions; AC acts as shock absorber, alleviates the friction between bones within joints, and maintains a biochemical homeostasis with the subchondral bone [93]. The composition and structure of hyaline cartilage are closely related to the tissue functions. While this tissue is aneural and avascular, the high glycosaminoglycan (GAG), collagen and water contents within the extracellular matrix (ECM) act as an essential microenvironment for chondrocyte homeostasis and provide the necessary mechanical integrity for articulation of the limbs.

Due to its role in body's daily movements, AC is highly susceptible to damage or disease by physiological wear and tear, and traumatic injuries. With the end goal of repairing or regenerating cartilage through various tissue engineering strategies, the biochemical and biomechanical requirements of the native tissue must be taken into account for long term success. Therefore, a thorough understanding of the structure-function relationship of native articular cartilage with a comprehensive analysis of the physiochemical parameters is a prerequisite for engineering cartilage for therapeutic applications.

2.2.3 – Physiochemical requirements of engineered cartilage

To engineer functional articular cartilage, the physiological requirements should closely mimic the characteristics of the native tissue in both biochemical composition and mechanical integrity. The native structure of AC is comprised of three primary zones including the superficial, middle and deep zones (Figure 2.1). Each of the zones independently, yet cohesively, contribute specific functions of lubrication and compressive strength due to the organization and composition of the ECM accompanied by cells.

The superficial zone of AC contains the largest cell population although only being roughly 10-20% by volume. The tissue primarily acts as the area for friction reduction in

the tissue [94]. In this zone, the chondrocytes have a flat morphology and run parallel to the surface of the joint along with the collagen fibers. In addition to these structural characteristics, the chondrocytes in this secrete lubricin, a lubricant protein, reducing friction experienced from joint movement [80].

The middle zone acts as the primary shock absorbing layer in AC. In this portion of cartilage, mature chondrocytes are round in morphology and are sparsely dispersed in a rich proteoglycan ECM consisting of approximately 40-60% of AC by volume. The cells are perpendicularly aligned to the joint surface along with the thicker collagen fibers, which provides the structural integrity of AC. Additionally, while aggrecan is prominent throughout the tissue, the middle zone contains the highest content of this proteoglycan by volume, which helps contribute to the intrinsic compressive strength of AC [95].

The closest zone to underlying subchondral bones is the deep zone, which makes up about 30-40% of AC by volume. Located at the interface of cartilage and bone, this transitional zone possesses the characteristic feature known as the tidemark. The tidemark is the boundary of the calcification of the tissue and allows for proper integration between AC and the underlying subchondral bone. Beyond the definitive tidemark, while still contributing to ECM production, chondrocytes begin to show signs of hypertrophy. The increase in their mineral content as the transition from interfacial cartilage to bone is gradual. This transitional calcified cartilage zone is important for

proper neo-cartilage tissue integration because its close proximity to vasculature in subchondral bone [95]. The calcified cartilage also mediates the mechanical stresses and biological stimuli between the interfacial tissues, in addition to providing interstitial fluid transport to cartilage above [96].

Chondrocytes, the only cell type in found in cartilage, are responsible for producing and maintaining the ECM in AC, and the subsequent resulting anisotropic biomechanics within the mature tissue. Considering the fact that chondrocytes compose roughly 1-5% of the total volume, designing a scaffold with zonal structure is a key component for proper and facilitated regeneration of cartilage tissue [95, 97]. In this regard, electrospun scaffolds have shown to be an attractive methodology for AC tissue engineering due to the ability to tailor both the structure and function of the scaffolds with high porosity. Therefore, mimicking the zonal architecture and relative cell distribution should also reduce the discontinuities in mechanical properties by matching the local strain at the implant-tissue interface and aid in long-term tissue replacement strategies [98].

This chapter will discuss the method of electrospinning as a promising fabrication technique for scaffolding, current applications of electrospun scaffolds for cartilage tissue engineering, as well as limitations with the use of such scaffolds for translational applications.

2.3 – Synthesis of Electrospun Scaffolds

Electrospinning is a simple, yet powerful method for synthesizing highly porous micro- and nano-fibrous scaffolds for cartilage tissue engineering. These easily tunable and tightly regulated microstructures are ideal for controlling cell-scaffold interactions and subsequent tissue development. In comparison to scaffolds fabricated by other techniques, such as hydrogel based materials [99], porogen leaching of polymeric materials [100] or 3D printing [101], electrospun scaffolds provide several mechanical and biochemical advantages, which will be further discussed in this section.

2.3.1 – Electrospinning overview

Electrospinning is a versatile technique with a variety of finely tunable parameters to achieve desired material, chemical, and mechanical properties of a non-woven nano- or micro-fibrous mesh (Figure 2.2). This common term has been developed from the early description ‘electrostatic spinning’, and has been widely studied and used in both academic and industrial settings [102]. Electrospinning provides a means for synthesizing a network of elongated one dimensional nanostructures, which mimics the native nanoscale ECM present in AC.

Electrospinning requires a polymer to be soluble in a solvent at specific ranges of viscosity, conductivity, vapor pressure, and other solution properties. The solution is fed to a spinneret, a small orifice to generate a droplet at the tip, at a known flow rate. A high voltage is applied to the solution droplet to form what is known as the Taylor cone. In the Taylor cone, the charges which are carried throughout the solution mixture begin to separate. This charge separation elongates and ejects the polymer solution in the stable jet region of the Taylor cone to the direction of electric field. As the ejected polymer jet begins to dry within the distance of travel from the spinneret to the collection substrate, the current flow changes from an Ohmic to convection as the charges begin to move to the outer surface of the fiber. Beyond a critical point where the energy of these charges overcome the surface tension of the mixture, the solution experiences an electrostatic repulsion from one another resulting in a whipping instability, known as 'spinning,' to occur. This instability of the ejected polymer solution results in the rapid evaporation of the solvent creating nano- and microfibers. Finally, these fibers are then collected on a grounded substrate of desired geometry, producing vertically deposited non-woven fiber mats.

One of the greatest advantages of electrospinning is its processing capacity of various materials to yield scaffolds with diverse chemical and mechanical properties, which can invoke various biological responses from the cells. Natural polymers such as collagen, gelatin, fibrinogen, elastin, and fibrin, have been electrospun for tissue

engineering applications [103, 104]. A plethora of synthetic biodegradable polymers such as poly (lactic acid) (PLA), poly (glycolic acid) (PGA), poly (ε-caprolactone) (PCL), and composites of the monomer units [105-107] were also utilized for electrospinning. Table 24.1 lists commonly used polymers for electrospinning in the applications of cartilage tissue engineering. Many of these polymers have been approved by the Food and Drug Administration (FDA) for various *in vivo* applications, and can be selectively used to tailor the mechanical, chemical and degradation properties of electrospun scaffolds.

There are a variety of different configurations to produce electrospun scaffolds having different compositional and microstructural characteristics (*e.g.*, co-electrospinning, co-axial electrospinning, and blend electrospinning). Such diversity in electrospun fibers enables synthesis of scaffolds with tailored properties. By selectively determining materials and methodologies for electrospinning, scaffolds can be engineered to induce cell/tissue specific responses, facilitate tissue morphogenesis, and maintain phenotypical characteristics of the tissue.

Co-electrospinning is a technique where two or more polymeric solutions are simultaneously collected onto a single collection device (Figure 2.3). This is an attractive method for producing fibers that are on different orders of magnitude in fiber diameters or chemical compositions contained within a single scaffold [108-110]. By modifying the

collection medium or materials used for electrospinning, cellular responses can be tailored to address shortcomings of a single polymeric material.

Co-axial electrospinning, also referred to as core-shell or core-sheath electrospinning, is the process of enclosing one material around the other through the use of concentric needles (Figure 2.4). It has been demonstrated that this procedure can incorporate materials that are unable to be processed alone, where the sheath acts as a carrier of the core solution [111]. With this method, unspinnable materials can be used for tuning the intrinsic mechanical properties of the fibers, or a drug of interest can be loaded into the core material to control tissue morphogenesis [112, 113].

Blend electrospinning is where two or more miscible solutions are combined into a single feed system and fed through a common spinneret for desired final material properties (Figure 2.5). While this procedure is not the most common technique, the benefit of using this particular method has shown to help modify the chemical and mechanical properties of the scaffolds for aiding in cell proliferation, differentiation, and survivability [111, 114, 115].

There are many variables which need to be carefully determined for successful electrospinning. The detailed description of electrospinning parameters that determine

the structural and morphological characteristics of electrospun fibers as well as spinnability, is as follows in the subsequent section.

2.3.2 – Fundamental principles of electrospinning

The fundamental principles of electrospinning are dictated by three primary parameters including solution, processing, and environmental conditions (Table 24.2). Each fabrication setting must be taken into close consideration to properly synthesize a scaffold with structural and functional characteristics similar to native cartilage.

Solution parameters: user-defined variables

The first step to determine the properties of the final end product are solution parameters, which consist of the polymer and solvent material properties, as well as those of the solution mixture. The high solubility of the polymer of interest in a particular solvent is prerequisite for uniform electrospinning. The major scaffold characteristics such as chemical composition, mechanical integrity, degradation rate and by-products will be determined by polymeric materials. On the other hand, the solvent properties will determine morphological characteristics of electrospun scaffolds such as fiber size, porosity and fiber morphology.

Different polymeric materials have different solubility characteristics in any given solvent. Some polymers are fully, partially, or even insoluble in different solvents, which will impact the electrospinnability of those materials. The selected solvent, or combination of solvents, also have varying intrinsic chemical, electrical, and solubility characteristics which will significantly affect the fabrication of the fibers [116]. There is a critical range of polymer concentration, which determines electrospinnability [117]. Below a certain threshold, there are an insufficient amount of polymer chain entanglement to generate continuous fibers, resulting in fragmented polymer droplets called electrospraying. This critical concentration depends on a balance of the polymer chemical composition, chain length, the accompanying solvents and the combined solution viscosity. In contrast, an extremely high polymer concentration results in overly large polymer chain entanglements, and entrapped solvent prevents the fibers to sufficiently dry before being collected. This results in wet fibers binding to another, creating a thin film rather than porous fibrous membranes [118]. Similarly, when the polymer molecular weight increases, large, smooth, continuous fibers are formed, whereas a low molecular weight polymer is insufficient in forming fibers due to low polymer chain entanglement [119].

An additional solution parameter for electrospinning is the conductivity of the fluid. The polymer solution conductivity (*i.e.,* charge density) assists in the jet formation from the Taylor cone and resulting whipping instability of the electrospun fibers. As the

conductivity increases the distribution of the charge density of the applied voltage overcomes the tangential electric field along the surface of the solution droplet [120]. Higher solution conductivities will result in smaller fiber diameters, whereas lower values generate larger electrospun fiber diameters. When the polymer solution conductivity is too low, surface charging is insufficient to form a Taylor cone failing the electrospinning process. In contrast, when the solution conductivity is too high the reduced tangential electric field also resists the formation of the Taylor cone [120]. The addition of ionic salts such as KH_2PO_4 and NaCl can increase the ion contents, which enhances the surface charge density of the solution, and improves the electrospinnability of the polymer [121].

Finally, the dielectric properties of the solvent used in electrospinning polymers also affect the electrospinnability of the polymer solution in conjunction with the conductivity. The dielectric constant of a solvent represents the amount of “free” charge that can be induced into the polymer solution during spinning [122]. Polymer-solvent solutions consisting of low-dielectric constants limit the initiation of the whipping instability and thinning of the polymer jet. By reducing the available charge on the surface of the polymer jet, the electrostatic repulsive force which initiates the whipping instability of the fiber is also decreased. This leads to the stable jet to become elongated, resulting in an extended duration for the charge density to migrate to the surface of the fluid. This delay results in larger electrospun fiber diameters or loss of electrospinnability. This

suggests that there is a critical window of “free” charge available to initiate the whipping instability that induces spinning of any polymer-solvent systems.

Process parameters: experimental variables

Process parameters are defined as experimental variables to control electrospinning process. These parameters include the polymer solution flow rate, the working distance from the tip of the spinneret to the collection target, the type of grounded collection target, as well as the applied voltage at the spinneret.

The polymer solution flow rate has been shown to influence the overall fiber diameters. While low flow rates typically result in smaller fiber diameters and vice versa for higher flow rates, there is a range of optimal flow rates for any given polymer/solvent combination [123, 124]. If the flow rate is too low for a given solution, an overcharging of the solution may occur, resulting in electrospraying to deposit particles on the collector. If the solution flow rate is too high, the applied electric field cannot generate a whipping instability within the polymer jet, preventing ‘spinning’ of the polymer solution. In addition, the solvent contained within the solution will not evaporate rapidly enough to form fibers.

The working distance between the spinneret tip and the collection substrate dictates the resulting fiber morphology. By changing the working distance, the applied electric field between the tip and collector is also altered, impacting the formation of the fibrous membranes. As the distance increases, the fibers are continually stretched and thinned within the whipping region, resulting in smaller fiber diameters [125]. However, there's a critical voltage threshold that can be applied to the spinneret as proportional to the increased working distance without causing instability in the Taylor cone formation. The applied voltage that creates an electric field between the spinneret and the collector, is the key driving factor for electrospinning, determining the electrospun fiber diameter [126, 127]. High applied voltage levels increase the surface charge density of the polymer-solvent solution resulting in greater repulsion of the fibers, which in-turn increases the whipping instability and thinning of the jet formation, ultimately generating fibers on a smaller dimensional scale.

Finally, the collection target has significant effects on the macro-structure of the synthesized scaffolds [128]. While the most common collection substrate is a grounded static metallic collection plate, a wide variety of collectors including grounded solution baths [129], rotating mandrels [130], and patterned devices [131] have been used. Each of these result in patterns or macro-structures allowing for tailored cellular responses in migration, proliferation, and differentiation of the cells. The macro-structure of

electrospun scaffolds is especially important for cellular migration including angiogenesis, thus determining engineered tissue integration to native tissues [132, 133].

Ambient parameters: environmental variables

While the ambient parameters have a distinct impact on electrospun fibers, these systemic parameters present challenges for dynamic control. Furthermore, the effects of these environmental factors depend on polymer-solution combinations (*i.e.*, sensitivity to temperature, hygroscopic nature of solution and optimum vapor pressure) and simultaneously influence solution properties (*i.e.*, viscosity and evaporation rate). Therefore, it is difficult to make direct correlations between final scaffold production and these variables.

The temperature during electrospinning has been shown to influence the final fiber diameters. Both the solvent evaporation rate and the intrinsic solution viscosity are affected by ambient temperature during electrospinning [134]. There have been two proposed mechanisms on the effects of environmental temperature on electrospinning, both of which affect fiber diameters in a biphasic manner. Firstly, as the temperature decreases, the solvent evaporation is reduced. The prolonged solidification of the polymer induces increased fiber elongation and jet thinning, resulting in smaller fiber diameters. Secondly, at higher temperatures the polymer chains have greater freedom to

move, resulting in lower solution viscosity, also reducing the fiber diameters [135]. In most cases, ambient room temperature (20-23°C) conditions are typically used, unless more specific conditions are required to successfully generate fibers.

Next, the relative humidity also determine the morphological characteristics of electrospun fibers. When the environmental humidity is too low, the solvent evaporation rate increases and can completely dry the solvent before proper solution elongation to form fibers. In contrast, when the humidity is too high, the solvent cannot completely evaporate resulting in continuing elongation of the fibers resulting in small diameters. Therefore, depending on the polymer-solvent selection there is an ideal range of relative humidity for successful continuous fiber formation [135]. The humidity has also been shown to impact the surface morphology of the electrospun fibers where lower levels of humidity generate smooth fibers and higher humidity levels create pores on the surface of the fibers [136]. Although the exact mechanism for surface pore formation is unclear, it was proposed that the evaporation of the solvent cools the fibers during electrospinning and ambient moisture condenses on the surface of the fiber resulting in pitting and pore formation. Similarly, the cabin air velocity also has an influence on fiber generation by affecting solvent evaporation [137]. When the cabin air velocity is too low, solvent evaporation is decreased resulting in insufficient drying of the fibers.

The electrospinning process is a potent technique to mass-produce nano- and microstructures utilizing a wide array of polymeric materials to guide cellular activity in tissue engineering applications. Therefore, while the fabrication process has many interconnected variables to consider, this methodology is attractive for cartilage tissue engineering due to its highly-tunable nature to produce tightly regulated cellular microenvironments.

2.4 – Electrospun Scaffolds for Cartilage Regeneration

Designing scaffolds with appropriate chemical, mechanical and biological properties is essential for guiding proper functionality and integration of engineered cartilage. Therefore, the scaffolds should strive to address the following criteria.

· Scaffold materials are biocompatible to minimize any immunogenic response of the surrounding tissues.

· Scaffolds are biodegradable at a designed degradation rate, resulting in proper integration of the engineered tissue to the native tissues while maintaining structural and mechanical integrity during maturation.

· The microstructure and composition of scaffolds provide proper microenvironments either to differentiate native progenitor cells to the necessary phenotype of the tissue or to maintain the phenotype of cultured mature cells within the scaffolds.

These prerequisites ensure the development of the engineered tissue to match the mechanical and biochemical properties of the native tissue.

Electrospinning has shown to be an attractive method to produce chondro-inductive scaffolds in meeting the above criteria due to its ability to tailor the structural, mechanical, and chemical parameters simulating the extracellular (ECM) microenvironments for cell migration, proliferation, and/or differentiation of chondrocytes or chondrocyte-precursor cells. Therefore, it provides an opportunity to devise a scaffold mimicking the architecture of native cartilage in the structure, function, and biochemical composition for cartilage regeneration. Herein, a discussion of the materials used in the synthesis of electrospun scaffolds will be given, followed by the effects of such scaffolds on directing cellular behavior for cartilage regeneration.

2.4.1 – Materials selection

When selecting proper polymers to be used for cartilage regeneration, it is important to consider how the chemical and mechanical properties of these materials correlate to the structure and function of articular cartilage. The appropriate materials selection is essential for controlling cellular behaviors and the impacts on the surrounding native tissues. The following will describe the biocompatible materials that are most commonly used for electrospun scaffolds for cartilage regeneration.

Natural/biological materials

The use of natural or biological polymers for electrospun scaffolds is advantageous due to their natural biocompatible and biodegradable properties. The balance between hydrophilicity for proper cellular interaction and hydrophobicity for structural maintenance during tissue maturation is critical for cartilage regeneration. Additionally, the by-products from these biodegradable scaffolds induce little, to no, innate immune responses from the surrounding tissues. Although a few promising natural polymers may not have intrinsic material properties to be electrospun individually, co-axial electrospinning and/or post-modification techniques can provide an opportunity to exploit excellent biological properties of these natural polymers to elicit the desired cellular interactions.

Being one of the primary components within cartilage, collagen is commonly used because of the ability to impart natural bioactivity on the localized cell population as RGD binding domains present in collagen promote cellular attachment and proliferation [138]. Furthermore, electrospinning produces nanofibers ranging from 50 to 500 nm, similar to the sizes of natural collagen fibrils [139]. The degradation rate of the as-spun collagen nanofiber mats can be controlled by the *in situ* crosslinking to enhance the mechanical integrity of the scaffold, a typical shortcoming of natural products [140]. Electrospinning of collagen has been studied extensively [104], along with the combinatory blends of

other natural materials such as chitosan, elastin, and silk fibroin for various tissue engineering applications [141-143]. In addition to use as an electrospinning material, this natural protein can be conjugated to the surface of synthetic electrospun fibers to enhance cellular attachment, which may possess critical mechanical characteristics necessary for cartilage tissue engineering. Gelatin, a denatured collagen product, is also a naturally derived protein extracted from a variety of tissues in xenogenic sources. It is commonly used for electrospinning due to its biocompatibility and chemical composition similar to collagen while providing economic advantages over the high costs associated with pure collagen [144]. The mechanical properties of electrospun gelatin can be modulated by tailoring the degree of crosslinking similarly to collagen [145].

Hyaluronic acid (HA) is a glycosaminoglycan found in the ECM of many soft connective tissues. The function of HA is especially important for cartilage as its charged nature attracts water molecules to render resistance to compressive forces. However, the polyelectrolytic nature, in addition to very high molecular weight which significantly increases solution viscosity, inhibits the use of HA as a stand-alone material for electrospinning. Therefore, many studies have focused on blending HA with uncharged carrier polymers such as gelatin [146] and poly (ethylene oxide) (PEO) [147] to enable electrospinning. Recently, Brenner, Schiffman [148] demonstrated that the use of aqueous ammonium solutions can overcome these limiting characteristics of HA for electrospinning, making it an attractive material for cartilage regeneration.

Finally, chitosan, a polysaccharide, is another natural material commonly used for electrospinning. By creating a nanofibrous topography of chitosan on top of a 2D membrane it has been shown to enhance chondrocyte attachment, proliferation, and conservation of the chondrocyte phenotype when compared to a chitosan based film [149]. More commonly, blending of chitosan and other natural and synthetic components in scaffold fabrication for cartilage regeneration have been shown to be beneficial for cell attachment, proliferation, and viability [150, 151].

Synthetic polymers

While there are numerous synthetic materials successfully used for electrospinning in various tissue engineering applications such as vascular [152], bone [153], neural [154], and tendon/ligament [155], the following will focus on three of the main polymers for cartilage tissue regeneration. Synthetic polymers typically have enhanced mechanical properties over their natural counterparts, as well as a customizable chemical structure through modification in functional groups to control cell-scaffold interactions.

Poly (lactic acid) (PLA), poly (glycolic acid) (PGA), and poly (ε-caprolactone) (PCL) have all been approved by the FDA for various *in vivo* applications. Therefore, each of

these synthetic polymers are attractive for cartilage regeneration to address specific cellular responses based on their chemical and mechanical traits. Each of these materials have been shown to be beneficial in promoting or maintaining chondrogenic phenotype over commonly used cell culture methods, such as chondrogenic differentiation of MSCs on PCL nanofibers over tissue culture polystyrene (TCPS) [156] or providing a suitable substrate for chondrocyte culture without dedifferentiation [157].

The use of PLA alone for electrospun scaffolds in cartilage regeneration has had little to no attention probably due to the slow clearance rates of the material during degradation and the acidic by-products of the polymers. Thus, it has typically used as a component for blends or co-block polymers in electrospinning applications [158, 159]. Additionally, different techniques were incorporated to PLA electrospinning to optimize the scaffolds for cartilage applications. Laser ablation was used on electrospun nanofibrous PLA scaffolds to increase the pore dimensions, which could enhance cell infiltration for tissue engineering [160]. In addition, nanofibrous PCL fibers were coated on microfibrous PLA fibers in an attempt to fabricate highly porous scaffold with nanofibrous topographical features for cartilage generation [161].

A semicrystalline polyester, PGA, is an attractive polymer for scaffolding material due to the relatively quick degradation period of only a few weeks *in vivo* [162]. Prior to the popularity of electrospinning for tissue engineering applications, the development of

non-woven microfibrous mesh via extrusion of fine fibers of PGA was developed. Using isolated chondrocytes, these fibrous scaffolds were shown to induce the formation of cartilaginous tissue consisting of high GAG and collagen content [163]. Although this polymer has shown to be more beneficial for soft tissue engineering applications [164], combining this material with other synthetic or natural polymers can greatly enhance the chondroinductive properties for maintaining cellular phenotype or influencing chondrogenesis of multipotent stem cells due to the capacity of tailoring the composition of these materials to control the subsequent biodegradation rates and resulting mechanical properties.

Another polyester based synthetic polymer, PCL, has been extensively studied in electrospinning for cartilage applications. Although the degradation time for this material is much greater than PGA (>24 months), this may be an ideal polymer due to the low clearance rate of acidic by-products in native cartilage. With this relatively soft material characteristic in consideration, nanofibrous scaffolds have been developed for 2D cell culture to enhance cartilage tissue formation [156, 157, 165]. Additionally, its excellent processability in a variety of organic and inorganic solvents increases its utility as a composite material for cartilage tissue applications [166].

Composite materials

Alloying materials among natural and synthetic polymers provide an opportunity to tune the chemical, mechanical and biological properties of scaffolds to modulate functionality of the final chondro-inductive scaffold and subsequent the cellular behaviors. In order to facilitate cartilage regeneration, the composites utilize the beneficial aspects of the various natural and synthetic polymers incorporating their mechanical properties, biocompatibility, and degradation rates. These composites are typically fabricated by simple blending or using the coaxial or co-electrospinning procedures as previously described.

More common examples of composite materials used for cartilage regeneration utilize a combination of both synthetic and natural polymers, such as chitosan-PEO [151], gelatin-PCL [167], gelatin-PLLA [144]. While each of these composites of materials address different applications of cartilage regeneration, they combine the chemical and mechanical strengths of the two materials to alleviate the limitations of their counterpart. Therefore, the optimization of composition, whether it be combinations of synthetic-synthetic or natural-synthetic polymers, is critical for potential uses in cartilage regeneration as well as electrospinning processability.

In addition to simple alloy of materials, synthesis of co-block polymers from the previously mentioned synthetic materials (PLA, PGA, and PCL) are commonly used to tailor the chemical and mechanical properties of electrospun fibers. One example of synthetic co-block polymers used for cartilage regeneration is poly (D,L-lactide-co-glycolide) (PLGA). This co-polymer has been investigated for the mechanical properties, degradation, and cellular responses to different lactic acid to glycolic acid ratios, and has been used in the fabrication of both 2D [168] and 3D [169] nanofibrous scaffolds for cartilage reconstruction.

2.4.2 – Applications of electrospun scaffolds for cartilage regeneration

The capability of synthesizing scaffolds with highly tunable chemical and mechanical characteristics positions electrospinning as one of the viable methods to produce a tightly regulated microenvironment for desired cellular behaviors. Applicability to a wide variety of materials and mass-scalability add significant values to electrospun scaffolds for therapeutic applications. Typical use of these electrospun scaffolds includes cell culture substrates for chondrocyte expansion or MSC differentiation to chondrocytes, and 3D tissue scaffolds for cartilage tissue engineering.

Electrospun cell culture systems

Limited cell source is a primary concern for cartilage regeneration [170]. Mature primary chondrocytes dedifferentiate or lose their phenotypic characteristics during typical *in vitro* culture involving common cell culture labwares [171, 172]. They change their morphology, a feature that is closely linked to the functions of the cells, from round to flat shape primarily due to changes in the configuration of cell-ECM adhesion from 3D to 2D [173]. By this reason, hydrogel systems such as agarose or alginate have been used to culture chondrocytes to maintain their phenotype. However, their application in the mass production of chondrocytes is limited by its difficulty in cell retrieval from 3D matrices. On the other hand, topographical features associated with the non-woven nature of electrospun fibers provide a microenvironment suitable for maintaining chondrocytes' natural morphology, thus functionality in a 2D format ideal for cell retrieval.

In an earlier study by Li, Danielson [157], electrospun PCL nanofibers showed enhanced maintenance of chondrocytic phenotype over TCPS culture systems. A more round or spindle shape of chondrocytes with less actin stress fiber formation on the nanofibrous scaffolds was observed, in contrast to a more flat morphology on the TCPS. This morphological difference was related to the cells' functionality, demonstrated by greater expression of chondrocytic proteins including Collagen II and IX, aggrecan, and

cartilage oligomeric matrix protein on the electrospun scaffolds. This enhancement in maintaining phenotypic characteristics of chondrocytes is likely due to physical features of electrospun fibrous structure rather than specific chemical traits. The superiority of electrospun fibrous structure as a cell culture system for chondrocytes was demonstrated when a chitosan and poly (ethylene oxide) (PEO) blend of nanofibers was compared to a thin film of similar composition [151].

Interestingly, in addition to the topographical feature of electrospun scaffolds, the fiber size significantly affects the phenotypic stability of chondrocytes. Noriega, Hasanova [174] reported that submicron size topography was preferential for chondrocyte culture when compared to larger micron sized fibers. While the differences in the fiber size did not show significant changes in RhoA activity that governs cytoskeletal organization, the increased ROCK expression, a downstream of RhoA, in nanofibers appears to enhance chondrocytic protein expression and phenotypic maintenance [174]. RhoA is a central protein that is regulated by integrin-related cell-ECM interactions and mechanotransduction [175]. It is unclear that the enhanced chondrocytic activity on nanofibers is due to the increased binding sites that change the quantity of cell-matrix adhesion or the decreased substrate stiffness that frustrates stress fiber formation. Nevertheless, the study by Noriega, Hasanova [174] provides insight to the influence of fiber diameter on cellular behaviors, and confirms the utility of electrospun nanofibers as a promising substrate for chondrocyte culture systems.

One of the approaches to overcome limited quantities of native chondrocytes from a patient for cartilage regeneration is to use various types of stem cells by differentiating them into chondrocytes. In this regard, electrospun scaffolds demonstrated a great potential promoting chondrocytic differentiation of stem cells. Utilizing PCL nanofibrous scaffolds, Li, Tuli [165] demonstrated the enhanced differentiation potential of MSCs toward chondrocytes. More specifically, the results showed that the high MSC seeding density, similar to commonly used differentiation protocols such as micro mass [176] or pellet culture [177], may not be required when an electrospun system is used. This observation further signifies the beneficial effects of topographical features in electrospun fibrous structure for promoting the differentiation of stem cells toward chondrocytes and the subsequent maintenance of mature chondrocytic phenotype.

Among many physiochemical properties of electrospun fibers, the mechanical properties of fibrous network are one of the dominant factors that delineate the enhanced chondrogenesis of stem cells on electrospun scaffolds. Nam, Johnson [156] showed that softer electrospun scaffolds exhibited greater chondrogenesis as compared to stiffer scaffolds when the same surface chemistry was maintained by utilizing core-shell electrospinning. MSCs cultured on soft PCL nanofibrous scaffolds exhibit a more round chondrocyte-like morphology with less actin stress fiber formation, in contrast to

the elongated fibroblastic-like structure of the MSCs cultured on TCPS shown in Figure 2.6. These results indicate that the compliance or pliability of individual electrospun fibers controls the cell morphology and its subsequent differentiation, which further emphasizes the importance of material selection for optimized mechanical properties.

The topographical cues of nanofibrous scaffolds have been shown to significantly influence cellular signaling of stem cells during chondrogenic differentiation. Nanofibers provide adequate focal points for stem cell adhesion, proliferation, and chondrogenic differentiation [178]. Zhong, Zhang [179] investigated the roles of the RhoA/ROCK and Yes-associated protein (YAP)/transcriptional co-activator with PDZ-binding motif (TAZ) signaling pathways in fibrochondrogenic differentiation of MSCs, showing that these signaling pathways play an imperative role in cytoskeletal dynamics and stem cell differentiation [180]. The activation of ROCK on nanofibers enhances Sox9 activity, which is a primary transcription factor necessary for promoting chondrogenesis [181]. Simultaneously, the YAP/TAZ signaling that upregulates Runx2 and collagen I, while downregulating Sox9, collagen II, and aggrecan gene expression, was effectively suppressed, further enhancing chondrogenesis. This study provides a critical insight on the cell signaling responses of stem cells to their local microenvironment, demonstrating the utility of electrospun nanofibers for directing chondrogenesis.

Overall, these results demonstrate the superiority of electrospun scaffolds over typical tissue culture plates as a cell culture platform for cartilage regeneration. The nanofibrous structure not only enhances the phenotypic maintenance of mature chondrocytes, but also promotes the differentiation of stem cells toward chondrocytes.

Electrospun scaffolds for cartilage tissue engineering

In contrast to the monolayer culture systems described above, the construction of engineered cartilage requires placement of appropriate cells within a 3D electrospun scaffold while maintaining the mechanical integrity in the defect site of the host under physiological conditions. Considering the main function of cartilage being load-bearing, it is important to consider promoting tissue morphogenesis while maintaining structural integrity during the maturation of the engineered tissue, both of which associate with the porosity and degradation rate of scaffolds. For cartilage tissue engineering, two main approaches include 1) the use of acellular scaffolds followed by the recruitment of endogenous cells into the scaffolds and 2) the culture of appropriate cells within scaffolds *in vitro* and their subsequent implantation after tissue maturation.

To assess the feasibility of utilizing electrospun scaffolds for cartilage regeneration, acellular electrospun PLGA scaffolds were implanted into osteochondral defects in the femoral condyles of rabbits [169]. The results showed the ingrowth of

endogenous cells into the scaffolds and enhanced tissue formation over untreated tissue damage. However, the degree of regeneration depended on the availability of macro-pores for cellular infiltration; scaffolds having a cannulated configuration induced greater tissue morphogenesis as compared to a solid form, indicating that intrinsically small pore size in electrospun nanofibers is a limiting factor impeding tissue regeneration. A recent study using an *in vitro* cell-scaffold culture approach demonstrated a similar observation regarding cellular infiltration-dependent cartilage regeneration by electrospun scaffolds [167]. Different ratios of gelatin to PCL electrospun scaffolds were implanted *in vivo* in a rodent model to evaluate their potential for 3D cartilage regeneration. PCL enhanced the mechanical integrity of the scaffolds, whereas the biocompatibility and facilitated biodegradation of gelatin increased the cellular infiltration and subsequent tissue morphogenesis. It was shown that scaffolds with high PCL content were less favorable for 3D cartilage regeneration due to limited cellular infiltration demonstrating the importance of the balance between chondrogenesis-favorable nanofiber structure and cell ingrowth-allowing macroporous structure.

To overcome the shortcoming of electrospun nanofibrous structure, various methods have been incorporated into electrospinning process to increase pore size for enhanced cellular infiltration. Some of these methods of enlarging pore dimensions include removing salt particles incorporated into the fibers during the synthesis [182, 183], ultrasonication to enlarge the inter fiber spacing [184], as well as the selective

dissolution of sacrificial PEO fibers after scaffold fabrication [185]. Another approach includes the utilization of microfibers to increase intrinsic pore size in electrospun scaffolds [186]. Figure 2.7 shows articular chondrocytes cultured in microfibrous PCL scaffolds, secreting their own nanofibrous ECM within microfiber networks. One of the caveats utilizing microfibers, however, is extensive culture period for tissue maturation due to the large pore volume that needs to be filled by the cells.

A novel method for addressing the benefits and pitfalls of solely using electrospun nano- or microfibers is to employ a multiscale, or multidimensional electrospun fiber approach. The benefits of multiscale approach stems from the cell-favorable topographical scales accomplished through nanofiber formation and the cellular infiltration enhancing macropores by microfibers. One method used to address this multiscale approach was accomplished via combining PCL microfibers and fibrin nanofibers by utilizing the co-electrospinning technique on a rotating mandrel [187]. The combination of using both micro- and nanofibers in a 3D scaffold demonstrated the enhancement of cellular proliferation throughout the scaffold while enabling the cells to maintain cellularity and secrete chondrocytic ECM. Another similar study utilizing multiscale electrospun fibers to enhance the porosity of 3D scaffolds employed nanofiber-coated microfibers. A combination of PCL nanofibers electrospun onto PLA microfibers was utilized to synthesize highly porous scaffolds ranging 95-97% porosity while providing nano-topography for cell-scaffold interactions [161]. While the authors

did not focus on the biochemical aspects of maintaining chondrocyte phenotype or enhancing chondrogenesis, this study demonstrated a possibility of inducing synergistic effects between nanofibers and microfibers for enhance cellular behaviors and infiltration, which may be applicable for cartilage regeneration.

As previously described, articular cartilage is structured to exhibit depth-wise anisotropy in cell population, morphology, orientation as well as ECM composition and structure. This gradient structure is essential for depth-dependent cartilage functions such as load-bearing and joint lubrication. In an effort to address the structure and function for this zonal architecture, a combinatory approach for sequential electrospinning has been attempted to produce distinct fiber dimensions and organizations in a depth-dependent manner [188]. Varying the polymer concentration and velocity of a rotating mandrel collector, a 3D trilaminar composite microfibrous culture system mimicking the articular cartilage zonal architecture was developed. Culture of mature chondrocytes in this scaffold over the course of a 5-week period, resulted in cartilage-like ECM deposition with a depth-dependent organization. This study demonstrates the importance and feasibility of electrospun scaffold structure-dependent cellular functions for articular cartilage regeneration.

Overall, electrospinning finds a great utility in the fabrication of *in vitro* cell culture systems and in vivo tissue engineering scaffolds. However, there are still limitations and

drawbacks that need to be overcome to further enhance therapeutic applications of electrospun scaffolds in cartilage regeneration.

2.5 – Current Limitations of Electrospun Scaffolds in Cartilage Tissue Engineering

Many key factors must be considered and incorporated into material selection and fabrication process in order to ensure proper cartilage regeneration. For example, different scales of electrospun fibers (*i.e.*, nano- and micro-size) exhibit both benefits and shortcomings for cartilage regeneration. Nanofibrous structure produces a high surface-area to volume ratio which promotes cellular adhesion and proliferation, ideal for 2D cell culture. However, its intrinsically small pore size restricts cellular infiltration, limiting its use in 3D culture systems. In contrast, the microfibers allow for greater cellular penetration in 3D, but do not provide nanofiber-based topographical cues mimicking the ECM components present within native tissue [187].

While most studies focus on scaffold materials for electrospinning, the structural configuration of such as-spun fibers does not depict the 3D spatial orientation of cartilage ECM. Since cartilage is a complex tissue with varying ECM arrangements, both parallel and perpendicular to the surface to the joint, electrospinning techniques to mimic these organizations are currently limited to layered fiber networks [189]. Such a layered approach may impede its therapeutic applications due to compromised structural

integrity between layers. Therefore, a monolithic scaffold having gradient changes in structural and mechanical properties would present more appropriate platform for cartilage regeneration. Another aspect to consider for electrospun scaffolds as a vehicle to drive cartilage regeneration is the size and shape of the implant. So far, most studies have been limited to the size of local cartilage lesion with a cylindrical shape. To further facilitate the adaption of electrospun scaffolds for cartilage tissue engineering, methods that can scale up the size of scaffolds to full cartilage with a patient-specific shape need to be devised.

Electrospinning is a versatile technique which produces fibers on different orders of magnitude in size and mechanical properties, providing an opportunity to fabricate physiochemically tuned scaffolds for cartilage regeneration. Future focus for the field will likely address the zonal architecture of articular cartilage in both structure and function of engineered tissue through a thorough consideration of materials to match the chemical and mechanical aspects of physiological cartilage tissue. In conclusion, electrospun scaffolds show exemplary promise for cartilage regeneration.

2.6 – Tables & Figures

NATURAL POLYMERS	SYNTHETIC POLYMERS
Collagen	PGA – Poly(glycolic acid)
Gelatin	PLA – Poly(lactic acid)
Chitosan	PLLA – Poly(L-lactic acid)
Fibrin	PLGA - Poly(lactic-co-glycolic acid)
Hyaluronic Acid	PCL – Poly(ε-caprolactone)
	PEO – Poly(ethylene oxide)
	PEG – Poly(ethylene glycol)

TABLE 2.1. COMMON POLYMERS USED IN ELECTROSPINNING.

List of natural and synthetic polymers commonly used for electrospinning nano- and microfibrous scaffolds for cartilage tissue regeneration.

PARAMETER	SUB-PARAMETERS
SOLUTION: **USER-DEFINED VARIABLES**	Polymer/solvent solubility
	Polymer/solvent concentration
	Polymer molecular weight
	Solution viscosity
	Solution conductivity
	Dielectric constant
PROCESSING: **EXPERIMENTAL VARIABLES**	Polymer solution flow rate
	Electric field strength
	Working distance
	Applied voltage
	Fiber collection geometry and composition
AMBIENT: **ENVIRONMENTAL VARIABLES**	Temperature
	Relative humidity
	Air cabin velocity

TABLE 2.2. LIST OF COMMON ELECTROSPINNING PARAMETERS.

Experimental parameters addressed during the electrospinning process.

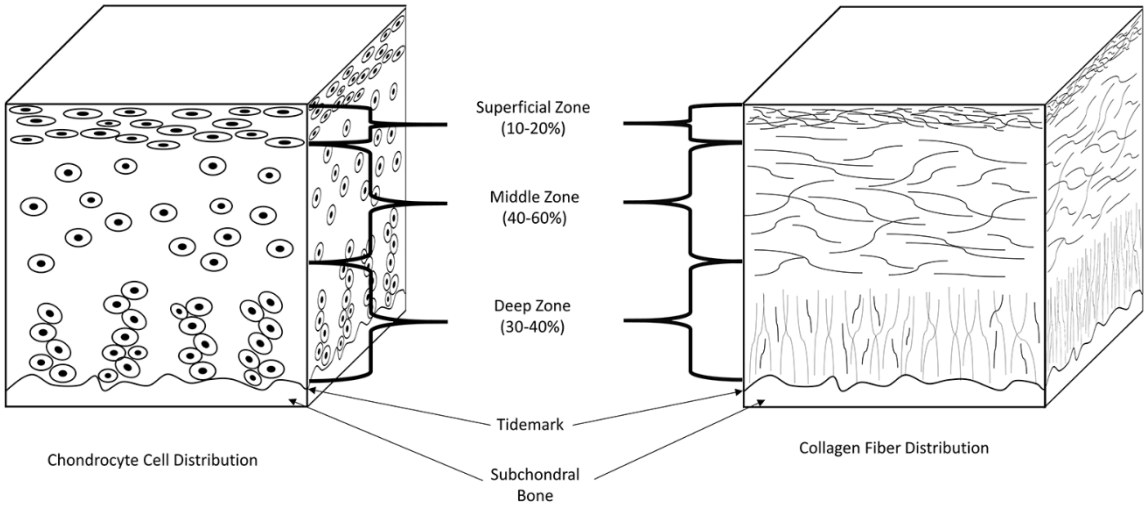

FIGURE 2.1. CROSS-SECTIONAL SCHEMATIC OF ARTICULAR CARTILAGE.

The tissue consists of the superficial, middle/transitional, and deep zones with a distinct tidemark of calcified cartilage and the underlying subchondral bone (from top to bottom). Both cellular organization and collagen fiber orientation are shown with respect to the zonal structure of cartilage.

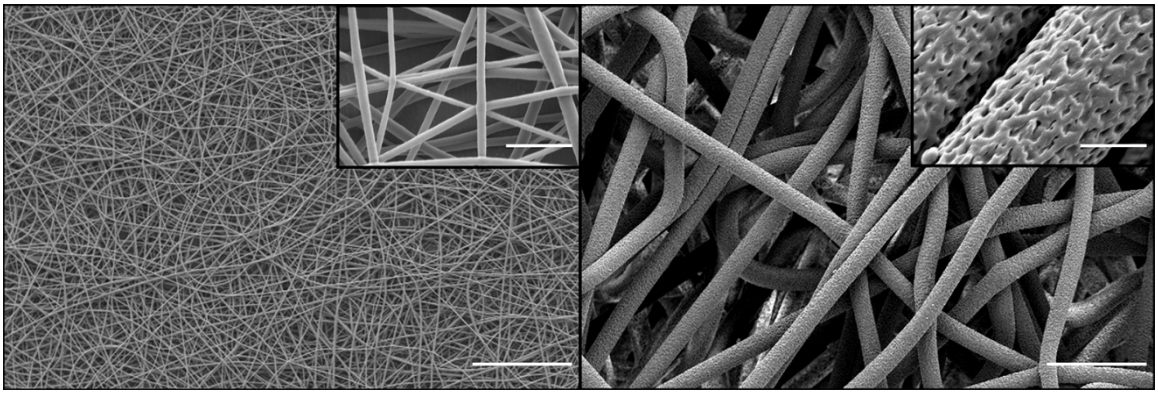

FIGURE 2.2. RANDOMLY ORIENTED ELECTROSPUN FIBER MORPHOLOGY.

SEM images of electrospun nano- and microfibrous poly (ε-caprolactone) scaffolds demonstrating fiber dimensions of different orders of magnitude (Scale bars: 5μm for subset and 50μm for full images).

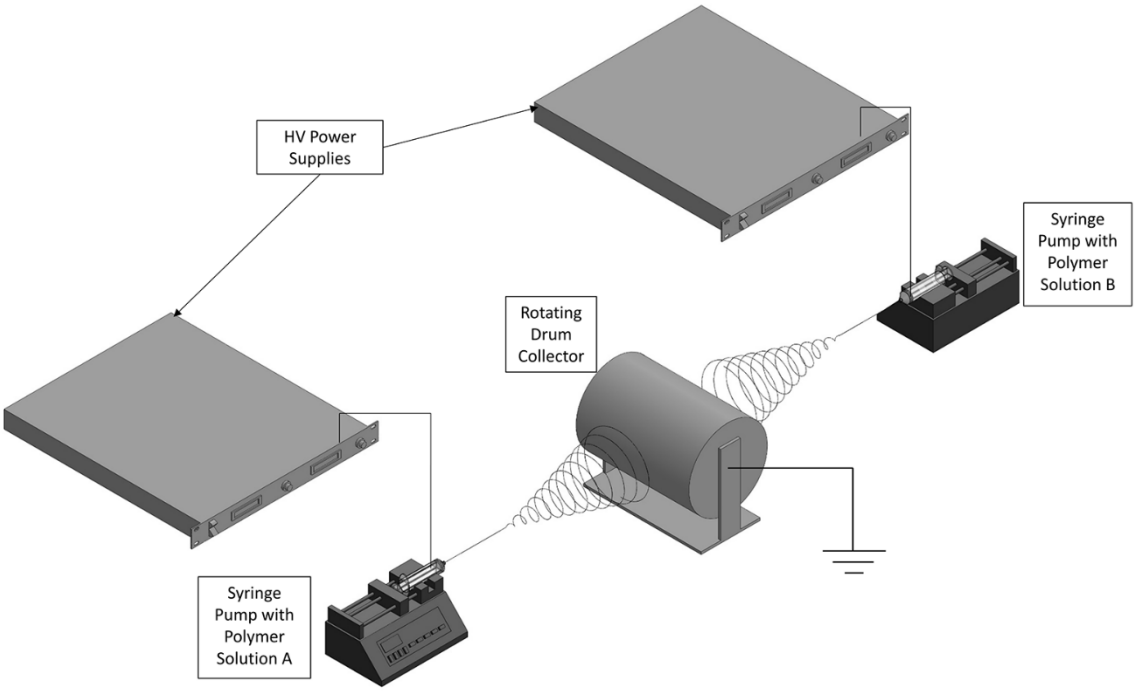

FIGURE 2.3. CO-POLYMER ELECTROSPINNING SETUP.

A schematic of co-electrospinning setup where two different solutions are simultaneously electrospun and acquired on a common collector.

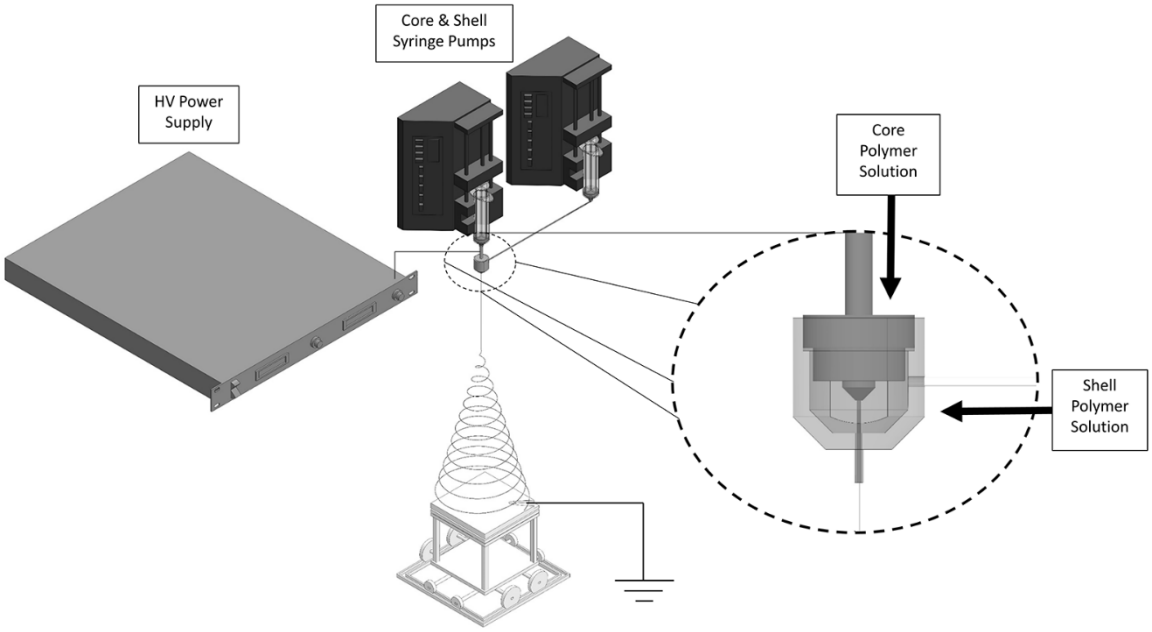

FIGURE 2.4. CORE-SHELL FIBER ELECTROSPINNING SETUP.

A schematic of coaxial or core-shell electrospinning setup where one polymeric solution is fed into an inner reservoir (core), whilst a secondary polymer is fed to the surrounding reservoir (shell).

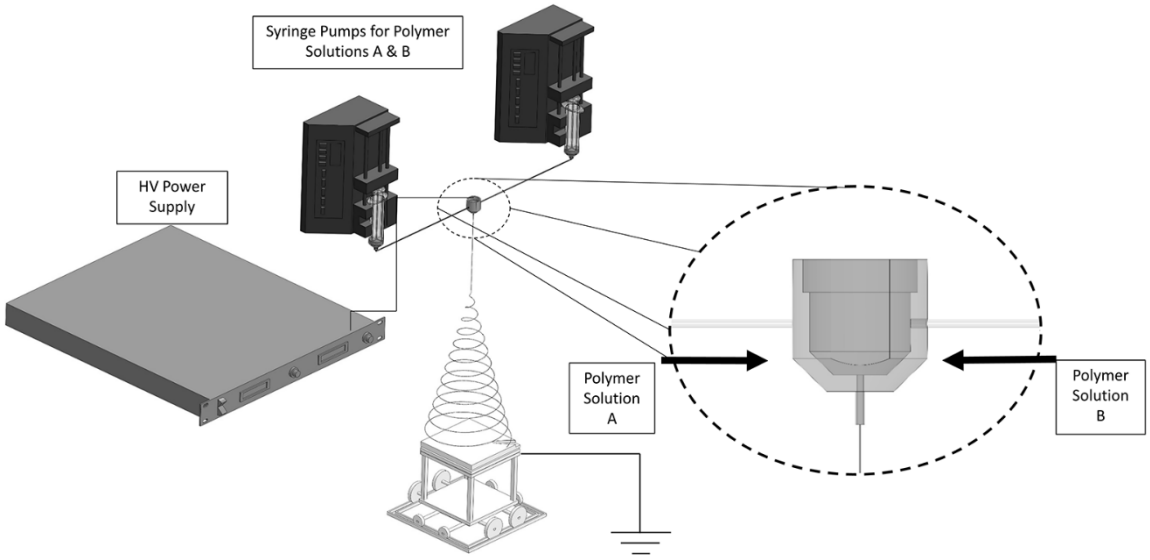

FIGURE 2.5. SINGLE NOZZLE POLYMER BLENDING ELECTROSPINNING SETUP.

A schematic of blend electrospinning where two different polymeric solutions are independently fed into the same reservoir, mix together, and are emitted through a single capillary.

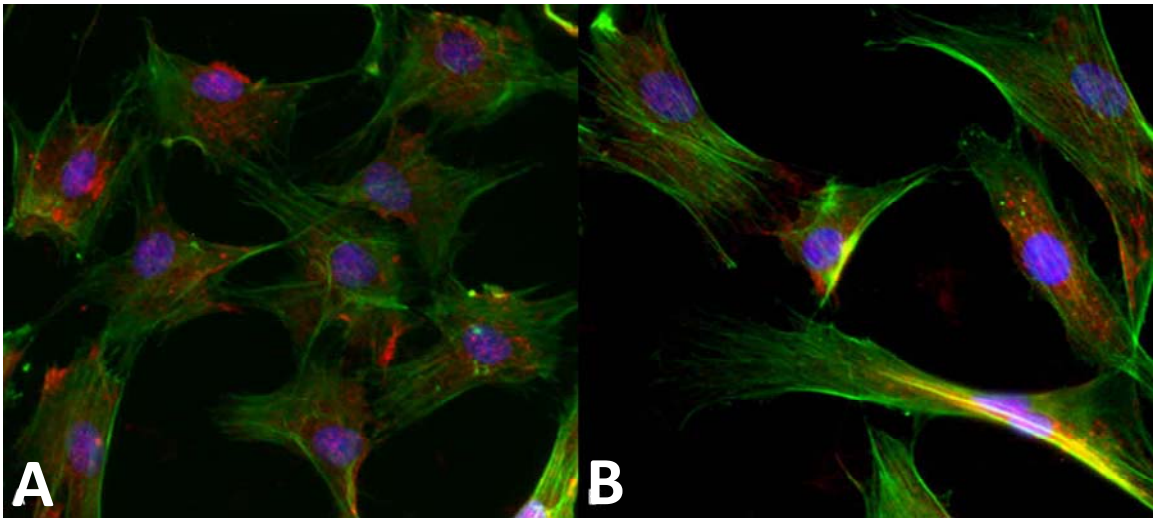

FIGURE 2.6. MESENCHYMAL STEM CELLS (MSCS) CULTURED ON VARIOUS TWO-DIMENSIONAL SUBSTRATES.

Immunofluorecent images of MSCs cultured on (A) nanofibrous poly(ε-caprolactone) scaffolds and (B) tissue culture polystyrene plate showing different cytoskeletal organization (actin and nucleus were stained with Phalloidin and DAPI, respectively).

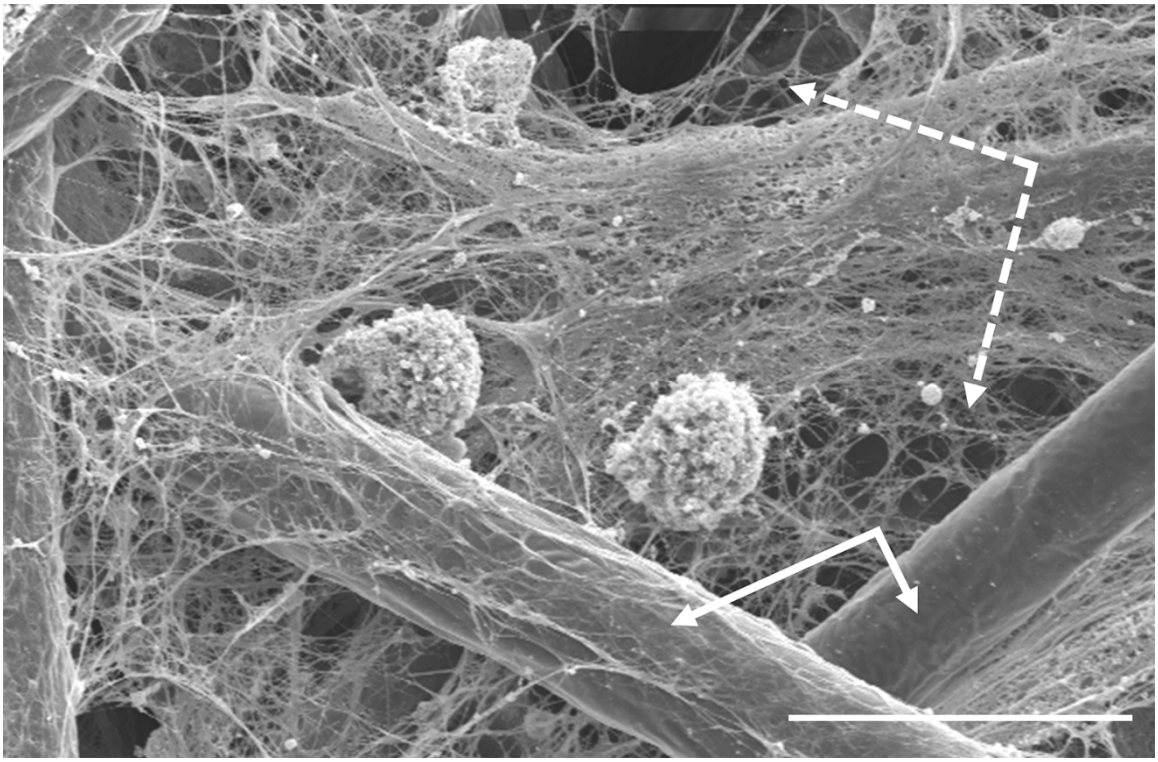

FIGURE 2.7. MICROSTRUCTURE MORPHOLOGY OF CELLS CULTURED IN THREE-DIMENSIONS.

SEM images of articular chondrocytes cultured on microfibrous poly (ε-caprolactone) scaffolds. Dashed arrows indicate cell secreted collagen fibers. Solid arrows indicate poly (ε-caprolactone) microfibers (Scale bar: 20μm).

CHAPTER 3 – MAGNITUDE-DEPENDENT AND INVERSELY-RELATED OSTEOGENIC/CHONDROGENIC DIFFERENTIATION OF HUMAN MESENCHYMAL STEM CELLS UNDER DYNAMIC COMPRESSIVE STRAIN

3.1 – Abstract

Biomechanical forces have been shown to significantly affect tissue development, morphogenesis, pathogenesis and healing, especially in orthopaedic tissues. Such biological processes are critically related to the differentiation of human mesenchymal stem cells (hMSCs). However, the mechanistic details regarding how mechanical forces direct MSC differentiation and subsequent tissue formation are still elusive. Electrospun three-dimensional scaffolds were utilized to culture and subject hMSCs to various magnitudes of dynamic compressive strains at 5, 10, 15, or 20% (ε = 0.05, 0.10, 0.15, 0.20) at a frequency of 1 Hz for 2 hours daily for up to 28 days in osteogenic media. Gene expression of chondrogenic markers (*ACAN, COL2A1, SOX9*) and glycosaminoglycan (GAG) synthesis were upregulated in response to the increased magnitudes of compressive strain, whereas osteogenic markers (*COL1A1, SPARC, RUNX2*) and calcium deposition had noticeable decreases by compressive loading in a magnitude-dependent manner. Dynamic mechanical analysis showed enhanced viscoelastic modulus with respect to the increased dynamic strain peaking at 15%, which coincides with the maximal GAG synthesis. Furthermore, polarization-sensitive optical coherence tomography (PS-OCT) revealed that mechanical loading enhanced the alignment of extracellular matrix to the

greatest level by 15% strain as well. Overall, we show that the degree of differentiation of hMSCs towards osteogenic or chondrogenic lineage is inversely related, and it depends on the magnitude of dynamic compressive strain. These results demonstrate that multi-phenotypic differentiation of hMSCs can be controlled by varying the strain regimens, providing a novel strategy to modulate differentiation specification and tissue morphogenesis.

3.2 – Introduction

Mesenchymal stems cells (MSCs) have shown a great potential as a cell source for the regeneration of diseased or damaged musculoskeletal tissues. They present capabilities to expand to a clinically relevant cell number and differentiate to multiple phenotypes for target tissues [190-192]. Furthermore, the use of autologous MSCs can also leverage their non-immunogenic or even immune-suppressive characteristics for enhanced host-tissue integration [193, 194]. For these reasons, there have been many clinical trials to utilize MSCs for tissue repair, typically by means of cell injection to the site of damage [195-197]. Although some of the trials have shown excellent efficacies, the control of stem cell differentiation into a desired phenotype *in vivo* still presents a great challenge, especially in the mechanically challenging areas like cartilage defects [198, 199]. In this regard, well-defining physiochemical microenvironments of the cells via *in-vitro* cell culture provides an opportunity to precisely control stem cell behaviors such as proliferation, differentiation and subsequent tissue formation.

Both biochemical and biophysical environments modulate cellular behaviors in skeletal tissues. Stimulating skeletal cells with biochemical factors utilizing growth factors and cytokines to initiate various signaling cascades has been the primary choice of directing tissue formation. However, mechanical stimulation has been also shown to be

an essential component to functionalize and mature the tissues, especially in the musculoskeletal system [200-203]. Indeed, a lack of mechanical stimulation during development results in malformation of bone and cartilage, substantiating its critical role in the regulation of skeletal tissue morphogenesis [204, 205]. In many *in-vitro* studies, both osteoblasts, the bone forming cell, and chondrocytes, the primary cell found in cartilage, are mechano-responsive regulating their metabolic activities under dynamic compressive loading [206-208]. Interestingly, we have previously shown that such mechano-responsiveness of osteoblasts and chondrocytes is magnitude-dependent, each having an optimal level of mechanical stimulation that led to the maximal osteogenic and chondrogenic activities [209, 210].

MSCs have also shown to be mechano-responsive as mechanical stimulation affects their phenotype specification. Specifically, dynamic compressive loading has been shown to induce the differentiation of MSCs towards osteoblastic or chondrocytic phenotypes [211-214]. For example, MSCs cultured in partially demineralized bone scaffolds and subjected to mechanical loading exhibited significant increase in alkaline phosphatase and osteopontin transcription levels, demonstrating the osteogenicity of mechanical stimulation [215]. Additionally, compressive loading has been shown to induce cartilaginous matrix formation from MSCs cultured in hyaluronan-gelatin composite scaffolds [216]. However, there's still a lack of comprehensive understanding in the phenotype specification of MSCs under mechanical stimulation as most studies

typically focus on the differentiation towards a single phenotype. Indeed, Grayson et al. has shown that MSCs can simultaneously differentiate to a mixture of cell phenotypes including both osteoblast and chondrocyte [73]. In addition, our previous studies showing the magnitude-dependency of cellular behaviors in skeletal cells under dynamic compressive loading suggest that the application regimen of mechanical stimulation may influence phenotype specification of MSCs [209, 210]. Therefore, it is important to comprehensively understand how biochemical and mechanical cues synergistically or antagonistically influence MSC differentiation and subsequent tissue formation, in order to achieve enhanced skeletal tissue morphogenesis.

In this study, we investigated the effects of mechanical stimulation on MSC differentiation in the presence of biochemical cues. More specifically, human MSCs (hMSCs) were seeded into 3D electrospun scaffolds with appropriate mechanical resiliency for various magnitudes of long-term dynamic compression. The differentiation of hMSCs and subsequent ECM maturation under mechanical stimulation were mechanically, biochemically, and optically characterized in a comprehensive manner to determine phenotype specification of the cells and subsequent tissue morphogenesis. Ultimately, these assessments will provide a clear insight to implement a certain regimen of dynamic mechanical stimulation to promote MSC differentiation towards a desired phenotype and tissue formation.

3.3 – Materials and Methods

All reagents and products were purchased from Sigma–Aldrich (St. Louis, MO) unless otherwise noted.

3.3.1 – Scaffold fabrication

Three-dimensional (3D) scaffolds were synthesized by electrospinning an 11 wt % poly (ε-caprolactone) (PCL) dissolved in 19:1 (v/v) chloroform-methanol solution. A vertical electrospinning setup was used with a tip-to-collector distance of 45 cm as previously described [217]. The polymer solution was dispensed at 11 mL/hr and the applied voltage was adjusted to approximately 16 kV to form a stable Taylor cone [218]. A 6 mm diameter biopsy punch (Integra Miltex, York, PA) was used to produce cylindrical scaffolds from approximately 3 mm-thick as-spun fiber mats. The cylindrical scaffolds were, then, plasma-treated at 30 W for 5 minutes, followed by collagen type I conjugation to improve cellular adhesion using a crosslinking agent, 100 mM N-hydroxysuccinimide (NHS)/N-(3-Dimethylaminopropyl)-N'-ethylcarbodiimide hydrochloride (EDAC) [202]. The scaffolds were sterilized by 70% ethanol for 12 hours followed by air dry. Sterilized scaffolds were stored at 4°C until cell seeding. The microstructure of the electrospun fibers was observed under a scanning electron microscope (SEM, TESCAN, Brno, Czech Republic).

3.3.2 – Cell culture

Human fetal bone marrow-derived mesenchymal stem cells (hMSCs) were purchased from Applied Biological Materials (Richmond, Canada) and were cultured until experimental use between passages 7 and 10. The hMSCs were expanded with growth media (GM) composed of DMEM-F12 (Lonza, Anaheim, CA) supplemented with 15% FBS, 1% Penicillin-Streptomycin, and 100ng/mL bFGF in T75 flasks until they reached approximately 85-90% confluency. The scaffolds placed in a 24 well-plate were seeded with 60 µL of cell-suspended media at a concentration of approximately 33 million cells/mL. The capillary forces of the sterilized and dry 3D scaffolds allowed for complete cellular infiltration throughout the thickness of each scaffold. The cell seeded scaffolds were incubated for 2 hours to induce cell attachment before filling with an additional 1 mL of GM. The cell/scaffold constructs were pre-cultured in GM for 5 days prior to being subjected to differentiation media and/or mechanical stimulation. The GM was exchanged to osteogenic differentiation media (OM) 24 hours prior to the application of mechanical stimulation. The OM was composed of low glucose DMEM supplemented with 10% FBS, 10 mM sodium-β-glycerophosphate, 200 µM ascorbic acid-2-phosphate, 100 nM dexamethasone, and 1% Penicillin-Streptomycin-Fungizone. The OM was exchanged at 50% volume every day, and a full volume exchange was conducted every fifth day. Except the duration of mechanical stimulation, the cell/scaffold constructs were

placed onto an orbital shaker at 200 RPM to ensure complete media exchange throughout the entirety of the experiment.

3.3.3 – Application of dynamic compressive strain and mechanical characterization of cell/scaffold constructs

A custom compression system modified from the previous report was utilized to apply various magnitudes of compressive strain to the cell/scaffold constructs [219]. Briefly, a nominal tare load of 0.02 N was used to ensure the scaffolds were in contact with the impermeable platens. Unconfined compression of the cell/scaffold constructs was conducted daily for 2 hours/day for up to 28 days of stimulation. Mechanical simulation was applied in four separate magnitudes of strain: 5, 10, 15, and 20% (*i.e.*, ε = 0.05, 0.10, 0.15, and 0.20) of the scaffold thicknesses, where statically cultured samples (ε = 0%) serve as a control. During the mechanical stimulation, force responses were recorded from individual samples using load cells in the compression system, used for the calculation of mechanical properties. The elastic and viscoelastic mechanical properties were deconvoluted by analyzing the dynamic responses of the cell/scaffold constructs using the following equation adapted from a study [220].

$$\sigma_0 = \varepsilon_0 G^* \sin(\omega t + \delta) \quad (1),$$

which can be further expanded to

$$\sigma_0 = \varepsilon_0 G' \sin(\omega t) + \varepsilon_0 G'' \cos(\omega t) \quad (2),$$

where σ_0 is the maximum stress, ε_0 is the maximum strain, ω is the compression frequency, δ is the phase delay between the force and displacement curves, G^* is the ratio of maximum stress to maximum strain, G' is the elastic modulus, and G'' is the viscoelastic modulus. Alternatively, control samples (ε = 0%) were cultured and subjected to a brief mechanical testing with ε = 10% at designated time points to assess the mechanical properties (n=6).

3.3.4 – Gene expression analysis

Total RNA from the cell/scaffold constructs cultured for 14 or 28 days was extracted using an RNeasy Mini Kit (Qiagen, Valencia, CA), and cDNA synthesis was performed using iScript cDNA Synthesis Kit (Bio-Rad, Hercules, CA). Negative control samples were collected from cells cultured on tissue culture plastic without exposure to OM, 3D culture in the scaffold, or mechanical stimulation. Real-time PCR was performed to determine osteogenic and chondrogenic gene expression with various differentiation markers using the following custom primers: *GAPDH (forward) 5'-*GCAAATTCCATGGCACCGT-*3' and (reverse) 5'-*TCGCCCCACTTGATTTTGG-*3'; COL1A1 (forward) 5'-*CAACCTGGATGCCATCAAAG-*3' and (reverse) 5'-*TGCTGATGTACCAGTTCTTCTGG-*3'; SPARC (ON) (forward) 5'-*TGGACTCTGAGCTGACCGAATT-*3' and (reverse) 5'-*AGAAGGTTGTTGTCCTCATCCC-*3'; RUNX2 (forward)5'-*GAATGCACTATCCAGCCACCTT-*3' and (reverse) 5'-*

TAGTGAGTGGTGGCGGACATAC-*3'; ACAN (forward) 5'*-GTGATCCTTACCGTAAAGCCCAT-*3'* *and (reverse) 5'*-TCTCATTCTCAACCTCAGCGA-*3'; COL2A1 (forward) 5'*-GGCAATAGCAGGTTCACGTACA-*3' and (reverse) 5'*-CGATAACAGTCTTGCCCCACTT-*3'; SOX9 (forward) 5'*-GAGGAAGTCGGTGAAGAACG-*3'* *and (reverse) 5'*-ATCGAAGGTCTCGATGTTGG-*3'*. PCR data was analyzed by the comparative threshold cycle (C_T) method using *GAPDH* as an endogenous control [221].

3.3.5 – Morphological analysis by histology, scanning electron microscopy and optical coherence tomography

Histology was used to determine the protein expression from either osteogenic or chondrogenic phenotypes via alizarin red or alcian blue staining, respectively as previously described [202]. Briefly, the scaffold sections were incubated in a 0.05% alizarin red or a 0.2% alcian blue solution before rinsing with DI water, mounted and observed under an inverted microscope (Nikon Eclipse, Melville, NY).

To examine cell secreted extracellular matrix (ECM) by scanning electron microscopy (SEM), the cell/scaffold constructs were fixed in 10% formalin overnight, and sectioned horizontal to the height of the sample. The sections were then dehydrated as previously described [182]. Briefly, a sequential dehydration of 50%, 70%, 80%, 95%, and 100% ethanol, followed by 3:1, 1:1, and 1:3 Ethanol:Hexamethyldisilazane (HMDS, Ted

Pella, Inc., Redding, CA) exchange was performed. Upon completion of drying the samples overnight, the sections were sputter-coated with platinum–palladium followed by imaging using an SEM.

The formalin-fixed samples were also imaged using a custom-built multi-functional spectral-domain optical coherence tomography system with a wavelength range centered in the 1300nm range [222]. Depth-resolved profiles of intensity and birefringence, with 512 points spanning 2.0mm, were acquired at a rate of 30Hz. Volumetric data sets composed of 200 frames with 2048 depth profiles each were acquired to span 1.5 x 1.5mm or 4 x 4mm lateral areas. Three-dimensional volumes of OCT intensity and cumulative phase retardation were used for structural imaging and quantification of the optical polarization properties of the samples.

3.3.6 – Statistical analysis

All experiments were conducted with at least 4 samples (n = 4), and data is represented as mean ± standard deviation or standard error of means. Each set of data was subjected to analysis using SPSS (v.19.0) to determine statistical significance by one-way analysis of variance (ANOVA) with Tukey's HSD post-hoc. Alternatively, to correlate scaffold properties and cellular behaviors as a response of mechanical stimulation,

bivariate relationship was determined by Pearson's correlation. A value of $p \leq 0.05$ was regarded as statistically significant.

3.4 – Results

3.4.1 – Scaffold characterization

Mechanically resilient 3D electrospun microfibrous scaffolds were synthesized to investigate the effects of dynamic mechanical stimulation on the phenotype-specific differentiation of hMSCs. The scaffolds were composed of cylindrical fibers providing large pores for facile cellular infiltration upon cell seeding (Figure 3.1A). In addition, the microfiber possesses a porous surface morphology for enhanced cellular adhesion (Figure 3.1B). The average fiber diameter was 10.99 ± 0.42 μm (Figure 3.1C). The 3D scaffolds were cut from electrospun mats to have dimensions of 6 mm in diameter with an approximate thickness of 3 mm (Figure 3.1D).

3.4.2 – Cellular differentiation under static conditions

Human mesenchymal stem cells (hMSCs) were seeded into the scaffolds and statically cultured for up to 28 days in osteogenic media to determine the baseline differentiation behavior of the cells. The degree of differentiation towards osteogenic and

chondrogenic lineages was determined by gene and protein expression (Figure 3.2). The gene expression of osteogenic markers *COL1A1, SPARC (ON) and RUNX2* were all upregulated proportionally to the culture duration in OM over the cells cultured on tissue culture plate (TCP) in GM. These results positively correlate with the osteogenic ECM synthesis as evidenced by the calcium deposition within the cell/scaffold constructs (Figure 3.2D). In contrast, the same static culture conditions did not induce any significant degree of chondrogenesis as expected, evident by statistically insignificant regulation of chondrogenic markers including *ACAN, COL2A1* and *SOX9* (Figure 3.2E-G). The insignificant differentiation of hMSCs in the static conditions was confirmed by a low level of GAG staining, indicating that the cells preferentially differentiated towards the osteogenic lineage.

3.4.3 – Dynamic mechanical analysis of cell/scaffold constructs

After establishing the baseline differentiation behaviors under the static condition, the cell/scaffold constructs were subjected to various magnitudes of dynamic compressive strain to elucidate the effects of mechanical stimulation on phenotype specific differentiation of hMSCs. During the course of 28 days of culture duration, the mechanical properties of the cell/scaffold constructs were simultaneously measured during dynamic mechanical stimulation (Figure 3.3A). The viscoelastic properties of the cell/scaffold constructs were revealed by the phase delay between the applied strain and

the corresponding force under sinusoidal unconfined compression (Figure 3.3B). Given that the compression frequency of the scaffolds was maintained at 1 Hz for the different magnitudes of strain, the resulting strain rates varied depending on the magnitudes. Since the viscoelastic properties of the cell/scaffold constructs is strain rate-dependent, the overall mechanical responses were deconvoluted to elucidate elastic and viscoelastic moduli by using Equation (2) based on the observed phase delay (δ) (Figure 3.3C).

Figure 3.3D and 3.3E show the evolution in the elastic and viscoelastic moduli of the cell/scaffold constructs, respectively, during the culture period of up to 28 days. At Day 0 of culture immediately after cell seeding, the cell/scaffold constructs exhibited an elastic modulus of 30.43 ± 6.90 kPa, and a viscoelastic modulus of 4.09 ± 0.88 kPa (data not shown). There was not significant changes in the elastic modulus in all conditions after 7 days of mechanical stimulation with various magnitudes. The constructs that were not subjected to mechanical stimulation (0%) exhibited greater increases throughout the culture duration as compared to other conditions except the samples that were subjected to higher strain magnitudes (15% and 20%) at the later culture periods. In contrast, the viscoelastic moduli of the constructs that were subjected to dynamic strains greater than 10% exhibited significant increases over the statically cultured constructs. In general, both elastic and viscoelastic moduli increased over the course of culture duration regardless of mechanical stimulation conditions. More importantly, the 15% strain condition induced the greatest increase in viscoelastic modulus as well as elastic modulus at 20.59 ± 4.67

kPa and 145.42 ± 24.64 kPa, respectively, suggesting the most significant ECM deposition over other conditions.

3.4.4 – Magnitude-dependent osteogenic/chondrogenic differentiation of hMSCs under mechanical stimulation

To determine the effects of mechanical stimulation at the transcriptional level that modulated the differentiation of hMSCs, the expression of osteogenic or chondrogenic genes were examined. These genes are known to regulate phenotype-specific ECM deposition, which likely affected the evolution of mechanical properties. As previously noted in Figure 3.2, the static culture condition (ε = 0%) in osteogenic media induced gradual osteogenesis, indicated by increases in all osteogenic markers *COL1A1, SPARC (ON) and RUNX2* over the course of 28 days (Figure 3.4A-C). Interestingly, the application of dynamic compression suppressed many of these osteogenic markers except *RUNX2* which had a significantly greater expression in the 20% strain condition as compared to the statically cultured condition at Day 28.

Unlike osteogenesis, dynamic compressive strains enhanced the chondrogenesis of hMSCs cultured in the 3D scaffolds in general (Figure 3.4D-F). Both *COL2A1* and *SOX9* exhibited upregulation by mechanical stimulation in the most conditions while *ACAN* showed the greatest expression at the 15% strain. As expected, the expression pattern of

chondrogenic genes were closely related to the mechanical properties of the cell/scaffold constructs, especially viscoelastic properties: both showed the maximums when dynamic compressive strain of 15% was applied during the culture.

3.4.5 – Magnitude-dependent ECM deposition/alignment by dynamic mechanical stimulation

In order to assess tissue maturation, ECM deposition was examined by SEM and histology at the culture durations of 14 and 28 days for the cell/scaffold constructs that were either subjected (ε = 5, 10, 15 & 20%) or not subjected (ε = 0%) to dynamic compression (Figure 3.5). The horizontal sections of both the top and the middle were observed to determine the uniformity of cellular growth/ECM secretion. In all cases, the pores within the scaffolds were densely populated by cell-secreted ECMs as early as the culture duration of 14 days. These ECMs were further specified by histological examination with osteogenic and chondrogenic-specific stains, *i.e.*, alizarin red for calcium deposition and alcian blue for GAG, respectively. For alizarin red staining, the static culture condition showed the greatest calcium deposition, which gradually decreased with increasing the magnitude of dynamic compressive strain for both 14 and 28 days of culture. In contrast, GAG deposition determined by alcian blue staining was gradually enhanced with the increased magnitude of dynamic compression, peaking at 15% strain, followed by a slight decrease at 20% strain.

The morphological changes of the cell/scaffold constructs after 28 days of culture under various magnitudes of dynamic compression were further examined by OCT (Figure 3.6). Differences between the samples can be seen in 3D reconstructed volumes of the samples (Figure 3.6A, Supplementary Data). The cylindrical structure of the fibers that is very clearly evident in the absence of cells becomes obscured in the sample seeded with cells under no compression, and becomes visible under compression. Interestingly, polarization-sensitive OCT (PS-OCT) reveals more quantifiable differences between the samples that relate to their differences in ECM organization (Figure 3.6B). Quantitative analysis of the cumulative phase retardation as a function of depth was done for cell/scaffold constructs of all conditions as compared to acellular scaffolds. PS-OCT detects from birefringence, which is proportional to the density and organization of fibrous structures and can be quantified through determination of the rate at which the cumulative phase retardation between orthogonal polarization states changes with depth in a sample. The alignment of deposited ECM, characterized by the initial offset and the slope of depth-dependent phase retardation, was closely related to the magnitude of applied strains during culture; 0% exhibited the most random ECM orientation, evident by a uniform low phase retardation before an increase due to signal weakening. In contrast, the cell/scaffold constructs subjected to dynamic compression during culture exhibited greater intensities and rapid increases in phase retardation, suggesting alignment of ECMs as compared to the statically cultured constructs. Among the dynamic

culture conditions, 15% strain induced the greatest alignment of the ECM, coinciding with the observed greatest elastic and viscoelastic moduli.

3.5 – Discussion

Biomechanical factors continuously modulate tissue morphogenesis throughout development, especially in the musculoskeletal system. It has been shown that limited mechanical loading (*e.g.*, immobilization or disuse) during development prevents or retards musculoskeletal tissue morphogenesis [204], suggesting the critical role of mechanical stimulation in tissue specification including stem cell differentiation and maturation. In this regard, many studies have utilized dynamic mechanical stimulation in a variety of forms such as compression, tension and shear, as a biological cue to enhance tissue morphogenesis for bone and cartilage from MSCs [213, 223-225]. Although those exploratory studies clearly demonstrated the anabolic effects of mechanical stimulation, they were often limited to feasibility studies, lacking a comprehensive understanding in the effects of dynamic mechanical stimulation on MSC differentiation and subsequent tissue morphogenesis. With the end goal of producing physiologically relevant tissue constructs which can ultimately be used as *in-vitro* tissue models or replacements for diseased or damaged skeletal tissues, we present here the fundamental aspects of mechano-modulation in hMSC differentiation and maturation. Specifically, our systematic

approach revealed the magnitude-dependent and inversely related osteogenesis and chondrogenesis of hMSCs under dynamic compressive strain.

Both biochemical and biophysical factors modulate stem cell differentiation [226]. When hMSCs were seeded into the scaffold and subjected to osteogenic media, they preferentially differentiated towards osteoblasts as expected. Interestingly, when the cell/scaffold constructs were subjected to dynamic compression in the same osteogenic media, however, the cells concurrently differentiated towards both osteoblasts and chondrocytes. This strongly suggests the critical role of biomechanical factors determining cellular fate, even overcoming local biochemical environments. More significantly, such mechano-responsiveness is magnitude- and phenotype-specific. The cells not subjected to mechanical loading exhibited mostly osteoblastic traits, whereas those exposed to dynamic compression decreased the degree of osteogenic differentiation, inversely proportional to the magnitude of strain applied. This cellular response conflicts with the previous report, where the dynamic compression enhanced the anabolic activities of mature osteoblasts [209], likely demonstrating phenotype-specific actions of mechanical stimulation. Conversely, the degree of chondrogenic differentiation was positively correlated to the magnitude of dynamic compression, peaking at 15% strain. Interestingly, there was a decrease in the chondrogenic expression for gene and protein expression, as well as mechanical properties, in the 20% applied strain condition. In addition, the upregulation of *RUNX2* at the later stage of

differentiation independent of other osteogenic markers may indicate inflammation-induced hypertrophy of chondrocytes [227]. These results suggest that over-stimulation of the cell/scaffold constructs beyond a specific threshold may actually be detrimental to mature tissue development.

In addition to phenotype specification of hMSCs, mechanical stimulation strongly affected ECM production and organization. Evident from histological imaging, the magnitude of dynamic compressive strain differentially regulated phenotype-specific ECM production. Greater amount of mineral deposition at lower magnitudes was observed while higher magnitudes enhanced GAG production. This observation is well aligned with the mechanical characterization of the cell/scaffold constructs, where viscoelastic modulus was clearly correlated to the amount of GAG production. In addition to ECM production, mechanical stimulation also modulated the organization of ECM. PS-OCT was utilized, for the first time in engineered tissues at the best of our knowledge, to determine dynamic strain magnitude-dependent ECM alignment. Indeed, the cell/scaffold constructs subjected to 15% strain showed the greatest ECM alignment, demonstrating the capability of mechanical stimulation to organize ECMs as often observed *in vivo* in cartilage and bone [228]. The direction of the alignment with respect to the depth of the cell/scaffold constructs was not investigated in this study. Nevertheless, these results suggests a great potential of dynamic compressive loading to mimic the organized structure of cartilage ECMs.

The comprehensive analysis of the biochemical and mechanical properties of the dynamically cultured scaffolds provides insight into how various magnitudes of strain differentially influence musculoskeletal tissue development. Our results indicate that stem cell differentiation is dynamic strain magnitude-dependent in the presence of a biochemical cue. These results provide a greater understanding in how mechanical cues may override the directed biochemical cues to provide a foundation for tissue engineering. This also may address the challenges to form neo-tissue composed of multi-cell types, regulated by both the local biochemical traits and the mechanical factors. Our study therefore suggests a new outlook on directing MSC differentiation towards musculoskeletal tissues by utilizing synergistic effects of biochemical and magnitude-dependent mechanical cues.

3.6 – Conclusions

Mechanical stimulation provides a facile means to direct stem cell differentiation in lieu of biochemical cues. In this study, we demonstrated that MSCs differentiate in a magnitude-dependent and phenotype-specific manner in response to different magnitudes of applied dynamic compressive strain. Ultimately, these results suggest that MSCs are mechano-responsive and their multi-phenotypic differentiation can be controlled by varying the strain regimens. The results, therefore, provide a novel strategy

to modulate phenotype-specific MSC differentiation and subsequent tissue morphogenesis.

3.7 – Figures

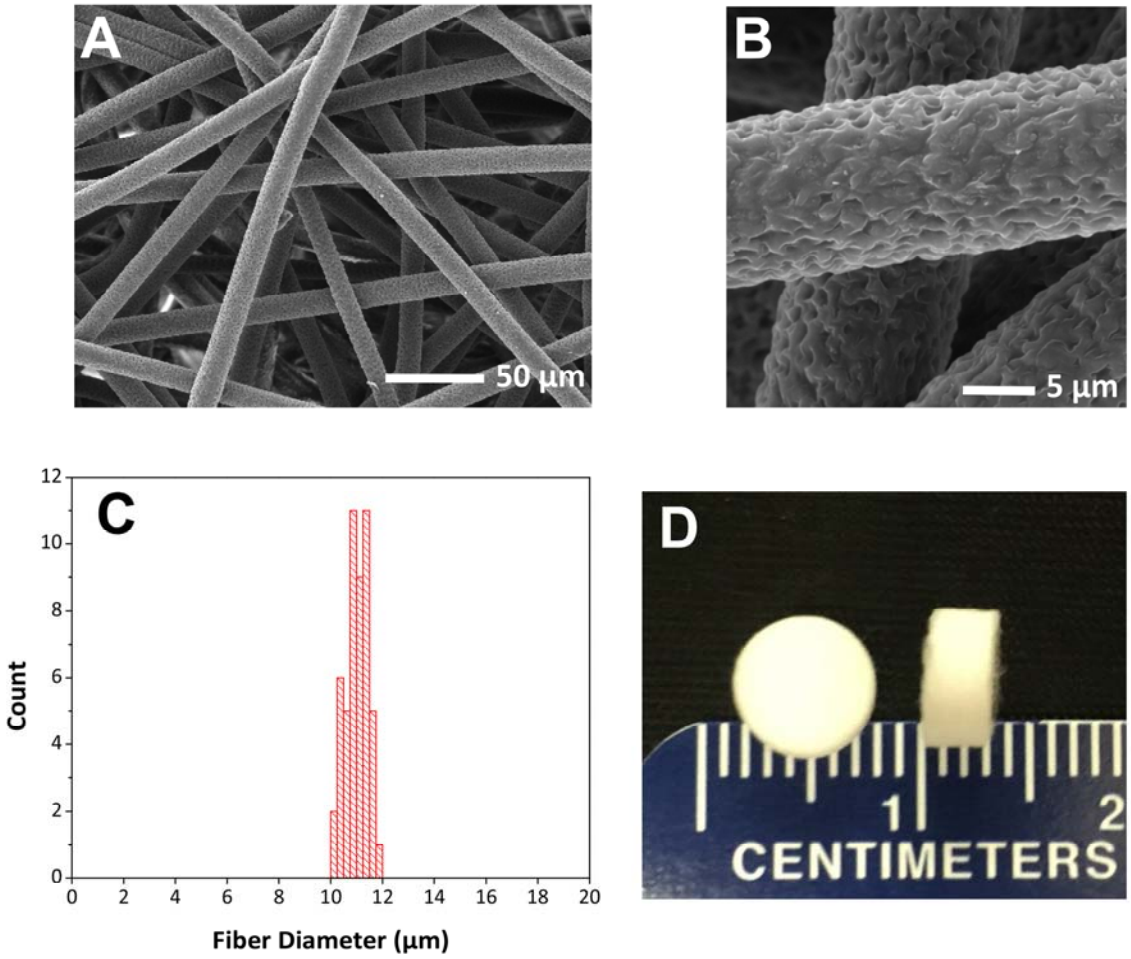

FIGURE 3.1. MORPHOLOGICAL CHARACTERIZATION OF ELECTROSPUN SCAFFOLDS.

Representative SEM images showing (A) the microstructure of the fibrous network of fibers having (B) the porous surface morphology and (C) a relatively uniform fiber size distribution. (D) A representative optical image showing the gross morphology and shape of the scaffolds for cell culture.

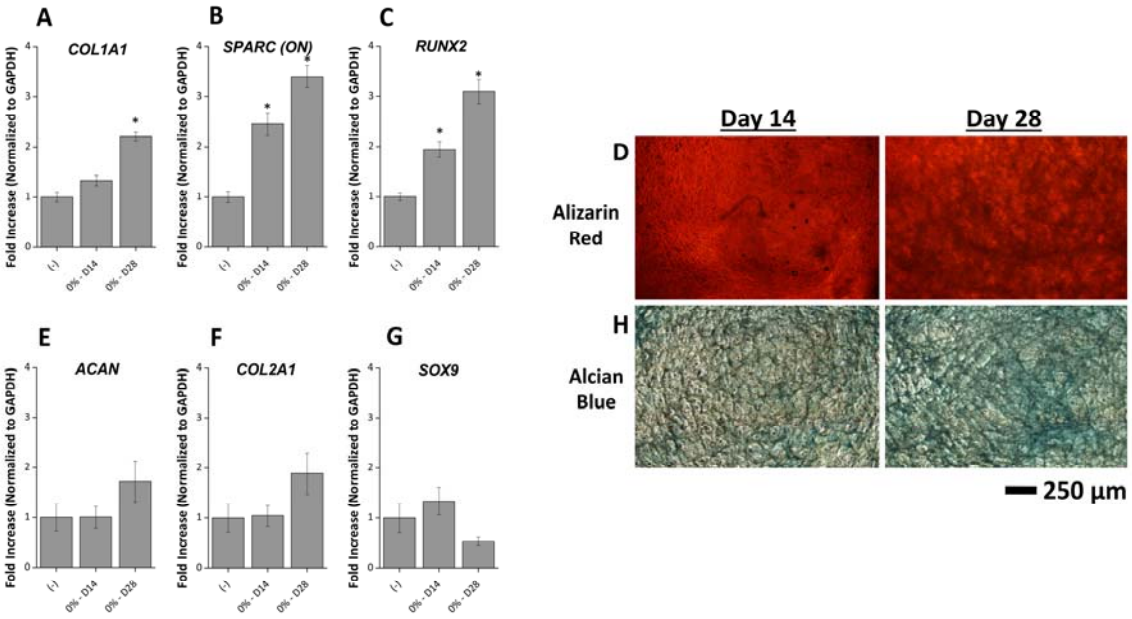

FIGURE 3.2. THE OSTEOGENIC OR CHONDROGENIC DIFFERENTIATION OF HMSCS CULTURED IN 3D ELECTROSPUN SCAFFOLDS FOR VARIOUS DURATIONS.

(A-C) Greater osteogenic gene expression (*COL1A1, SPARC (ON),* and *RUNX2*) and (D) ECM deposition (calcium by alizarin red) as compared to (E-G) chondrogenic gene expression (*ACAN, COL2A2,* and *SOX9*) and (H) ECM deposition (glycosaminoglycan by alcian blue) indicate preferential differentiation of hMSCs towards osteogenic lineage under static culture conditions.

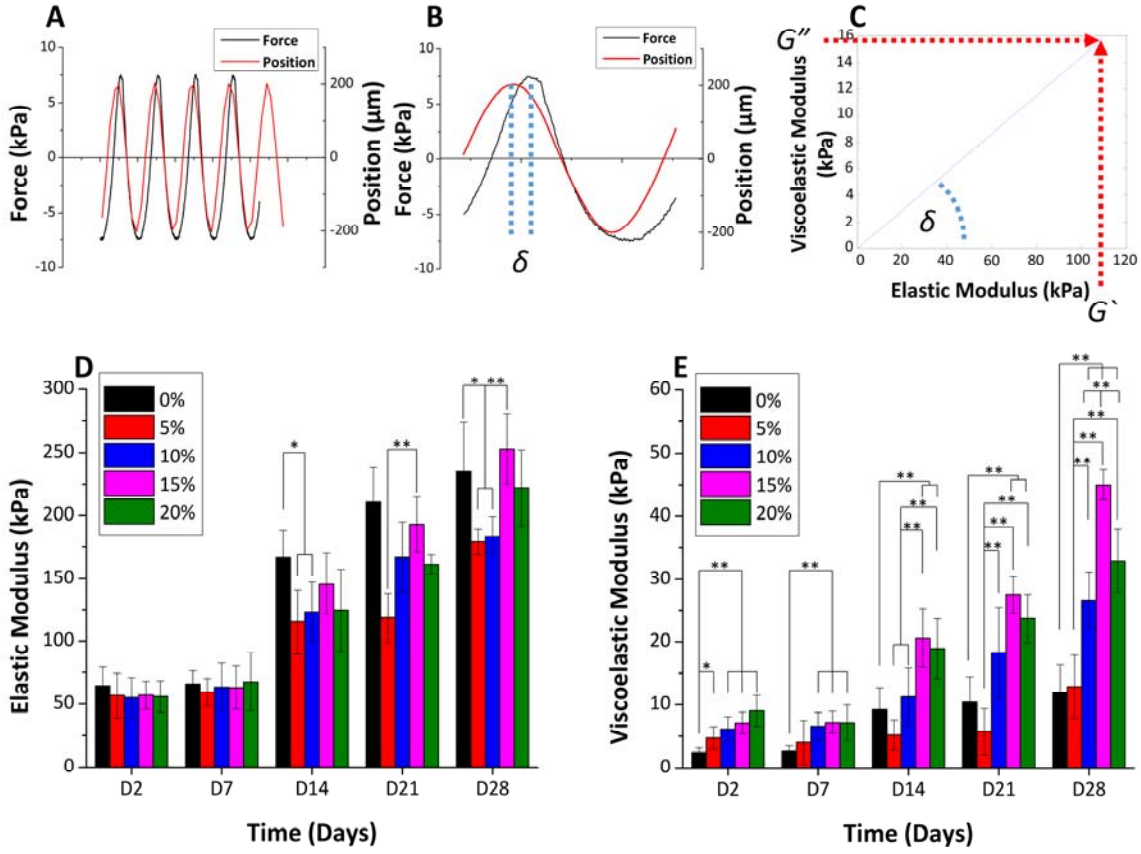

FIGURE 3.3. DYNAMIC MECHANICAL ANALYSIS OF CELL/SCAFFOLD CONSTRUCTS CULTURED UNDER DAILY MECHANICAL STIMULATION WITH VARIOUS DYNAMIC COMPRESSIVE MAGNITUDES AND CULTURE DURATIONS.

(A) A representative force and position curves acquired from a cell/scaffold construct under sinusoidal dynamic compression, and (B) a detailed force-position curves showing a phase delay (δ) between the applied strain and the responding force, which was used to deconvolute (C) the of elastic (G') and viscoelastic (G") moduli. (D) Deconvoluted elastic and (E) viscoelastic mechanical properties of the cell/scaffold constructs cultured under different magnitudes (5, 10, 15 and 20% strain) of dynamic compression analyzed at different time points up to 28 days. * and ** denote $p < 0.05$ and $p < 0.01$, respectively (n=6).

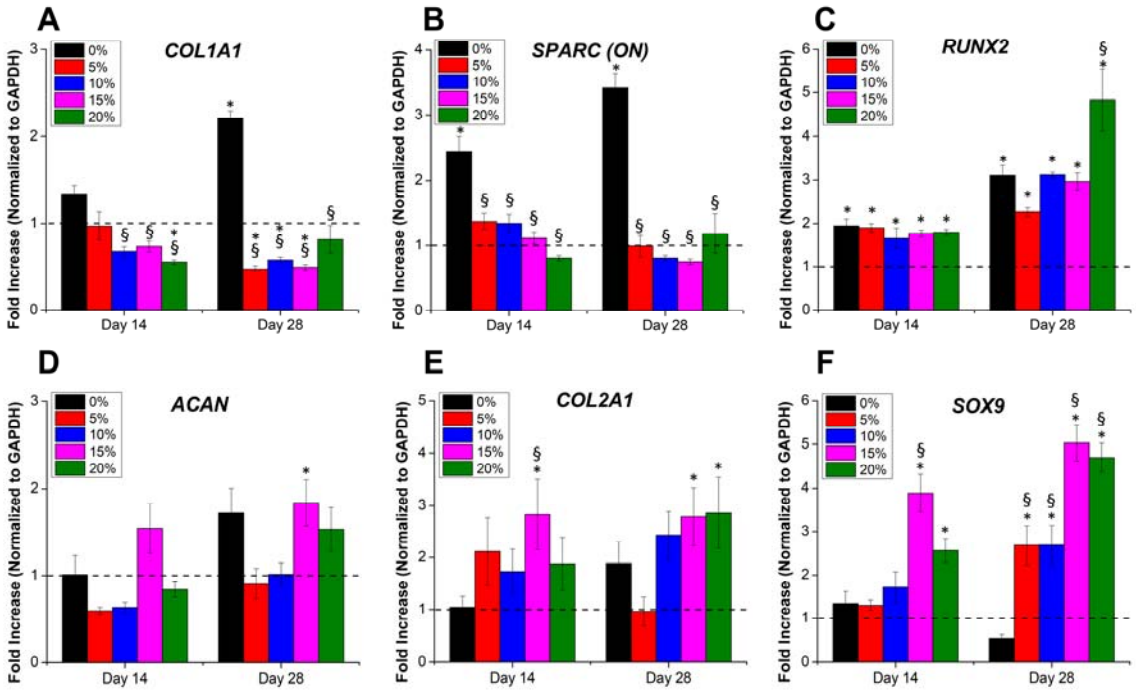

FIGURE 3.4. THE OSTEOGENIC OR CHONDROGENIC DIFFERENTIATION OF HMSCS BY SDURATIONS.

The relative gene expression of hMSCs dynamically cultured in electrospun scaffolds for up to 28 days determined by qRT-PCR for (A-C) osteogenic markers, *COL1A1, SPARC (ON) and RUNX2*, and (D-F) chondrogenic markers *ACAN, COL2A1* and *SOX9*. Each gene expression was normalized to that of the cells before being cultured in the scaffold (dashed lines). * and ** denote $p < 0.05$ and $p < 0.01$, respectively, as compared to the negative control samples (represented as dashed lines); § and §§ denote $p < 0.05$ and 0.01, respectively, as compared statically culture samples (0%).

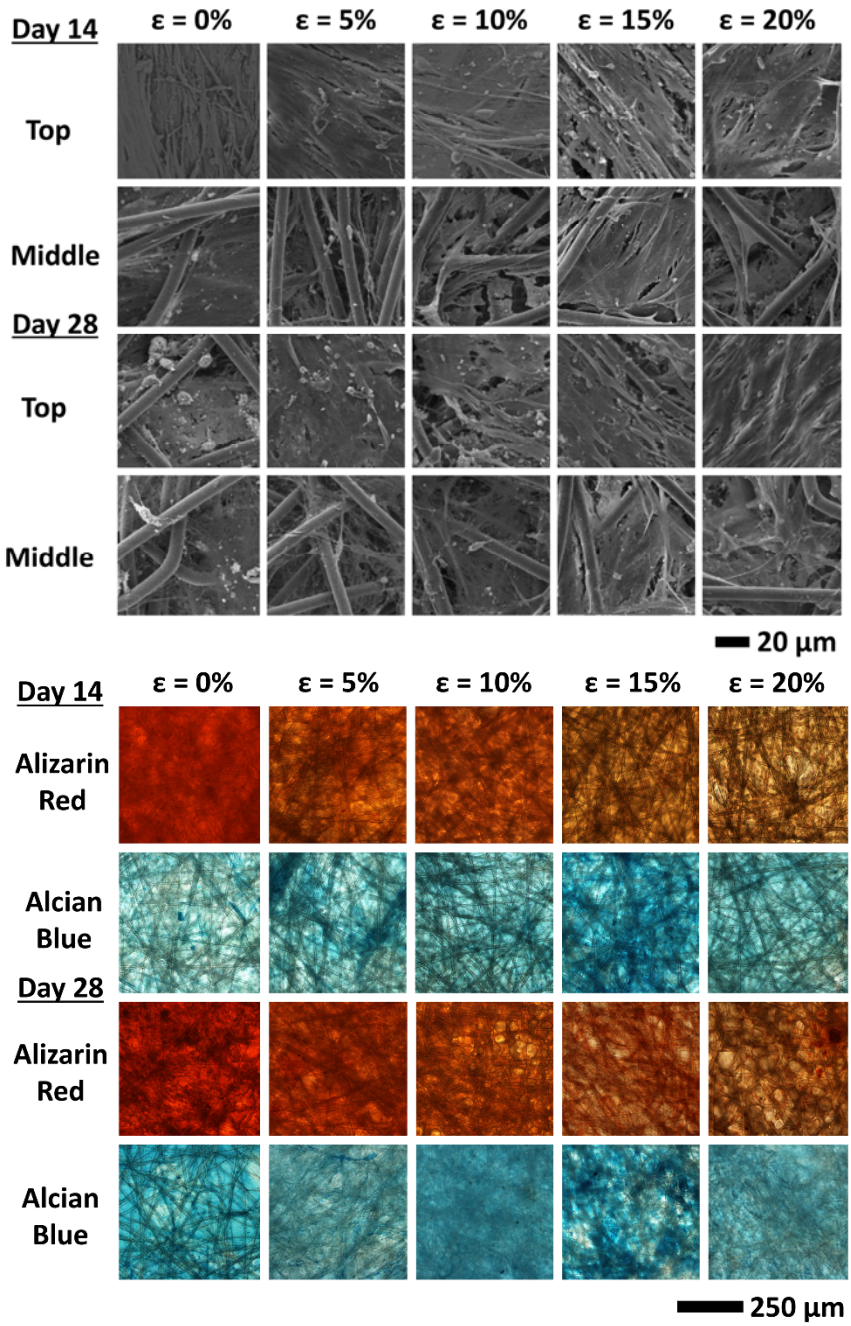

FIGURE 3.5. REPRESENTATIVE SEM AND HISTOLOGY IMAGES OF CELL/SCAFFOLD CONSTRUCTS CULTURED UNDER VARIOUS CONDITIONS EXHIBITING DIFFERENT ECM COMPOSITIONS FROM HMSCS.

The cell/scaffold constructs cultured under different dynamic compressive stimulation (0, 5, 10, 15 and 20% strain) for 14 or 28 days were subjected to SEM or histology imaging

(alizarin red for calcium and alcian blue for glycosaminoglycan) to assess overall ECM deposition.

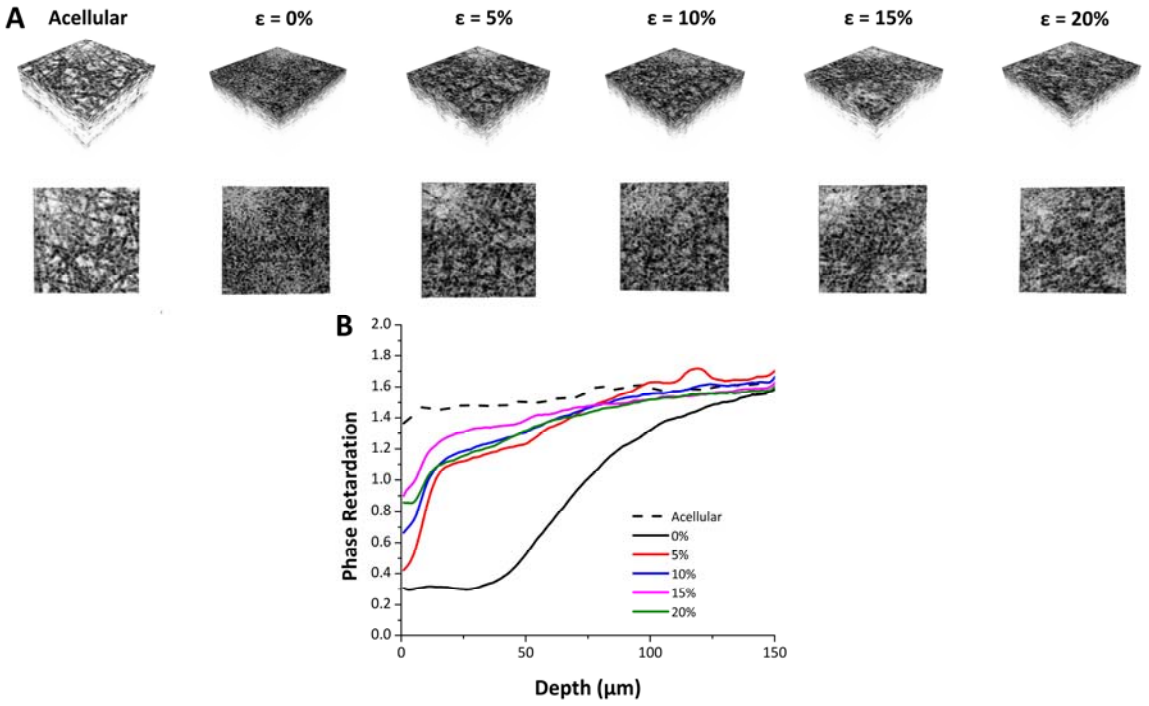

FIGURE 3.6. OPTICAL COHERENCE TOMOGRAPHY (OCT) OF ACELLULAR AND CELLULAR SCAFFOLDS CULTURED WITH OR WITHOUT DYNAMIC COMPRESSION.

OCT intensity images of (A) acellular scaffold, cell/scaffold constructs cultured (B) without or (C) with dynamic compression, and (D-F) corresponding graphs of double-pass cumulative birefringence from polarization-sensitive OCT analysis.

CHAPTER 4 – MICROSTRUCTURE-DEPENDENT MECHANICAL PROPERTIES OF ELECTROSPUN CORE-SHELL SCAFFOLDS AT MULTI-SCALE LEVELS

4.1 – Abstract

Mechanical factors among many physiochemical properties of scaffolds for stem cell-based tissue engineering significantly affect tissue morphogenesis by controlling stem cell behaviors including proliferation and phenotype-specific differentiation. Core-shell electrospinning provides a unique opportunity to control mechanical properties of scaffolds independent of surface chemistry, rendering a greater freedom to tailor design for specific applications. In this study, we synthesized electrospun core-shell scaffolds having different core composition and/or core-to-shell dimensional ratios. Two independent biocompatible polymer systems, polyetherketoneketone (PEKK) and gelatin as the core materials while maintaining the shell polymer with polycaprolactone (PCL), were utilized. The mechanics of such scaffolds was analyzed at the microscale and macroscales to determine the potential implications it may hold for cell-material and tissue-material interactions. The mechanical properties of individual core-shell fibers were controlled by core-shell composition and structure. The individual fiber modulus correlated with the increase in percent core size ranging from 0.55 ± 0.10 GPa to 1.74 ± 0.22 GPa and 0.48 ± 0.12 GPa to 1.53 ± 0.12 GPa for the PEKK-PCL and gelatin-PCL fibers, respectively. More importantly, it was demonstrated that mechanical properties of the

scaffolds at the macroscale were dominantly determined by porosity under compression. The increase in the compressive elastic modulus corresponded to the decrease of scaffold porosity ranging from 14.55± 1.43 kPa to 227.67 ± 20.39 kPa for the PEKK-PCL scaffolds and 17.57± 1.40 kPa to 484.01 ± 30.18 kPa for the gelatin-PCL scaffolds. and partly in tension rather than by individual core-shell fiber mechanics The biphasic profiles from tensile mechanical loading results from both the individual fiber modulus and scaffold porosity ranging from a low of 5.42 ± 1.05 MPa to a high of 12.00 ± 1.96 MPa for the PEKK-PCL scaffolds, and 10.19 ± 4.49 MPa to 22.60 ± 2.44 MPa for the gelatin-PCL scaffolds. These results suggest a feasible approach for precisely controlling the local and global mechanical characteristics, in addition to independent control over surface chemistry, to achieve a desired tissue morphogenesis using the core-shell electrospinning.

This chapter has been reproduced from *Horner C.B., et al. 2016, Microstructure-dependent mechanical properties of electrospun core-shell scaffolds at multi-scale levels, *Journal of the mechanical behavior of biomedical materials*, **59**: 207-219., with permission from Journal of the Mechanical Behavior of Biomedical Materials.

*Adapted from manuscript: Figures: 4.1–4.11 and Tables: 4.1–4.3

4.2 – Introduction

Tissue engineering approaches provide a viable method for the replacement or regeneration of damaged/diseased tissues. Tissue scaffolds need to be specifically designed for target tissues in order to modulate cells to elicit appropriate phenotypic behaviors and subsequent tissue morphogenesis [229, 230]. When designing and engineering such tissue replacements, it is critical to address various requirements to meet the biochemical and physical traits of the native tissues. Thus, an in-depth understanding of the interaction between the cells and the physiochemical properties of the scaffolds is essential for enhancing efficacy of the implanted tissue for successful therapeutic tissue regeneration [231-234]. This fundamental understanding is especially important when stem cells are considered as a cell source for the regeneration of tissues. The behaviors (*i.e.*, proliferation and differentiation) of stem cells such as induced pluripotent stem cells (iPSC), adipose-derived stem cells (ASC), and mesenchymal stem cells (MSC), have shown to be controlled by their microenvironments or 'cell niche' [235-237]. In addition to soluble factors, physical environmental factors significantly affect stem cell behaviors. Specifically, mechanical properties of scaffolds have shown to direct stem cell differentiation via their intrinsic characteristics in static environments (*e.g.*, stiffness) [238, 239] independently of surface chemistry. This is in comparison to the scaffold compliance to extrinsic mechanical forces in dynamic culture environments, which have also been shown to modulate stem cell behavior [240] A more comprehensive

overview for the wide array of uses for these scaffolds can be gained by investigating compositions of varying core-shell dimensional ratios and polymer systems.

The mechanical characteristics of the scaffold influence the differentiation of progenitor cells towards desired phenotypic tissue possibly via modulating the attachment and spreading of the cells that regulate cell morphology. Several studies have shown that control of stem cell morphology via substrate stiffness determines subsequent stem cell differentiation, suggesting the mechanical properties as an important design criterion for scaffolds [235-237, 241, 242]. In addition to the 'intrinsic' mechanical properties of scaffolds, their performance under extrinsic mechanical stimuli, *i.e.*, forces generated by bodily movement *in vivo* or 'mechanical training' of engineered tissues *in vitro*, is just as influential for directing stem cell differentiation. For example, dynamic compressive or tensile loading to stem cell/scaffold constructs that mimics the native mechanical environments has shown to induce phenotype-specific differentiation of stem cells, *e.g.* compressive and tensile forces for chondrogenesis and tendonogenesis, respectively [243-246]. Such *in-vivo*-like extrinsic mechanical stimulation to the cells within scaffolds is likely determined by the bulk or macroscale mechanical properties of the scaffolds. Not only the mechanical loading direct stem cell differentiation, but it is also essential for maintaining tissue-specific phenotypes of the differentiated cells to support tissue maturation [246-248]. Therefore, tissue engineers must simultaneously take into account the macroscale mechanical characteristics of scaffolds for controlled

tissue morphogenesis as well as the microscale level properties that control cellular behaviors through modulating the localized cell-material interactions.

With this in mind, electrospinning presents a cost-effective and versatile technique for fabricating nano-/micro-structures possessing a high surface area-to-volume ratio, suitable for tissue engineering scaffolds. It also provides precise control over the physical and biological properties via control over various electrospinning parameters including solution properties (natural or synthetic polymer/solvent concentration, viscosity, conductivity) and processing parameters (solution flow rate, applied electric field, collection distance) [249]. The fibrous scaffolds that resemble the morphology of native extracellular matrix (ECM) have shown to be capable of addressing a vast array of potential bioengineering applications [240, 244, 246, 250, 251]. Recently, we have shown that the stiffness of electrospun scaffolds modulates self-renewal of iPSCs [242] and differentiation of MSCs [239]. In addition, we have also shown that electrospun scaffolds provide an appropriate platform to actuate scaffold-seeded cells with physiological mechanical stimulation, resulting in enhanced tissue morphogenesis [186].

In this regard, core-shell (also referred to as coaxial or core-sheath) electrospinning further allows for tight control over the physiochemical properties of the scaffolds. The method utilizes concentric needles to encapsulate one material within another in the form of monolithic fibrous structure. Advantages of the core-shell

structure include the capability of embedding growth factors or drugs [252, 253], or more relevantly in this study, the modulation of the intrinsic mechanical properties while maintaining the homogenous surface chemistry of the shell [250, 254]. Utilizing an identical shell material with varied core size/material composition enables decoupling of the mechanical factors from the surface chemistry of the scaffolds. This provides a means in maintaining a uniform exterior to which cells will directly interact with can solely impart mechanical cues independently of the surface chemistry the cells experience [255, 256]. More importantly, individual electrospun fiber mechanics can be controlled independently from the macroscale scaffold mechanics, presenting further engineering control over the physiochemical properties for various *in vitro* and *in vivo* applications.

The objective of this study is to understand the relationship between the microscale (*i.e.* individual fibers) and macroscale (*i.e.* bulk fibrous scaffolds) mechanical properties of electrospun core-shell scaffolds. The influence of polymer materials and dimensions of the core-shell structures on the mechanical characteristics of these scaffolds were evaluated. Ultimately, we demonstrate a methodology to control the intrinsic individual fiber mechanics independent of the bulk scaffold properties, which is useful to develop scaffolds having tissue-specific mechanical properties required for tissue engineering applications.

4.3 – Materials and Methods

4.3.1 – Scaffold fabrication

All reagents and materials were purchased from Sigma-Aldrich (St. Louis, MO) unless otherwise noted. Core-shell composite scaffolds of poly(etherketoneketone) (PEKK, core)-poly(ε-caprolactone) (PCL, shell) or gelatin (core)-PCL (shell) were synthesized by coaxial electrospinning as described previously [239]. Briefly, the shell polymer solution was prepared by dissolving 11 wt. % of PCL (*Mw* = 80,000) in 1,1,1,3,3,3-hexafluoro-2-propanol (HFIP, Oakwood Products, Inc., West Columbia, SC). For the core polymer solutions, gelatin (type A, from porcine skin in powder form) or PEKK (OXPEKK-IG100, Oxford Performance Materials, South Windsor, CT) were dissolved in HFIP at a concentration of 10 wt.%. A custom dual concentric nozzle 16G (OD: 1.65 mm, ID: 1.26 mm) - 22G (OD: 0.70 mm, ID: 0.41 mm) was utilized to synthesize the core-shell electrospun fibers (Figure 4.1A). Programmable syringe pumps (NE-1010, New Era Pump Systems Inc., Farmingdale, NY) were used in tandem to independently feed the core and shell polymeric solutions (Figure 4.1B). An electrical field ranging from 500-600 kV/m was applied to polymer solutions using a high voltage D.C. power supply (Model: FC60R2, Glassman High Voltage, Inc., High Bridge, NJ) to achieve a stable Taylor Cone. Non-woven electrospun fibrous mats were collected on a grounded 3” x 3” aluminum plate. A total of ten different conditions were utilized to synthesize scaffolds with the two previously

mentioned core (PEKK or gelatin)-shell (PCL) compositions having different core sizes; each electrospun core-shell fiber composition was fabricated by reciprocally varying the ratio between the core flow rate and the shell flow rate while maintaining the overall flow rate at 11 mL/hr at the following core-shell (C-S) ratios: 1:10, 2:9, 3:8, 4:7, and 5:6. These conditions have a percent core flow rates defined as 9%, 18%, 27%, 36%, and 45%, respectively.

4.3.2 – Morphological characterization of electrospun fibers

The morphology of the electrospun core-shell fibers was characterized using a scanning electron microscope (SEM, Phillips/FEI XL30-FEG, Hitachi, Japan). The average fiber diameter was determined from the measurements of at least 50 fibers per condition using ImageJ software. To observe the cross-section of the core-shell fibers for core-to-shell dimensional measurements, cryogenic fracturing was performed by submerging the fiber mat into liquid nitrogen. The cryo-fractured cross-sections were then characterized by SEM to assess the core and overall fiber diameters. Additionally, samples were submerged in PBS for one month to determine the stability of the scaffolds in an aqueous solution. SEM images were taken for the 9% and 45% core flow rate fibers both before and after submersion.

A liquid displacement method was used to determine the pore volume of the bulk scaffolds as described elsewhere [257]. Briefly, a 6 mm diameter biopsy punch (Integra Miltex, York, PA) was used to make cylindrical samples from the as-spun fiber mats. Thicknesses of punched cylinders were measured with digital calipers with a ±0.01 mm precision. Each sample was weighed out, submerged into ethanol, and placed under vacuum to allow complete ethanol penetration into the scaffolds. Residual ethanol on the surface of the cylinders was removed, then reweighed to obtain the mass and subsequent volume of ethanol contained within the interconnected porous network of fibers (n=6).

4.3.3 – Mechanical characterization of electrospun fibers/scaffolds

Individual core-shell electrospun fibers were collected on square copper grids with a 100 µm gap distance (Figure 4.2). The mechanical properties of the individual fibers were then tested by three point bending using an MFP-3D atomic force microscopy (AFM) system (Asylum Research, Santa Barbara, CA) [258, 259]. A silicon tetrahedral cantilever (AC240TS, Olympus, Japan) with a nominal spring constant of approximately at 2 N/m was used to deflect the mid-point of the fibers to a pre-determined trigger force of 20 nN. The indentation/retraction speed was 2 µm/s. The force-displacement curves were utilized to determine the elastic modulus of the core-shell fibers. All conditions were tested with at least 7 independent samples (n=7).

To measure the macroscale compressive properties of the scaffolds, a custom compression device was utilized as previously described (Figure 4.3) [186]. Briefly, a static impermeable platen with the dimensions of 9.5 mm in diameter was attached to a 1 kg load cell (Model 11, Honeywell Sensing and Control, Columbus, OH). A submicron linear translational stage (AVL-125, Aerotech, Pittsburgh, PA) was used to incrementally deliver a compressive strain along the fiber deposition direction (Figure 4.1C). A tare load of 0.02 N was used to ensure that scaffolds were in contact with the impermeable platen. The samples were then compressed at 5% strain increments of the scaffold thickness where the load was held for 90 s until achieving a total of 20% applied strain per sample [260]. The modulus was then calculated from a linear range of the stress-strain curve. All conditions were tested with at least 6 samples per condition (n=6).

In addition, tensile dog bones of the electrospun fiber mats were cut to have the dimensions of an overall length of 40 mm, and a sample gauge width of 20 mm, where the length of the grip section was 10 mm. The gauge length for the reduced section was 15 mm, and the width was 4 mm. The fillet radius shoulders were cut using a 6 mm biopsy punch to create a 3 mm radii to ensure a smooth transition from the grip section to the reduced section. Tensile testing parallel to the direction of the fiber deposition layer (Figure 4.1D) was carried out using a load frame (model 1322, Instron, Norwood, MA) equipped with a 1 kg load cell. A cross-head speed of 5 mm/min was utilized until

complete sample failure. All conditions were tested with at least 5 samples per condition (n=5).

4.3.4 – Theories of Mathematical Relationship between Mechanical Properties and Morphology

The mathematical relationship between the microscale/macroscale mechanical properties and morphology of the fibrous structures was investigated using mechanical analysis. First, the relationship between the Young's modulus of individual core-shell fibers and its geometry was explained by the rule of mixtures in Eqn. (1)

$$E_f = fE_c + (1-f)E_s \quad (1),$$

$$f = \frac{V_c}{V_s} = \frac{\pi \cdot {r_c}^2 \cdot l}{\pi \cdot {r_s}^2 \cdot l} = \left(\frac{r_c}{r_s}\right)^2 \quad (2),$$

where V_c, V_s, r_c, r_s, and l represent volume of the core, volume of the shell, radius of the core, radius of the shell, and the length of the fiber, respectively. Here, a geometric parameter f was introduced to represent the cross-sectional volumetric fraction of the core, which was experimentally determined. Young's moduli of materials that comprises the core or shell are 0.345 GPa, 3.45 GPa, and 2.5 GPa for PCL, PEKK, and gelatin, respectively [261-263].

Secondly, the relationship between the bulk compressive modulus and scaffold porosity was determined by Eqn. (3) [264, 265]:

$$E = C(100 - P)^n \quad (3),$$

where *C* is a material-specific constant, *n* is a structural constant, and *P* is the porosity of the electrospun fiber mat. For materials which possess a relatively high porosity (*P* > 50%), a structural constant of *n* = 2 can be used. Experimentally determined porosities were compared to respective compressive moduli to derive a constant, *C,* for each combination of materials used in this study.

Finally, the relationship between the bulk tensile modulus and the mass density was determined by Eqn. (4) [265, 266]:

$$\left(\frac{E}{E_0}\right) = \left(\frac{\rho}{\rho_0}\right)^2 \quad (4),$$

where the ratio between apparent Young's modulus of porous scaffolds (*E*) and Young's modulus of the individual solid fiber (E_0) is proportional to the ratio of the square of the relative mass density of the scaffold (ρ) to the mass density of the individual solid fiber (ρ_0).

The Pearson's *r* correlation coefficient is reported to compare these model prediction to the experimentally determined results for the individual fiber, compressive and tensile scaffold moduli for both the PEKK-PCL and gelatin-PCL polymer systems [267].

4.3.5 – Statistical Analysis

All experiments presented here within were conducted with at least 5 samples (n = 5), and data is represented as mean ± standard deviation. Each set of data was analyzed using SPSS (v.19.0) to determine significance by one-way ANOVA. To correlate individual fiber and scaffold properties as a response of mechanical stimulation, univariate correlation was determined by Pearson's correlation coefficients. $P \leq 0.05$ was regarded as statistically significant.

4.4 – Results

Various core (C)-shell (S) dimensional ratios of coaxial electrospun fibers were synthesized to systematically investigate how composition and morphology affect the mechanical properties of electrospun scaffolds at different length scales. Two different solution systems, PEKK-PCL and gelatin-PCL, were utilized to produce electrospun fibers. Distinctive C-S dimensional ratios were achieved by systematically modulating feeding flow rate of the core and shell components. The overall microstructures of these fibers showed a similar cylindrical morphology with an average of 5.16 ± 0.43 μm and 4.58 ± 0.35 μm in diameter (Figure 4.4A-E & K-O) for the PEKK-PCL and gelatin-PCL systems, respectively. The cross-sectional examination revealed that the core diameter increases with the greater percent core flow rate for both the PEKK-PCL (Figure 4.4F-J) and gelatin-

PCL (Figure 4.4P-T) systems. The percent core flow rates of 9%, 18%, 27%, 36%, and 45% resulted in varying percent core sizes for the different polymer systems used, and are listed in Table 4.1 along with their respective core and fiber diameters. The results demonstrate that approximately 100% increase in core diameter can be achieved while maintaining relatively the same overall fiber diameter for both systems (Figure 4.5A & 4.5B). Porosity measurements showed that the variation in the C-S ratios resulted in significant changes in the scaffold porosity, ranging from 70.2 ± 1.0% at the 9% core flow rate condition to 93.2 ± 0.5% for the 45% core flow rate condition for the PEKK-PCL scaffolds, and from 54.5 ± 4.2% for 9% core flow rate to 89.6 ± 0.4% for 45% core flow rate for gelatin-PCL fibers (Figure 4.5C & 4.5D). In general, the scaffold porosity increases with the increased volume ratio of the core material to the total fiber volume. Additionally, the 9% and 45% core flow rate scaffolds were subjected to soaking in an aqueous solution (Figure 4.6) for one month to test the stability of the fibrous structure. As shown in Figure 4.7 there were no noticeable changes in the structural conformation of the scaffolds. This is evident by comparing the fibers before soaking for both the 9% core flow rate (Figure 4.7A, 4.7E, 4.7I & 4.7M) and 45% core flow rate (Figure 4.7C, 4.7G, 4.7K & 4.7O) to after soaking (Figure 4.7B, 4.7F, 4.7J, 4.7N, 4.7D, 4.7H, 4.7L & 4.7P) for both polymer systems.

The elastic moduli of individual PEKK-PCL and gelatin-PCL fibers (shown in Figure 4.8C & 4.8D) were determined from the force-displacement curves by a three point

bending test using AFM (Figure 4.8A & 4.8B). As expected, the elastic modulus of individual core-shell fiber was positively related to the percent core flow rate. The elastic modulus of the PEKK-PCL core-shell fibers ranged from 0.55 ± 0.96 GPa for the 16% core size, up to 1.74 ± 0.22 GPa for the 59% core size. Likewise, the gelatin-PCL fibers exhibit values ranging from 0.48 ± 0.12 GPa to 1.53 ± 0.12 GPa, for the 14% and 59% core size, respectively. The experimental measurements agreed well with the prediction by Eqn. (1) having a correlation coefficient of 0.995 for PEKK-PCL and 0.934 for gelatin-PCL. Additionally, one-way ANOVA for both polymer systems indicates that the data is statistically significant with P = 0.000 for the individual fiber moduli, and disproves the null hypothesis allowing for mathematical modelling comparison of the data. In comparison, solid PCL fibers having a similar fiber diameter to the overall fiber diameter of these core-shell fibers exhibit a modulus of 0.32 ± 0.04 GPa (data not shown), similar to the value reported in literature [261]. These results demonstrate that core-shell electrospinning can achieve more than 5-fold increase in individual fiber elastic modulus via modulating core dimension while maintaining the overall fiber dimension and the same surface chemistry (*i.e.*, shell material).

To determine the relationship between morphological characteristics and macroscale mechanical properties of core-shell fibers/scaffolds, three dimensional scaffolds were subjected to unconfined compressive loads (Figure 4.9). PEKK-PCL (Figure 4.9A) and gelatin-PCL (Figure 4.9B) scaffolds were subjected to the compressive strains

from 5% to 20% applied strain to determine compressive equilibrium modulus [260]. In general, the compressive modulus of core-shell scaffolds decreased as the percent core size increased. The compressive moduli of the PEKK-PCL composite fibers ranged from 14.6 ± 1.4 kPa at 59% core sized fibers to 227.7 ± 20.4 kPa for the 16% core sized fibers (Figure 4.9C). Similarly, the gelatin-PCL fiber mats ranged from 17.6 ± 1.4 kPa at the 59% core size, to a high of 484.0 ± 30.2 kPa at the 14% core sized fibers (Figure 4.9D). Interestingly, the experimentally determined compressive moduli were not proportionally related to the elastic modulus of individual fibers predicted by Eqn. (1) (Figure 4.9C & 4.9D). Rather, there was a clear relationship between the compressive modulus and the porosity and it well agrees with the mathematical predictions by Eqn. 3 (dotted lines in Figure 4.9E & 4.9F), with correlation coefficients of 0.997 and 0.996 for PEKK-PCL and gelatin-PCL scaffolds, respectively. Again, one-way ANOVA for both polymer systems indicates that the data is statistically significant with P = 0.000 for the compressive moduli of the scaffolds rejecting the null hypothesis. Overall, compressive mechanical properties of electrospun core-shell scaffolds were correlated highly with the macroscale porosity of the electrospun fiber mats rather than the elastic modulus of individual fibers.

The stress-strain curves for PEKK-PCL and gelatin-PCL scaffolds having various percent core sizes under tensile loading are presented in Figures 4.10A and 4.10B. As compared to gelatin-PCL scaffolds, PEKK-PCL scaffolds exhibited a ductile behavior, in

which the failure of the samples occurred beyond 100% strain. Interestingly, there was a biphasic relationship between the core-shell ratio and the tensile modulus (Figures 4.10C & 4.10D). Both the PEKK-PCL and gelatin-PCL scaffolds reached the maximum tensile moduli at approximately 45% and 32% core sized fibers, respectively. Greater than these thresholds in percent core size led to a decrease in the tensile moduli. Below the thresholds, *i.e.*, the 45% and 32% core sized fibers for the PEKK-PCL and gelatin-PCL, respectively, the change of the tensile moduli is proportionally related to the individual fiber modulus predicted by Eqn. (1) (dotted lines in Figure 4.10C & 4.10D). Beyond these core sizes, however, porosity appears to be the dominant factor that determines the tensile modulus. The tensile modulus decreased from 12.0 ± 2.0 MPa at the 45% core sized fibers to 5.4 ± 1.1 MPa for the 59% core sized fibers for the PEKK-PCL scaffolds. Similarly, the maximum tensile modulus of the gelatin-PCL scaffolds was 22.6 ± 2.4 MPa at the 32% core sized fibers while it decreased to 16.8 ± 3.6 MPa when the core size increased to 59%. Remarkably, the tensile modulus of the scaffolds above the scaffold porosities of 45% (PEKK-PCL) and 32% (gelatin-PCL) was well predicted by Eqn. (3), with the correlation coefficients of 0.878 and 0.995 for PEKK-PCL and gelatin-PCL scaffolds, respectively (Figure 4.10E & 4.10F). The one-way ANOVA for both polymer systems for the tensile moduli of the scaffolds rejects the null hypothesis, and proves that the data is statistically significant with P = 0.000.

4.5 – Discussion

When designing an electrospun scaffold for tissue engineering applications, it is important to consider the physical properties that will ultimately contribute towards the desired use or projected outcome of the material. Considering the fact that both intrinsic (*e.g.*, stiffness) and extrinsic (*e.g.*, compliance to external forces) mechanical properties of the scaffolds influences stem cell fate, it is especially vital to take into account the scaffold characteristics delineating mechanics at the micro- and macroscales. In this study, we have demonstrated that the mechanical properties of individual core-shell electrospun fiber can be modulated independent of the properties of the bulk scaffolds composed of such fibers. More specifically, we showed that the mechanical properties of individual core-shell fibers can be modulated by controlling the dimensional ratio of respective core-to-shell components. In addition, we described how such a structural control at the microscale impacts the mechanics at both microscale and macroscale. Several other studies have successfully tested the mechanical characteristics of individual electrospun fibers [268] and/or selective bulk scaffold traits [269-271]. However, to our best knowledge, this study is the first to systematically investigate the mechanical properties of individual core-shell fibers and their influence on bulk scaffold mechanics under both compressive and tensile loadings.

The mechanical properties of the two core-shell model systems investigated in this study, PEKK-PCL and gelatin-PCL, are robustly dictated by the volume fractions of core and shell components as predicted by a simple rule of mixtures. Interestingly, the compressive moduli (along the direction normal to the longitudinal axis of individual fibers) of the bulk scaffolds do not seem to strongly depend on the elastic moduli of individual fibers (Figure 4.11A). Instead, the bulk compressive mechanics has a strong dependency on the scaffold porosity. As the scaffolds are compressed, the packing density increases and they undergo a densification by reducing pore volume between the fibers (Figure 4.11B). Therefore, the compressive modulus decreases to the second order of the relative fiber density, agreeing well with previous studies that reported a power-law relating porosity to the compressive stiffness as in Eqn. 3 [264, 272].

Unlike mechanical behaviors under compressive loading, which was predominantly modulated by bulk porosity regardless of component materials, tensile moduli of the scaffolds (along the longitudinal direction of individual fibers) are apparently influenced by both individual fiber mechanics and bulk scaffold porosity. Both PEKK-PCL and gelatin-PCL core-shell fiber scaffolds exhibited an increase in the tensile modulus when the percent core size increased. However, the tensile modulus exhibits a biphasic profile when the porosity reached a certain threshold (which is approximately 85% porosity for both polymer systems). When the electrospun scaffold is subjected to a tensile loading in the parallel direction of the fibers, the fibers initially align longitudinally

to the applied force while increasing their packing density (Figure 4.11C) [273, 274]. We speculate that the balance between intrinsic material properties of individual core-shell fibers and bulk scaffold properties (*i.e.,* porosity or relative fiber density) determines tensile modulus. It implies that porosity is a critical factor determining core-shell scaffold mechanics, in addition to individual fiber modulus which was commonly regarded as a deterministic factor for electrospun scaffold mechanics under tensile loading. Indeed, Soliman *et al.* demonstrated the tensile mechanics (ultimate stress, ultimate strain, and Young's Modulus) of electrospun fibers to be dependent on the fiber packing density [275].

Together, these results clearly demonstrate the feasibility of core-shell electrospinning to decouple scaffold surface chemistry from mechanical factors, and enable modification of mechanical cellular environments at the microscale without negatively impacting mechanical properties of scaffolds against applied forces at the macroscale. The cell-material interface can be tailored to achieve desirable biochemical microenvironments via modifications in shell materials regardless of the core polymer used in electrospun core-shell fibers. This has the ability to directly regulate cellular behaviors from attachment, self-renewal to differentiation of stem cells [240, 251]. In addition, such surface chemistry modification can be achieved independent of mechanical properties of the scaffolds by utilizing core materials with different mechanical properties. For example, the cell-material interface of both PEKK-PCL and

gelatin-PCL scaffolds can be modified to accommodate MSC attachment. A comparable individual fiber modulus of the two is expected to induce a similar cellular behavior under a static condition. However, vastly different mechanical behaviors of the scaffolds under compressive loading will likely induce different degree of MSC differentiation, *e.g.*, towards more chondrogenic phenotype in the softer PEKK-PCL scaffolds as compared to more osteogenic differentiation in the stiffer gelatin-PCL scaffolds.

More importantly, all of the mechanical testing results presented in this study reveal a comprehensive outlook on both the microscale (*i.e.* individual fibers) and macroscale (*i.e.* bulk scaffolds) for the mechanical aspects of electrospun core-shell fibrous scaffolds (Tables 4.2 & 4.3). Although the increase in core content in these fibers increases the individual fiber modulus, this does not always affect the bulk material properties, especially under compression. Similarly, the overall scaffold porosity dominates over the individual fiber properties to determine tensile modulus when the porosity is above a certain threshold. Therefore, our results suggest that core-shell electrospinning can provide a means to simultaneously tailor mechanical properties of scaffolds at both micro- and macroscale to achieve the desired and controlled cell niche at the cell and tissue levels.

4.6 – Conclusions

We demonstrated that the mechanical properties of core-shell electrospun fibers can be modulated by controlling the composition and the dimension of core, decoupled from the cell-interfacing surface (shell) chemistry. More importantly, we showed that mechanical properties of such fibers/scaffolds at the micro- and macroscale can be independently regulated by modulating micro- (core size) and macro-structure (scaffold porosity). Considering significant influence of various physiochemical cell niche on cellular behavior and subsequent tissue morphogenesis, the ability to independently tailor surface chemistry, micro- and macro-mechanical properties substantially increases the freedom of scaffold design. By modulating the respective core-shell dimensional ratios we have not only shown that the mechanics of the scaffolds can be regulated, but these fibers hold an additional promise for use in controlled drug release applications for tissue engineering purposes. Our insights in the relationship between the mechanical-morphology dependency at the micro- and macroscale are, therefore, expected to provide a better understanding to scaffold synthesis and aid for developing artificial tissues in biomedical engineering.

4.7 – Tables & Figures

% Core Flow Rate	C:S, PEKK:PCL			C:S, Gelatin:PCL		
	% Core Size	Fiber Diameter ± S.D. (µm)	Core Diameter ± S.D. (µm)	% Core Size	Fiber Diameter ± S.D. (µm)	Core Diameter ± S.D. (µm)
9%	16%	4.85 ± 0.78	1.91 ± 0.16	14%	4.34 ± 0.46	1.61 ± 0.20
18%	26%	4.79 ± 0.61	2.42 ± 0.27	16%	4.29 ± 0.84	1.73 ± 0.28
27%	45%	5.29 ± 0.48	3.55 ± 0.43	32%	4.39 ± 0.69	2.49 ± 0.27
36%	46%	5.71 ± 0.51	3.89 ± 0.63	53%	4.83 ± 0.39	3.52 ± 0.37
45%	59%	5.86 ± 0.71	4.50 ± 0.72	59%	5.07 ± 0.67	3.91 ± 0.64

TABLE 4.1. ELECTROSPUN CORE-SHELL FIBER DIMENSIONS.

Percent core flow rate, the resulting percent core size of the fibers, and the respective average fiber and core diameters listed within their corresponding polymer condition, PEKK-PCL and gelatin-PCL.

% Core Flow Rate	C:S, PEKK:PCL				
	% Core Size	Single Fiber Modulus (GPa) ± S.D. (n=7)	Compressive Modulus (kPa) ± S.D. (n=6)	Tensile Modulus (MPa) ± S.D. (n=5)	Porosity (%) ± S.D. (n=6)
9%	16%	0.55 ± 0.96	227.67 ± 20.39	9.20 ± 2.01	70.2 ± 1.0
18%	26%	0.81 ± 0.14	82.20 ± 7.02	11.60 ± 3.92	82.5 ± 3.0
27%	45%	1.26 ± 0.16	57.85 ± 8.07	12.00 ± 1.96	86.1 ± 1.9
36%	46%	1.31 ± 0.34	17.06 ± 2.90	6.30 ± 0.65	89.7 ± 1.5
45%	59%	1.74 ± 0.22	14.55 ± 1.43	5.42 ± 1.05	93.2 ± 0.5

TABLE 4.2. MORPHOLOGICAL AND MECHANICAL PROPERTIES OF PEKK-PCL CORE-SHELL ELECTROSPUN FIBERS.

Percent core flow rate, the resulting percent core size of the fibers, and the respective mechanical properties of PEKK-PCL microfibrous scaffolds defined by the single fiber modulus, the compressive modulus, the tensile modulus, and the scaffold porosities.

% Core Flow Rate	C:S, Gelatin:PCL				
	% Core Size	Single Fiber Modulus (GPa) ± S.D. (n=7)	Compressive Modulus (kPa) ± S.D. (n=6)	Tensile Modulus (MPa) ± S.D. (n=5)	Porosity (%) ± S.D. (n=6)
9%	14%	0.48 ± 0.12	484.01 ± 30.18	10.19 ± 4.49	54.5 ± 4.2
18%	16%	0.93 ± 0.31	161.85 ± 14.51	17.13 ± 2.16	72.5 ± 1.2
27%	32%	0.96 ± 0.21	82.99 ± 8.15	22.60 ± 2.44	84.8 ± 0.5
36%	53%	1.36 ± 0.30	55.31 ± 9.28	20.14 ± 1.71	87.1 ± 1.0
45%	59%	1.53 ± 0.12	17.57 ± 1.40	16.79 ± 3.63	89.6 ± 0.4

TABLE 4.3. MORPHOLOGICAL AND MECHANICAL PROPERTIES OF GELATIN-PCL CORE-SHELL ELECTROSPUN FIBERS.

Percent core flow rate, the resulting percent core size of the fibers, and the respective mechanical properties of gelatin-PCL microfibrous scaffolds defined by the single fiber modulus, the compressive modulus, the tensile modulus, and the scaffold porosities.

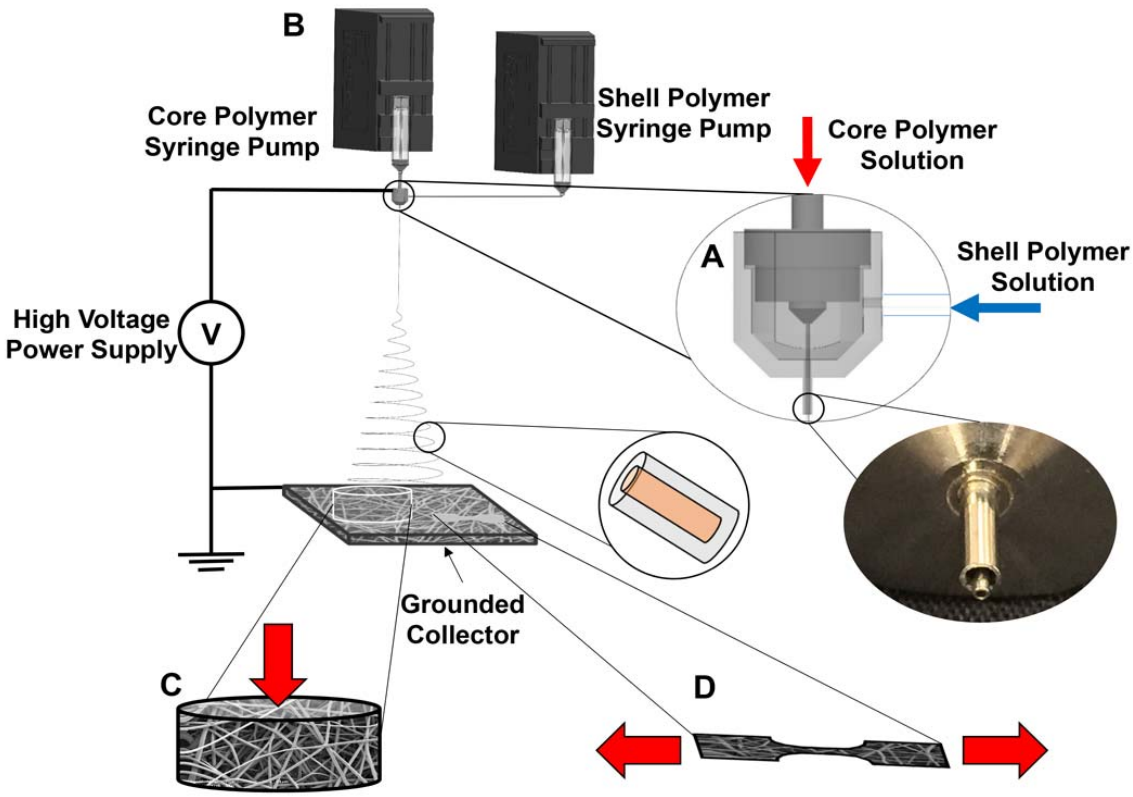

FIGURE 4.1. A SCHEMATIC OF THE CORE-SHELL ELECTROSPINNING SETUP.

(A) A custom concentric nozzle connected to (B) dual syringe pumps for independent supply of core and shell electrospinning solutions to produce various core-to-shell dimensional ratios. The orientations of the samples subjected to (C) compressive or (D) tensile testing were noted.

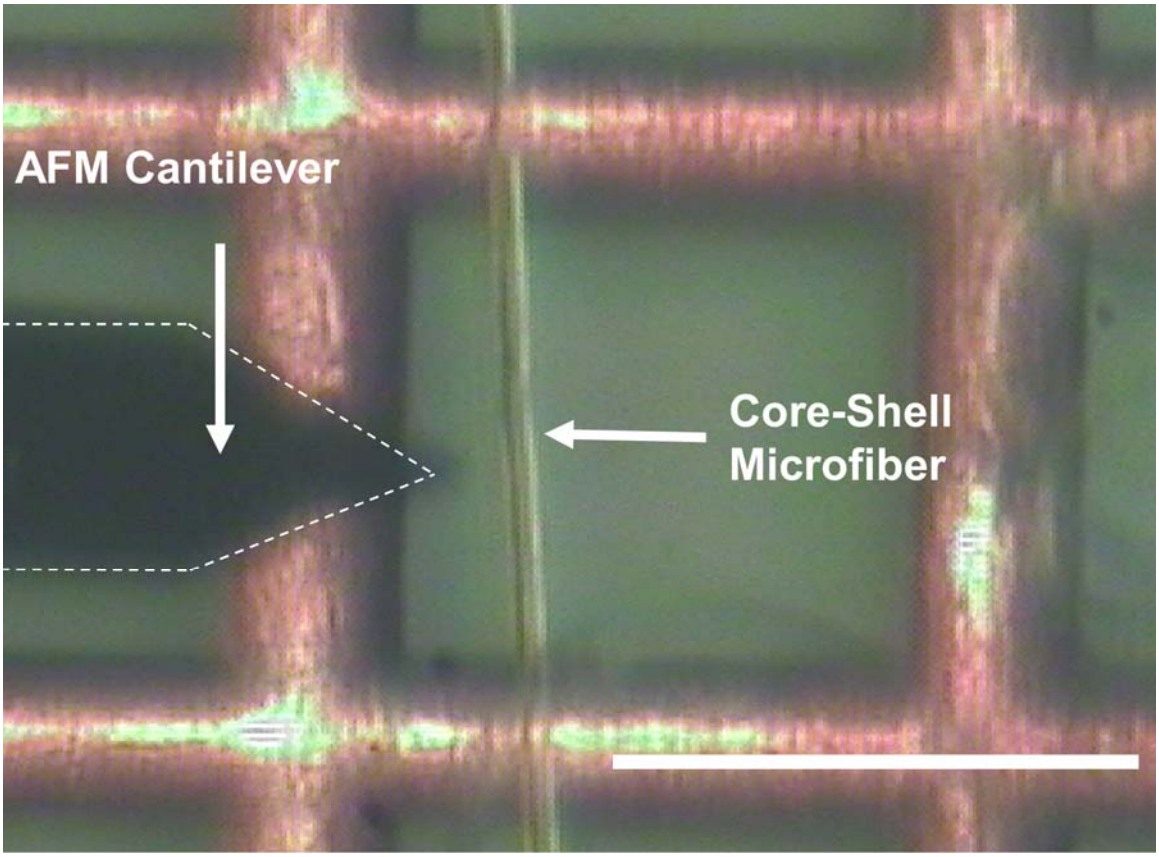

FIGURE 4.2. A REPRESENTATIVE IMAGE OF A THREE POINT BENDING TEST ON AN INDIVIDUAL ELECTROSPUN CORE-SHELL FIBER.

Mechanical characterization of an individual core-shell fiber was performed using atomic force microscopy (AFM). The image shows the AFM cantilever (outlined in dashed white line) positioned near a single fiber that was electrospun across a 100 µm gap prior to contact (Scale Bar: 100 µm).

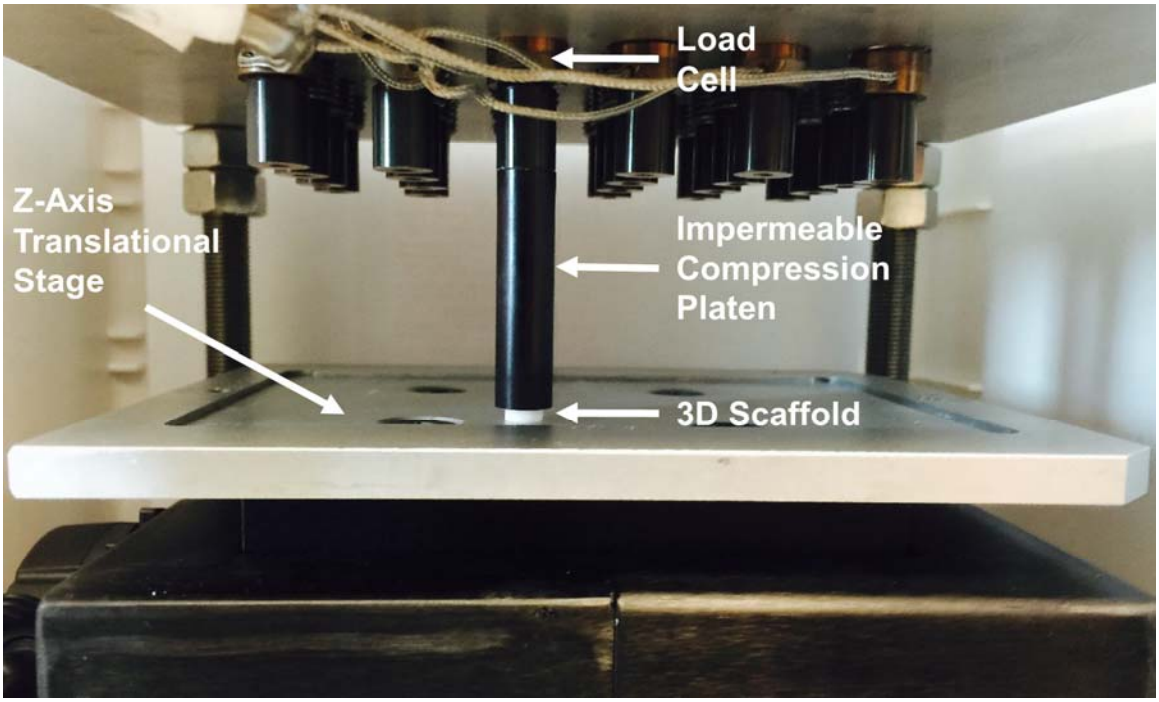

FIGURE 4.3. A CUSTOM COMPRESSION DEVICE FOR MECHANICAL TESTING.

An image shows a compression device composed of a z-axis translational stage and a load cell to test the macro-level compressive mechanics of bulk scaffolds.

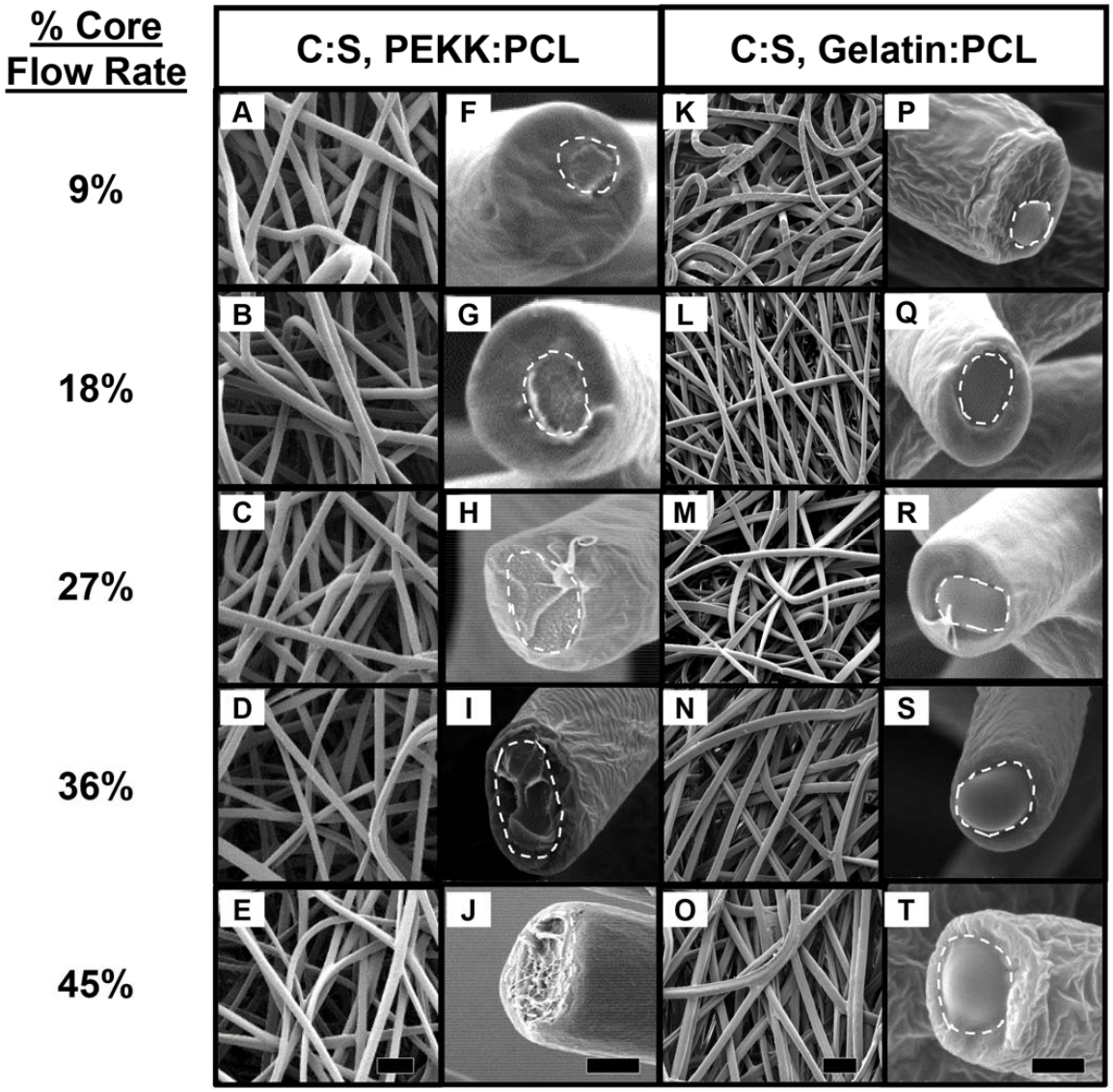

FIGURE 4.4. REPRESENTATIVE CROSS-SECTIONAL SEM IMAGES OF ELECTROSPUN CORE-SHELL FIBER WITH VARIOUS CORE-TO-SHELL DIMENSIONAL RATIOS.

Electrospun PEKK (core)-PCL (shell) and gelatin (core)-PCL (shell) microfibers with overall fiber morphology (A-E and K-O) and cross-section of individual fibers (F-J and P-T) for each system are shown (Scale Bars: 20 μm for A-E and K-O; 2 μm for F-J and P-T). Core materials are outlined by dashed white lines.

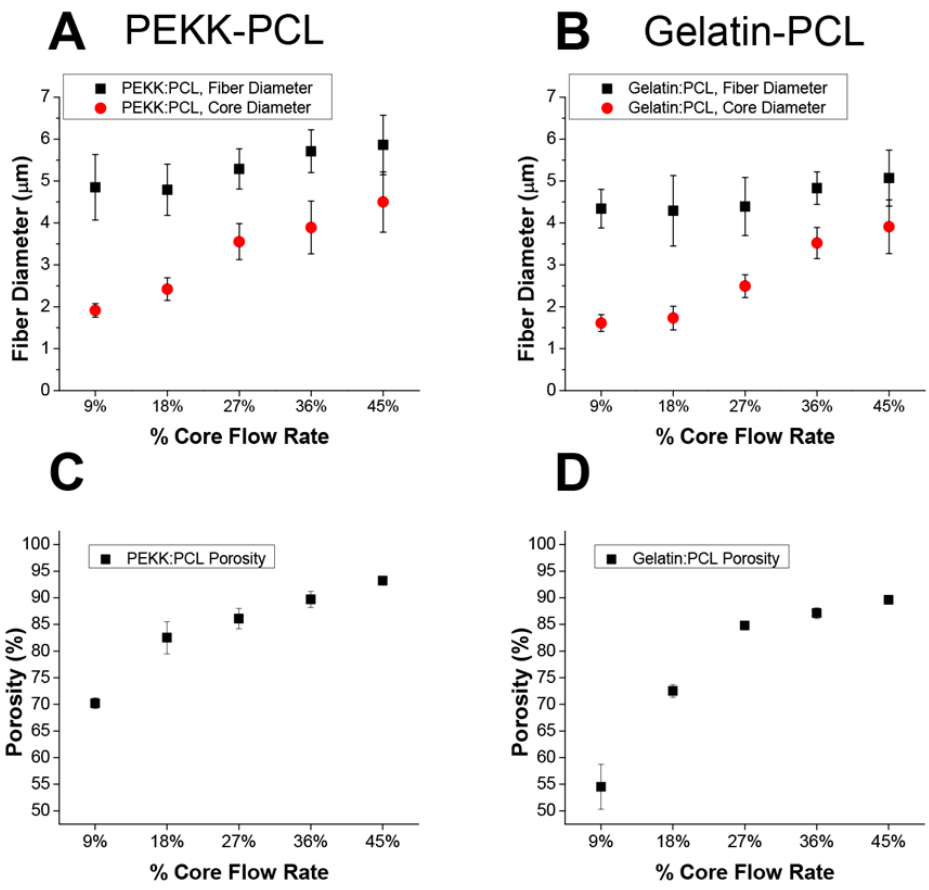

FIGURE 4.5. MORPHOLOGICAL CHARACTERIZATION OF ELECTROSPUN CORE-SHELL FIBER/SCAFFOLD WITH VARIOUS CORE/SHELL DIMENSIONAL RATIOS AT MICRO- AND MACROSCALES.

Characterization of core-shell polymer systems (A and C) PEKK-PCL and (B and D) gelatin-PCL for fiber diameter and scaffold porosities. (A and B) The overall fiber diameter and core diameter were measured with respect to the change of % core flow rate that was used to control the core/shell dimensional ratios. (C and D) At a macroscale, the porosity of the scaffolds composed of the core-shell fibers with various core-to-shell dimensional ratios was compared to % core flow rate. Standard deviation of samples is smaller than markers in some conditions.

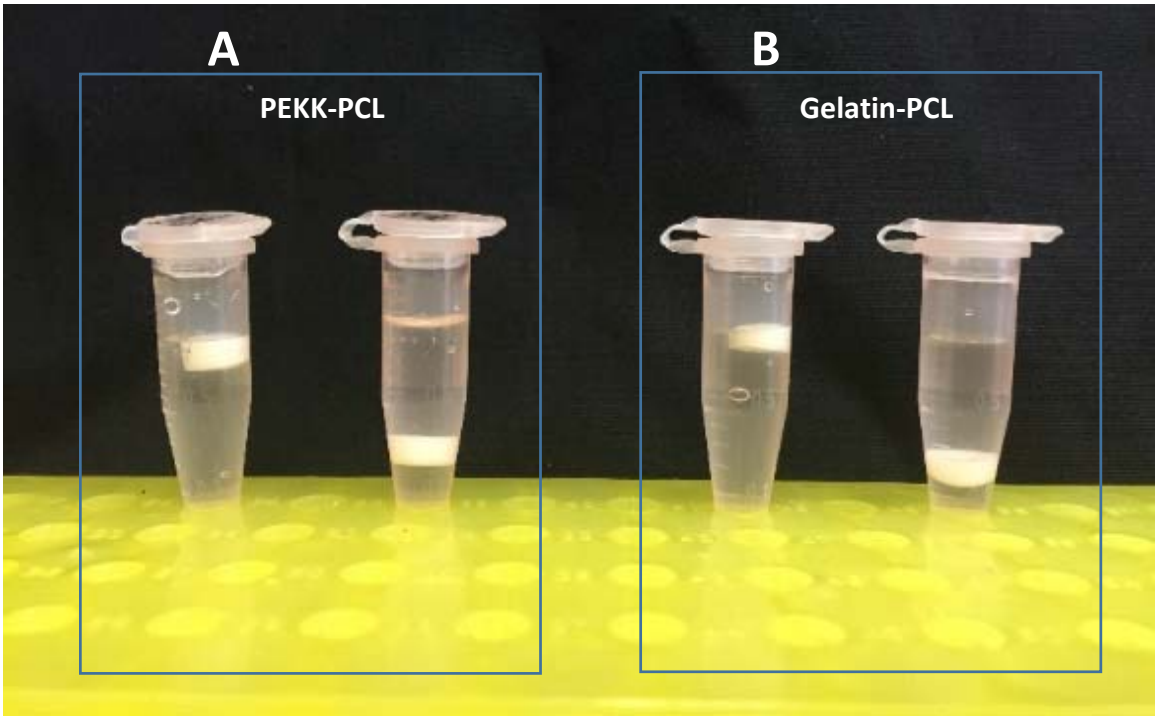

FIGURE 4.6. WETTABILITY OF ELECTROSPUN SCAFFOLDS.

The image above shows scaffolds from each core-shell polymer system, (A) PEKK-PCL and (B) gelatin-PCL, either just placed into solution (floating on left) or incubated for 5 minutes at 37 °C (submerged on right). Scaffolds were subjected to soaking in an aqueous solution for up to 1 month to test the stability of the fibrous structure.

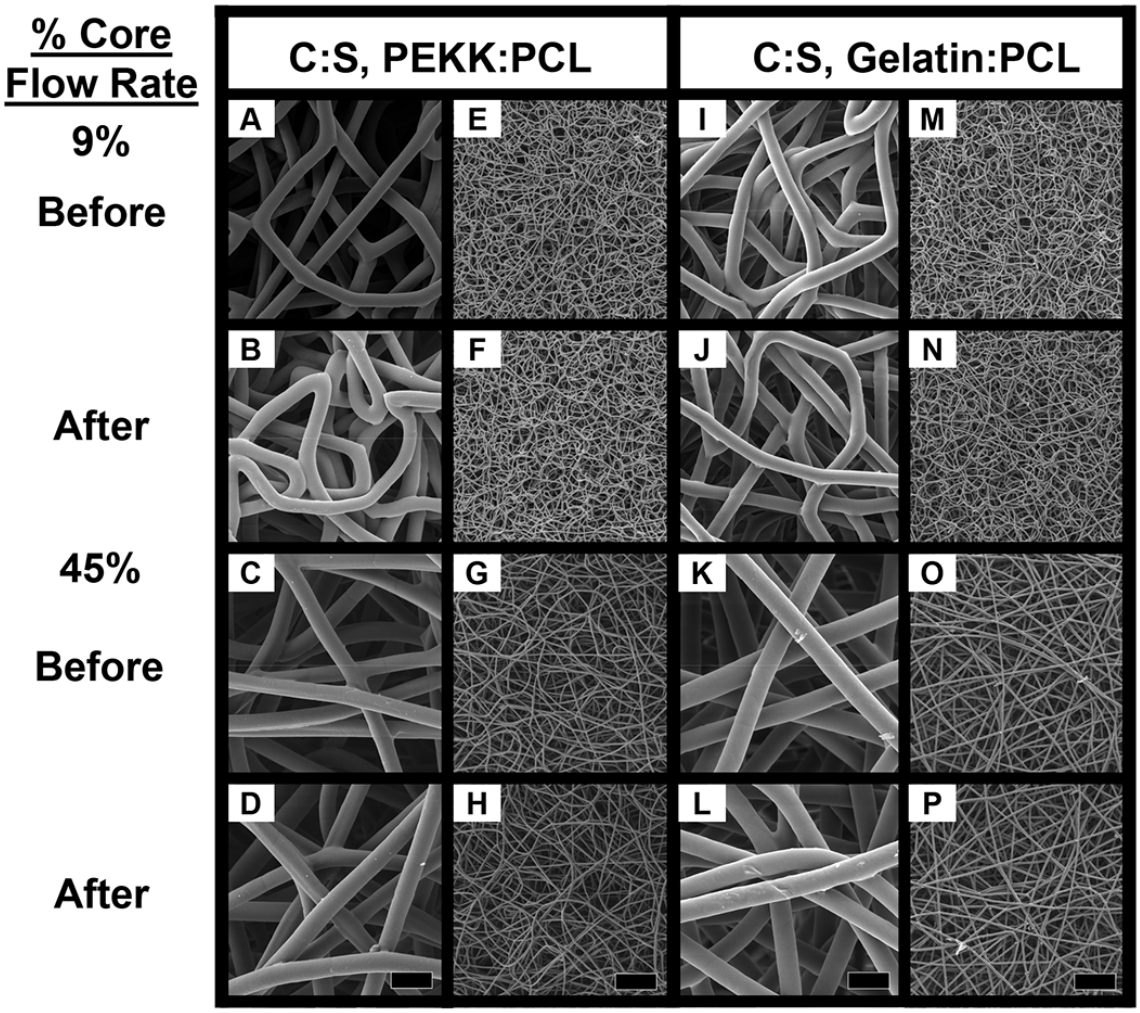

FIGURE 4.7. REPRESENTATIVE SEM IMAGES OF ELECTROSPUN FIBERS BEFORE AND AFTER SOAKING IN AN AQUEOUS SOLUTION.

Overall fiber morphology ((A-H) PEKK-PCL and (I-P) gelatin-PCL) before subjecting to PBS incubation (A, E, I, M, C, G, K and O) and after soaking in PBS for one month (B, F, J, N, D, H, L and P) for each system are shown (Scale Bars: 10 µm for A-D and I-L; 100 µm for E-H and M-P).

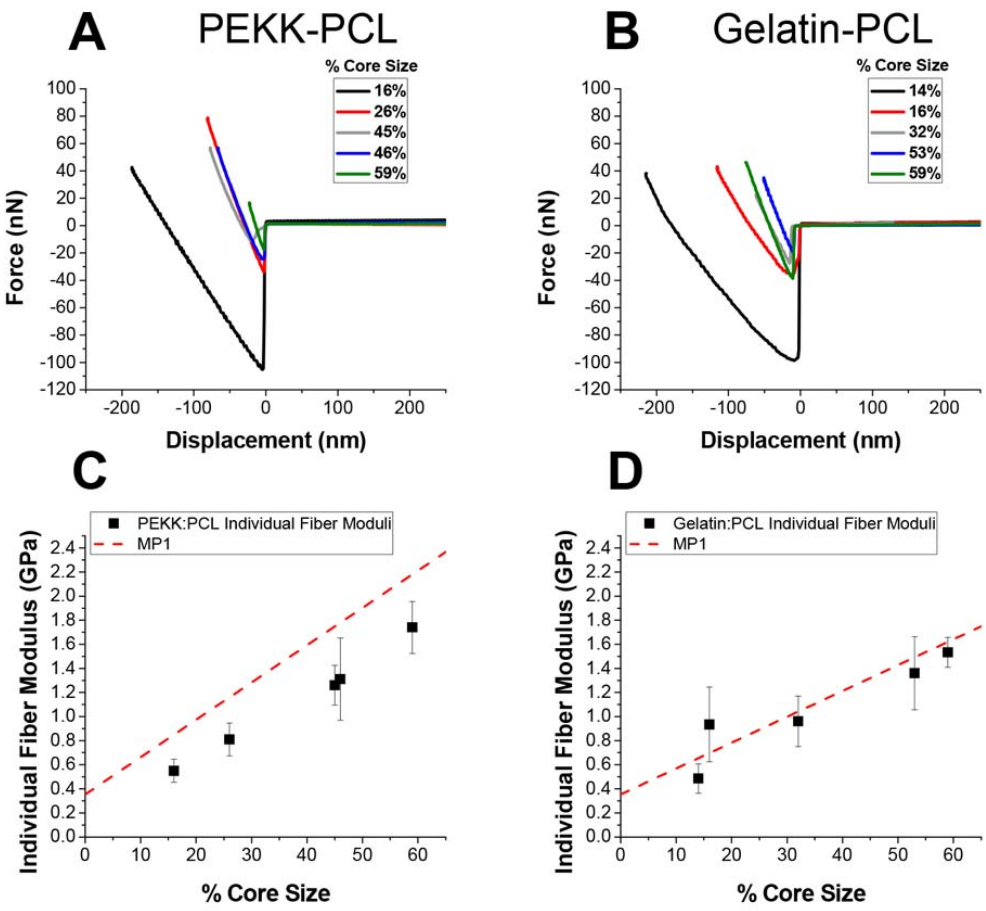

FIGURE 4.8. MECHANICAL CHARACTERIZATION OF INDIVIDUAL CORE-SHELL FIBERS WITH DIFFERENT CORE/SHELL DIMENSIONAL RATIOS BY A THREE POINT BENDING TEST USING AN AFM.

Characterization of core-shell polymer systems (A and C) PEKK-PCL and (B and D) gelatin-PCL by AFM. (A and B) Representative force-displacement curves of individual core-shell fibers with various % core sizes. (C and D) Experimentally determined elastic moduli of individual fibers having different % core sizes were compared to the mathematical prediction (MP1) by using Equation 1.

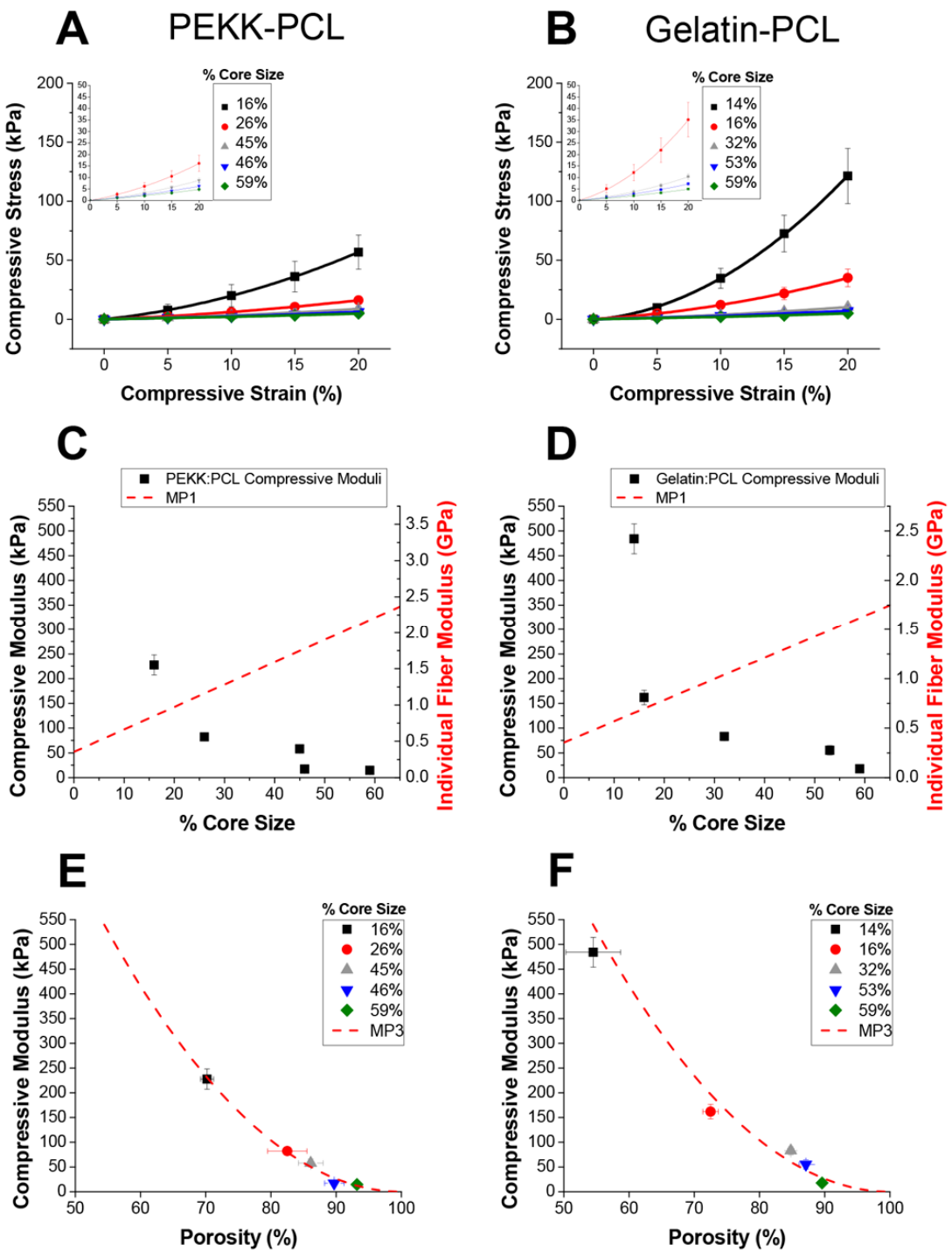

FIGURE 4.9. COMPRESSIVE MECHANICAL CHARACTERIZATION OF THE SCAFFOLDS COMPOSED OF CORE-SHELL FIBERS.

Characterization of core-shell polymer systems (A, C and E) PEKK-PCL and (B, D and F) gelatin-PCL by compressive loading. (A and B) Representative compressive stress-strain curves of scaffolds with various % core sizes. Insets show the curves for the core size greater than 26 and 16% for PEKK-PCL and gelatin-PCL, respectively to reveal the differences in mechanical responses. (C and D) Compressive modulus of scaffolds with different % core sizes shows a lack of proportional relationship to the individual fiber modulus predicted by Equation 1 (MP1, dashed line). (E and F) The relationship between compressive modulus and porosity was compared to a mathematical prediction by using Equation 3 (MP3, dashed line).

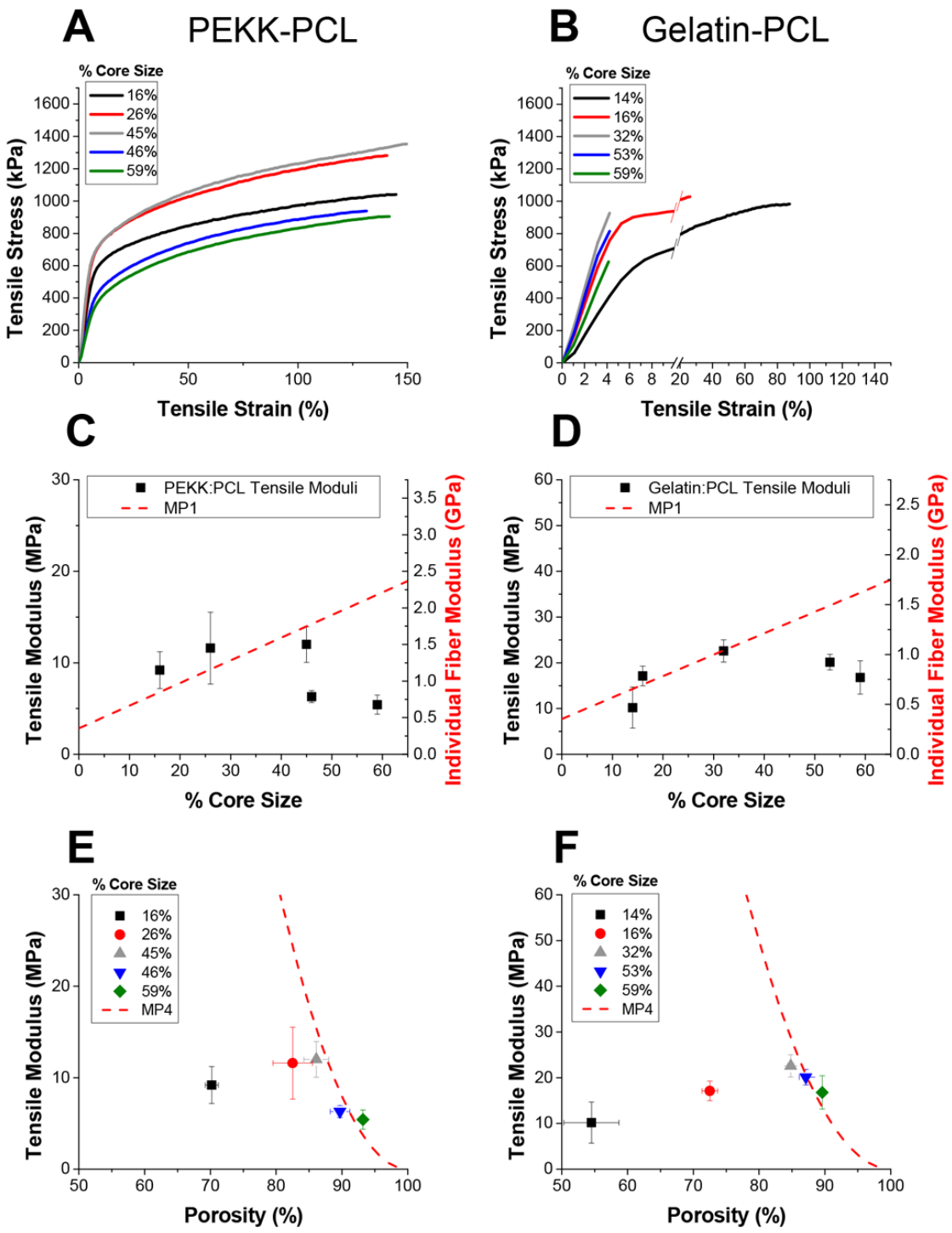

FIGURE 4.10. TENSILE MECHANICAL CHARACTERIZATION OF SCAFFOLDS COMPOSED OF CORE-SHELL FIBERS.

Characterization of core-shell polymer systems (A, C and E) PEKK-PCL and (B, D and F) gelatin-PCL by tensile loading. (A and B) Representative tensile stress-strain curves of scaffolds with various % core sizes. (C and D) Tensile modulus of scaffolds with different % core sizes shows a proportional relationship to the individual fiber modulus predicted by Equation 1 (MP1, dashed line) for smaller % core sizes. (E and F) The relationship between tensile modulus and porosity was compared to a mathematical prediction by using Equation 4 (MP4, dashed line).

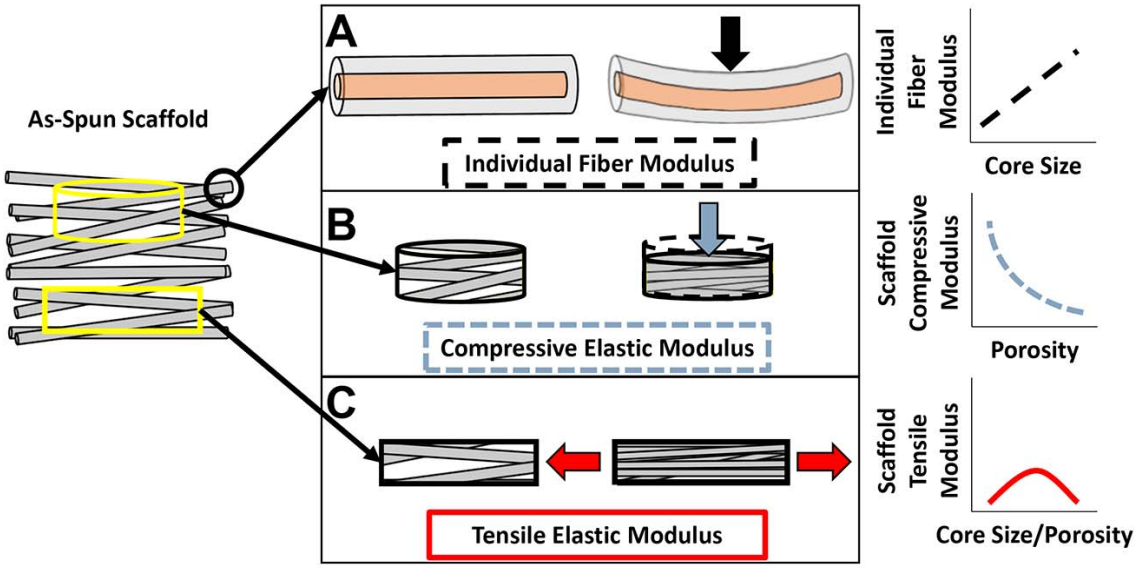

FIGURE 4.11. A SCHEMATIC DEMONSTRATING INDIVIDUAL FIBER AND SCAFFOLD DEFORMATION UNDER VARIOUS MODES OF LOADING.

(A) As the size of the core with the stiffer material increases, the individual fiber modulus linearly increases following the rule of mixture. (B) The compressive modulus of the scaffolds composed of such core-shell fibers significantly depends on the overall porosity of the structure rather than the single fiber modulus. (C) The dependency of the tensile modulus of the scaffolds changes from the individual fiber modulus at a low porosity to the overall structural porosity at a high porosity.

CHAPTER 5 – CONTROL OF MULTI-PHENOTYPIC DIFFERENTIATION OF STEM CELLS IN THREE-DIMENSIONS BY DYNAMICALLY CULTURED ENGINEERED GRADIENTS

5.1 – Abstract

Osteochondral tissue engineering has primarily revolved around the use of biphasic or multiphasic scaffolds to address regeneration of the interfacial tissue. While these methods allow for segmented development for tissue maturation they commonly require multiple steps and culture techniques, and do not recapitulate the continuous structure found within physiological tissue. Therefore, electrospun three-dimensional scaffolds consisting of linear and biphasic gradients were engineered. These scaffolds were utilized to culture and subject hMSCs to various magnitudes of dynamic compressive strains in a depth-dependent manner at a frequency of 1 Hz for 2 hours daily for up to 42 days in osteogenic media. Spatially controlled gene expression of chondrogenic markers (*ACAN, COL2A1*) were upregulated in response to areas of the scaffolds which had the increased magnitudes of compressive strain. Counter to this finding, osteogenic markers (*COL1A1, SPARC (ON)*) and calcium deposition all had observable downregulation and decreases in expression as a response to high compressive localized strain. Dynamic mechanical analysis showed good temporal development as a response to mechanical stimulation though was lower than the statically cultured controls. Overall, it has been shown that the degree of differentiation of hMSCs in monolithic scaffolds towards an

osteogenic or chondrogenic lineage is dependent on the magnitude of compressive strain. These results demonstrate that spatially-controlled multi-phenotypic differentiation of hMSCs can be controlled by varying the strain regimens in mechanical gradient constructs, providing a novel strategy to modulate differentiation specification and tissue morphogenesis.

5.2 – Introduction

Tissue engineering is considered to be a very promising strategy to regenerate the osteochondral interface, but oftentimes requires multi-layered scaffold designs to achieve distinct chondral and osseous layers. The simplest and most common approach to recapitulate tissue interfaces has been using multi-layered scaffolds designs, including our previous study [276]. For osteochondral tissue, segmental construction of tissue compartments using different cell sources and/or different scaffolding materials have been typically used to reconstruct such tissues. Many times mesenchymal stem cells (MSCs) which were pretreated with chondrogenic or osteogenic biochemical factors were sequentially seeded on a single scaffold with a cocktail medium to maintain both chondrogenic and osteogenic phenotypes [277]. Another method is to seed cells into two separate pieces of scaffolds with different materials and mechanical properties, have the MSCs undergo chondrogenesis and osteogenesis separately, and integrate the two compartments to form a singular assembled construct [38, 278]. In the case of different scaffold materials, oftentimes a stiffer, mineralized matrix is used for the bone region, whereas the cartilage region is often composed of a softer polymeric layer [49, 279-282]. Although these strategies provide a means to approximate overall tissue structure, they cannot depict a seamless transitional gradient morphology present in native tissues, which is essential for tissue integrity and functions.

Many tissues in the body possess cellular, extracellular matrix (ECM), and biochemical gradients, which is especially evident in load-bearing orthopaedic tissues. The osteochondral interface has a depth-wise transitional structure, composed of cartilage, calcified cartilage and subchondral bone. The gradients in cell phenotype and its associated ECM composition in a depth-dependent manner results in naturally varying elasticity in this interfacial tissue [283]. Additionally, it should be noted that the elastic modulus of cartilage is approximately more than four orders of magnitude less than that of subchondral bone, while that of calcified cartilage possesses an intermediate value [284, 285]. This concept provides a fascinating framework to focus research on continuous gradient scaffold approaches in comparison to multi-phasic constructs. Recently, several studies attempted to create continuous biochemical and/or mechanical gradients [286-288]. Notably, Mohan *et al.* developed a polymeric scaffold with bioactive signal gradients of BMP-2 and transforming growth factor β-1 (TGF β-1), and material gradient of hydroxyapatite [288]. The study demonstrated superior ability to regenerate osteochondral defect *in vivo* when both biochemical and material gradients were implemented. Although they did not analyze the mechanical gradient, it is likely that such gradient exists within the scaffold due to depth-wise differential loading of hard ceramic into polymer matrix. Therefore, it is hypothesized that the capability of regulating dynamic mechanical gradients in a quantitatively controlled manner is required to dissect the mechanistic details of gradient interfacial tissue morphogenesis. In this case, a mechanistic understanding of how a continuous osteochondral tissue gradient is being

developed is important for devising methodologies to treat tissue damage or for manufacturing full-scale replacements to recapitulate the tissue interface.

Due to their clinical relevance and vast potential in the regeneration of both cartilage and bone, human mesenchymal stem cells were investigated for their multi-phenotypic differentiation ability. It is well known that mechanical cues are important for inducing both osteogenesis and chondrogenesis of MSCs. In their multi-potent state, MSCs simultaneously contain a mixture of all mesenchymal genotypic factors at low levels of expression. These factors are able to cross-regulate each other to retain the cell in a multi-potent equilibrium. When an epigenetic cue (*i.e.*, mechanical stimuli) disrupts the equilibrium state, one factor becomes dominant while all the others are inhibited, leading to cell differentiation towards a certain cell phenotype [62, 289-293]. It has been shown that externally applied dynamic mechanical stimuli also modulate stem cell differentiation. In this circumstance, dynamic compressive loading has been reported to support both chondrogenesis and osteogenesis by upregulating chondrogenic transcription factor SOX9 and osteogenic transcription factor Runx2 in MSCs, respectively [63, 66-72]. Importantly, Michalopoulos *et al.* [71] and the recent study, discussed in Chapter 3, showed that dynamic compression-induced osteogenesis and chondrogenesis of MSCs are magnitude dependent, where preferential differentiation of MSCs towards osteoblasts at a low-strain magnitude changes to chondrogenic differentiation at a high-strain magnitude. Therefore, the overarching objective of this study was to engineer

mechanically distinct electrospun scaffolds consisting of mechanical gradients, and thus creating a respective strain gradient to induce site-specific multi-phenotypic stem cell differentiation of hMSCs within a monolithic scaffold when under dynamic compressive loading.

Therefore, the work described in this following chapter aims to direct the multi-phenotypic differentiation of a single population of hMSCs by modulating the mechanical properties of electrospun scaffolds and subsequent local strain in a depth-dependent manner. It is hypothesized that hMSC differentiation towards either an osteogenic or chondrocytic phenotype can be regulated by engineering scaffolds with a gradient of spatially controlled mechanical properties, and thus resulting local strains when subjected to dynamic compression. Interestingly, the application of a continuous dynamic mechanical gradient to subject stem cells to localized variations in compressive strain, to our knowledge, has yet to date been unexplored. This technique will prove to be important for understanding three-dimensional interfacial tissue morphogenesis from a single multi-potent stem cell population.

5.3 – Materials and Methods

All reagents and products were purchased from Sigma–Aldrich (St. Louis, MO) unless otherwise noted.

5.3.1 – Scaffold fabrication of various core-shell dimensional ratios

Three-dimensional (3D) scaffolds were synthesized by coaxially electrospinning a 25 wt % polyethylene glycol (PEG) in chloroform for the core polymer solution, and 11 wt % poly (ε-caprolactone) (PCL) dissolved in 19:1 (v/v) chloroform-methanol for the shell polymer solution. A custom dual concentric nozzle 16G (OD: 1.65 mm, ID: 1.26 mm) - 22G (OD: 0.70 mm, ID: 0.41 mm) was utilized to synthesize the core-shell electrospun fibers (NanoNC, Seoul, South Korea) was used. A vertical electrospinning setup was used with a tip-to-collector distance of 45 cm as previously described [217]. Relatively homogenous core-shell microfibers with varying dimensional ratios were fabricated by concurrently increasing and decreasing the core and shell flow rates in 1 mL/hr increments, respectively. The total polymer solution was dispensed at 11 mL/hr with varying ratios or 0:11, 1:10, 2:9, 3:8, 4:7, 5:6, and 6:5 mL/hr, while the applied voltage was adjusted to approximately 16 kV to form a stable Taylor cone [218]. A 6 mm diameter biopsy punch (Integra Miltex, York, PA) was used to produce cylindrical scaffolds from approximately 3 mm-thick as-spun fiber mats.

5.3.2 – Mechanical properties of monolithic scaffolds

Electrospun microfibrous scaffolds of varying core-shell dimensional ratios were subjected to compressive stress-relaxation testing for determination of the scaffold equilibrium moduli as previously described [217]. Briefly, scaffolds were submerged in PBS without Ca^{2+}/Mg^{2+} for 24 hours at 37ºC to remove the PEG from the core of the fibers and simulate the aqueous conditions experienced in cell culture conditions. An impermeable platen with the dimensions of 9.5 mm in diameter was attached to a 1 kg load cell (Model 11, Honeywell Sensing and Control, Columbus, OH) to ensure unconfined compressive loading of the samples. A submicron linear translational stage (AVL-125, Aerotech, Pittsburgh, PA) was used to incrementally deliver a compressive strain perpendicular to the direction of fiber deposition. In order to confirm that scaffolds were in contact with the impermeable platen a tare load of 0.02 N was used to signify detection of the scaffold surface. The samples were then compressed up to a total of 15% strain at 5% strain increments of the scaffold thickness where the load was held for 90 s per increment per sample. The equilibrium modulus was then calculated from a linear range of the stress-strain curve. All conditions were tested with at least 6 samples per condition (n=6).

5.3.3 – Gradient scaffold fabrication and characterization

In order to generate scaffolds composed of continuous engineered core-shell dimensional ratios, core and shell polymer solution flow rates were independently controlled in an inverse configuration while maintaining a total flow rate of 11 mL/hr using programmable syringe pumps. For a continuous linear gradient scaffold, the shell flow rate was held for 15 minutes at 11 mL/hr then decreased to 5 mL/hr over the course of 96 minutes, while the core flow rate was simultaneously increased from 0 mL/hr to 6 mL/hr over the same time course. These scaffolds will be referred to as linear gradient throughout the manuscript. Biphasic gradient scaffolds were fabricated in a similar manner to the linear gradient samples such that flowrates for the core and shell were started for 5 minutes at 0 mL/hr and 11 mL/hr, respectively, inversely increased and decreased to 6 mL/hr and 5 mL/hr, held for 5 minutes, and gradually returned to their initial states over the course of 100 minutes. Hereupon, these scaffolds are referred to as a biphasic gradient. Both linear and biphasic gradient scaffolds were electrospun to be approximately 3 mm thick. To observe the gradient core-shell dimensional ratios cryogenic fracturing was performed by placing the scaffolds into PBS for 24 hours followed by submerging into liquid nitrogen. The cryo-fractured cross-sections were then confirmed by observation under a scanning electron microscope (SEM, TESCAN, Brno, Czech Republic) to assess the gradient core diameter and while maintaining a relatively homogenous overall fiber diameters.

5.3.4 – Computational modeling of linear and biphasic mechanical gradient

In order to confirm that spatially controlled mechanical properties of electrospun fibers can indeed produce localized strain gradients we utilized COMSOL Multiphysics (v4.3) to analyze volumetric strain of a cylindrical solid. Using the experimentally determined equilibrium moduli of monolithic scaffolds, described previously, we are able to define a continuous or biphasic mechanical property gradient using the solid mechanics module along the depth of the scaffolds. With the assumption that the scaffold porosity of the linear and biphasic gradient is similar to that of the monolithic scaffolds tested previously, the only component that is changing is the core diameter of the fibers, and thus the resulting local mechanical properties of the bulk scaffolds. A prescribed global strain was then subjected to the top-surface of the cylindrical scaffolds, and the volumetric strain was analyzed in a depth-dependent manner with respect to the normalized distance from the top of the scaffold. A total strain of 6% was selected for analysis due to the local strains ranging from approximately 2-16% due to the results of cellular differentiation described in Chapter 3.

5.3.5 – Experimental validation of depth-wise strain gradients

In order to confirm the mechanical strain gradient in a depth-wise configuration a digital image correlation (DIC) technique was employed. Glass capillary tubing was heated and drawn into fine threads followed by inserting into the side of the scaffolds to track distinct features for the volumetric strain in a depth-wise manner. Acellular scaffolds were placed into PBS for 24 hours at 37ºC to remove any PEG from the core of the microfibers before being subjected to compression and sequential imaging. Scaffolds cultured with cells were fixed in formalin at designated time points prior to analysis. A custom compression system was assembled to subject the scaffolds to unconfined compressive loading. A CCD camera (DFK 41BU02.H, The Imaging Source, Charlotte, NC) with zoom lens was configured to capture still frames (7.5 fps) of the scaffold deformation under loading. At 6% applied strain of the scaffold thickness, determined from previous experiments, computational modeling, and dynamic compressive loading to constructs was used and location measurements of the glass capillaries were taken from the images and DIC was conducted to determine local strain with respect to the top of the scaffold. The experimental data was plotted against the computational modeling for comparison. Each scaffold was tested in triplicate for repeatability, three scaffolds per gradient type were analyzed for acellular scaffolds and at Day 42, while fewer samples were used for Day 14 and Day 28 of cell cultured constructs.

5.3.6 – Cell culture

Upon validation of both linear and biphasic strain gradients, scaffolds were then prepared for cell culture. PEG was removed from the core of the scaffolds by placing into PBS without Ca^{2+}/Mg^{2+} for 24 hours at 37°C. There was no measurable change in scaffold thickness due to removal of the core material. After drying at room temperature for an additional 24 hours the cylindrical scaffolds were plasma-treated at 30 W for 5 minutes. This was followed by collagen type I conjugation to improve cellular adhesion by using a crosslinking agent, 100 mM N-hydroxysuccinimide (NHS)/N-(3-Dimethylaminopropyl)-N'-ethylcarbodiimide hydrochloride (EDAC) [202]. The scaffolds were sterilized by 70% ethanol for 12 hours followed by air dry overnight. Sterilized scaffolds were stored at 4°C until cell seeding in 24-well tissue culture plates treated with 125µL/cm^2 of 0.5 mg/mL poly(2-hydroxyethyl methacrylate) (poly-HEMA) in 95% EtOH to prevent cellular attachment.

Human fetal bone marrow-derived mesenchymal stem cells (hMSCs) were acquired from Applied Biological Materials (Richmond, Canada) and were sub-cultured for expansion until experimental use at passage 6. The hMSCs were expanded with growth media (GM) composed of DMEM-F12 (Lonza, Anaheim, CA) supplemented with 15% FBS, 1% Penicillin-Streptomycin, and 100ng/mL bFGF in T75 flasks until approximately 85-90% confluency. The scaffolds placed in a 24 well-plate were seeded

with 60 µL of cell-suspended media at a concentration of approximately 33 million cells/mL. Capillary forces of the sterilized and dry 3D scaffolds provided complete and homogenous cellular infiltration of the cell-suspension throughout the thickness of each scaffold. The cell seeded scaffolds were incubated for 2 hours to induce cell attachment before filling each well with an additional 1 mL of GM. The cell/scaffold constructs were pre-cultured in GM for 7 days prior to being subjected to differentiation media and/or mechanical stimulation. The GM was exchanged to osteogenic differentiation media (OM) 24 hours prior to the application of mechanical stimulation. The OM was composed of low-glucose DMEM supplemented with 10% FBS, 10 mM sodium-β-glycerophosphate, 200 µM ascorbic acid-2-phosphate, 100 nM dexamethasone, and 1% Penicillin-Streptomycin-Fungizone. The OM was exchanged at 50% volume every day, and a full volume exchange was conducted every fifth day. With exception of time during mechanical stimulation, the cell/scaffold constructs were placed onto an orbital shaker at 300 RPM for the duration of the experiment to ensure complete and efficient media exchange throughout the entirety of the scaffolds.

5.3.7 – Application of dynamic compressive strain and mechanical characterization of cell/scaffold constructs

The same custom compression system used for testing the mechanical properties of electrospun scaffolds modified from previous reports was utilized to apply dynamic

compressive strain to the cell/scaffold constructs [217, 219]. Briefly, a nominal tare load of 0.02 N was used to ensure the scaffolds were in contact with the impermeable platens and determine the position of the scaffolds. The determined position was maintained over the length of the study. Unconfined compression of the cell/scaffold constructs was conducted daily for 2 hours/day for up to 35 days of stimulation. Mechanical simulation was applied at 6% strain (ε = 0.06) of the scaffold thicknesses for both the linear and biphasic gradients as determined by computational modeling and experimental validation of desired local strains, where statically cultured samples (ε = 0%) serve as a control. During the course of mechanical stimulation, force responses were recorded from individual samples acquired from load cells in the compression system, used for the calculation of mechanical properties. The elastic and viscoelastic mechanical properties were deconvoluted by analyzing the dynamic responses of the cell/scaffold constructs using the equations used in Chapter 3. Alternatively, control samples (ε = 0%) were cultured and subjected to a brief mechanical testing with ε = 6% at designated time points to assess and compare the developed mechanical properties (n=6).

5.3.8 – Gene expression analysis

RNA from the cell/scaffold constructs was extracted at 14 or 42 days of compression using an RNeasy Micro Kit (Qiagen, Valencia, CA), and cDNA synthesis was executed using iScript cDNA Synthesis Kit (Bio-Rad, Hercules, CA). Scaffolds were

tangentially sectioned into five layers along the thickness of the constructs to assess gene expression in response to localized compressive strain. Negative control samples were collected from cells cultured on tissue culture plastic without exposure to OM, and after the pre-culture period (at day 0 of 3D culture in the scaffold without OM or mechanical stimulation). Real-time PCR was performed to determine osteogenic and chondrogenic gene expression with various differentiation markers using the custom primers found in Table 5.1. PCR data was analyzed by the comparative threshold cycle (C_T) method using *GAPDH* as an endogenous control [221].

5.3.9 – Morphological analysis by histology

To determine the protein expression in a spatially-controlled manner, the cell/scaffold constructs were fixed in 10% buffered-formalin overnight and sectioned tangentially to the height of the sample, followed by cutting the sections in half to compare respective staining by histology. To determine the protein expression from either osteogenic or chondrogenic phenotypes, alizarin red or alcian blue staining, respectively was performed as previously described [202]. Briefly, each half of the scaffold sections were incubated in either a 0.05% alizarin red or a 0.2% alcian blue solution before rinsing with DI water, mounted and observed under an inverted microscope (Nikon Eclipse, Melville, NY).

5.3.10 – Statistical analysis

All experiments were conducted at minimum in triplicate (n = 3), and data is represented as mean ± standard deviation or standard error of means. Each set of data was subjected to statistical analysis using SPSS (v.19.0) to determine significance by one-way analysis of variance (ANOVA) with Tukey's HSD post-hoc. A value of $p \leq 0.05$ was regarded as statistically significant.

5.4 – Results

5.4.1 – Scaffold characterization

Monolithic core-shell scaffold characterization

Discrete monolithic three-dimensional electrospun microfibrous scaffolds with varied core-shell dimensional ratios were synthesized to investigate the effects of core size on the bulk compressive mechanical properties, while maintaining relatively homogenous overall fiber diameters. Electrospun scaffolds with varying core-shell dimensional ratios were fabricated by sequentially modulating the core to shell flow rates while maintaining a total volumetric flow rate of 11 mL/hr. Scaffolds consisting of microfibers with the presence of no core was generated by purely electrospinning purely

shell polymeric solution at a core:shell flow rate ratio of 0:11 mL/hr (Figure 5.1A). Through systematically electrospinning variations of the core:shell flow rate ratio at 1mL/hr increments (1:10, 2:9, 3:8, 4:7, 5:6 & 6:5 mL/hr) scaffolds composed of homogenous fibers with increasing core-shell dimensional ratios can be fabricated as seen in Figures 5.1 B-G. The respective core/overall fiber diameters, in μm, for each of these conditions are as follows: 0.00±0.00/11.50±0.78 for 0:11 mL/hr, 1.91±0.16/9.85±0.78 for 1:10 mL/hr, 2.42±0.27/9.79±0.61 for 2:9 mL/hr, 3.89±0.63/8.71±0.51 for 3:8 mL/hr, 4.50±0.72/8.86±0.71 for 4:7 mL/hr, 6.41±0.16/9.85±0.48 for 5:6 mL/hr, and 7.91±0.16/9.63±0.82 for 6:5 mL/hr.

All of the 3D scaffolds with varying core diameters which were tested were cut from electrospun mats to have dimensions of 6 mm in diameter with an approximate thickness of 3 mm. The scaffolds composed of monolithic cylindrical fibers were subjected to compressive stress-relaxation testing to determine the bulk mechanical properties. The stress-strain curves (Figure 5.1H) for scaffolds of different core diameters were used to measure the equilibrium moduli for each respective condition shown in Figure 5.1I. The resulting moduli was inversely related to the increase in core diameter gradually decreasing as the core:shell flow rate ratio increased. The measured equilibrium moduli for each flow rate ratios are 18.59±2.37 kPa for 0:11 mL/hr, 14.82±1.77 kPa for 1:10 mL/hr, 13.66±1.82 kPa for 2:9 mL/hr, 10.12±1.27 kPa for 3:8 mL/hr, 8.70±0.76 kPa for 4:7 mL/hr, 5.57±1.62 kPa for 5:6 mL/hr, and 3.11±0.81 kPa for 6:5 mL/hr.

Linear and biphasic gradient scaffold fabrication and characterization

Through temporal regulation of the core and shell polymeric flow rates, fabrication of monolithic scaffolds possessing continuous gradients of core-shell dimensional ratios were engineered. Linear and biphasic gradients were designed and fabricated by dynamically increasing and decreasing the core and shell flow rates, respectively, using the protocols shown in Figure 5.2A & Figure 5.3A. Representative cross-sectional SEM images of full-thickness scaffolds exhibit the spatial regulation of the core-shell dimensional ratios with core and overall fiber diameters similar to those seen in the discrete homogenous scaffolds used to determine the bulk scaffold equilibrium moduli. The linear gradient scaffolds have a continuous gradual increase in core diameter starting from the bottom to the top coinciding with the increase in core flow rate and decrease in shell flow rate (Figure 5.2B). Additionally, the biphasic gradient scaffolds exhibited a core-shell dimensional ratio continuously increasing from the bottom to the center of the scaffold and decreasing back down to a homogenous microfiber with no core present (Figure 5.3B).

Strain gradient modeling and experimental validation

With the successful generation of monolithic gradient scaffolds, and due to the variations in mechanical properties as a result of varying the core diameter of electrospun fibers, we analyzed the local strain of 3D scaffolds in a depth-dependent manner. Firstly, the localized strain gradients were modelled based upon the measured mechanical moduli for individual core-shell dimensional ratios. Continuous moduli equations were applied to three-dimensional cylindrical scaffolds to observed local changes in compressive strain when subjected to a single applied global compressive strain. Both the linear and biphasic gradient conditions were analyzed by a parametric sweep using total strain as a variable. It was determined that a 6% global strain will achieve a range of local stain approximately ranging from 3% to 16% (Figures 5.4A & B).

Next, experimental validation of designed gradients was confirmed using a DIC technique to track local changes in compressive strain with respect to the 6% global strain applied to the acellular scaffolds for both linear and biphasic gradients. Discrete features made on the scaffolds were used to calculate the local strains relative to the top of the scaffold (global strain). Both the linear gradient (Figure 5.4C) and the biphasic gradient (Figure 5.4D) electrospun scaffolds followed the trends of the computational modelling very well for several independent scaffolds confirming a gradient of mechanical properties based upon the variations in core-shell dimensional ratios. Furthermore, over

the course of the experiment, samples were collected at Days 14 and 42, and subjected to similar analyses to determine whether the scaffold either subjected to mechanical stimulation or cultured statically maintain their strain gradients. Interestingly, it was determined that the scaffolds in fact do maintain their local strain gradients over all experimental conditions. This includes both dynamically compressed (Figures 5.5A & B) and statically cultured (Figures 5.5C & D) linear gradients, as well as the biphasic gradients either subjected to mechanical stimulation (Figures 5.6A & B) or left alone to grow statically (Figures 5.6C & D).

5.4.2 – Dynamic mechanical analysis of cell/scaffold constructs

Over the course of 42 days of the daily dynamic mechanical stimulation culture duration, the mechanical properties of the cell/scaffold constructs were simultaneously measured at distinct time points. In Figure 5.7A and Figure 5.7B we are able to show the evolution in the elastic and viscoelastic moduli of the cell/scaffold constructs, respectively, during the culture period of up to 42 days. After 7 days of preculture, on Day 0 of culture, the cell/scaffold constructs were briefly compressed to determine the baseline mechanical properties of the gradients. The linear gradient exhibited an elastic modulus of 41.38 ± 18.04 kPa and a viscoelastic modulus of 1.24 ± 0.49 kPa whereas the biphasic gradient an elastic modulus of 42.38 ± 9.54 kPa and a viscoelastic modulus of 2.26 ± 0.75 kPa. There were no noticeable significant changes in the elastic or viscoelastic

modulus for all conditions after 7 days of mechanical stimulation for the daily stimulated gradient conditions. It should be noted that the control gradient constructs that were not subjected to mechanical stimulation, except for brief durations at designated time points, exhibited both greater increases in both elastic and viscoelastic moduli throughout the culture duration as compared to scaffolds of similar design and composition that were compressed daily. In a similar fashion, the viscoelastic moduli of the daily stimulated constructs were noticeably lower than the statically cultured constructs. Overall, both the elastic and viscoelastic moduli increased over the 42 day course of culture regardless of mechanical gradient scaffold conditions, but appeared to hit a saturation point after about 35 days. While the statically cultured linear and biphasic constructs had greater elastic and viscoelastic moduli as compared to the daily stimulated samples it is interesting that the compressed biphasic scaffolds had greater viscoelastic moduli compared to that of the linear gradient condition.

5.4.3 – Spatially-controlled osteogenic/chondrogenic differentiation of hMSCs under mechanical stimulation

To analyze the effects of spatially controlled compressive strain in response mechanical stimulation at the transcriptional level that modulated the differentiation of hMSCs, the expression of osteogenic or chondrogenic genes were examined in a spatially controlled manner. These genes (Table 5.1) are known to regulate phenotype-specific

ECM deposition, and are closely related to response of the mechanical properties and magnitude-dependent compressive strains of the engineered gradients as shown previously in Chapter 3. It should be noted that both types of these gradient constructs were cultured in osteogenic differentiation media. Confirmation that the gradient scaffolds are differentiating towards an osteoblastic-like phenotype is indicated by increases in osteogenic markers *COL1A1 and SPARC (ON)* over the course of 14 days (Figures 5.8A & B and Figures 5.9A & B) and 42 days (Figures 5.8E & F and Figures 5.9E & F) when comparing the statically cultured sampled to those subjected to 6% compressive strain. Interestingly, the application of dynamic compression suppressed many of these osteogenic markers in a spatially controlled manner due to regions of the scaffolds subject to high local values of compressive strain. This is especially evident in the trends seen for *COL1A1 and SPARC (ON)* expression at Day 14 and Day 42 where for the linear gradient scaffolds the top had the lowest expression (highest strain), the middle had an intermediate, and the bottoms had the greatest expression (lowest strain). The osteogenic expression for the biphasic samples was not as evident, but difference in expression was the greatest at day 14 where the top of the scaffolds (lowest strain) exhibited the greatest *COL1A1 and SPARC (ON)* fold change as compared to the middle of the scaffolds which had the greatest areas of strain.

In a contradicting manner towards osteogenesis, the spatially controlled strain regimens of the constructs enhanced the chondrogenesis of hMSCs cultured in the 3D

linear gradient scaffolds (Figures 5.8C & D and Figures 5.8G & H) as well as the biphasic gradient scaffolds (Figures 5.9C & D and Figures 5.9G & H). Both *ACAN* and *COL2A1* exhibited upregulation in comparison to the statically cultured samples within the regions of high localized compressive strain. Interestingly, the linear gradients showed the highest expression of these markers within the middle sections, and not as much in the very top regions which possessed the highest magnitudes of strain. Similarly, the biphasic gradients were able to enhance chondrogenic gene expression in the middle regions, which had the greatest strain levels as compared to statically cultured scaffolds, with the exception of *COL2A1* at the Day 42 time point. As designed and expected, the expression pattern of chondrogenic genes were closely related to the mechanical properties and compressive localized strains of the cell/scaffold constructs.

5.4.4 – Spatially-controlled ECM deposition by dynamic mechanical stimulation

To determine spatially controlled tissue development, ECM deposition was examined by histological staining in a depth dependent manner at 42 days of culture for both linear and biphasic gradient scaffolds dynamically or statically cultured in osteogenic media (Figure 5.10Figure 3.). The scaffolds were sectioned parallel to the deposition of fibers and the top, middle, and bottom constructs were cut in half to sequentially observe ECM secretion within the same sample layer. Histological examination was conducted with both osteogenic and chondrogenic-specific stains, *i.e.*, alizarin red for calcium

deposition and alcian blue for GAG, respectively. As expected, for alizarin red staining, the static culture condition showed the greatest calcium deposition throughout the entire thickness of the gradient scaffolds. Comparatively, there was a noticeable decrease in the intensity of staining coinciding with the areas of high compressive strain, the top of the linear gradient and middle of the biphasic gradient. Although, while GAG deposition was determined by alcian blue staining there was no significant observable differences in the intensity of stain between either type of gradient or culture condition.

5.5 – Discussion

It is well known that biochemical and biophysical factors modulate stem cell differentiation [226]. While most attention in the field of osteochondral tissue engineering is focused on using biochemical means for MSC differentiation, very little attention had been paid to the responsiveness of these cells to mechanical stimulation for development of chondro- and osteogenesis. As discussed in Chapter 3, MSC differentiation towards either a chondrogenic or osteogenic lineage is magnitude-dependent as a result of compressive strain. By modulating core and shell polymeric flow rates homogenous monolithic scaffolds of varying core dimensions were fabricated and tested for their bulk mechanical properties. Our data indicates that by using an aqueous soluble polymer for the core material, the microfibers can become hollow structures altering their mechanical properties. As the core dimension becomes larger with respect

to the overall fiber diameter, the bulk moduli of the scaffolds decreases, while to total apparent porosity within the scaffold increases. This finding is consistent with data presented in Chapter 4 showing that as the bulk porosity increase the mechanical properties will cohesively lower in a predictable manner. Therefore, the design and engineering of singular scaffolds containing continuous gradient structures of these core-shell dimensional ratios was carried out.

Three-dimensional electrospun scaffolds consisting of both linear and biphasic core-shell dimensional gradients were fabricated in a single-step fabrication technique. These dimensional gradients were modeled based upon the data acquired from the homogenous monolithic scaffold moduli to show that due to the material property gradient we can control localized strain gradients when subjected to a single global strain. Indeed, our experimental results confirmed the model strain gradients proposed to induce the desired magnitudes of compressive strain in a spatially-controlled manner, whereby stem cell culture and differentiation is highly influenced by mechanical stimulation. While the cell/scaffold constructs that were only subjected to biochemical cues for osteogenic differentiation showed preferential transformation towards osteoblasts as expected, we were able to observe a fantastic control of the differentiation of these cells towards both chondrocytes and osteoblasts in single constructs that were dynamically cultured in mechanical gradient scaffolds. The linear gradient samples not only maintained their strain gradients over the course of 42 days of culture, but areas of

high compressive strain downregulated the expression of both gene and protein expression toward an osteogenic lineage, while upregulating chondrogenic expression of similar analyses. Interestingly, this trend was also observed in the development of the biphasic gradient scaffolds where the top and bottom most surfaces of the scaffolds preferentially differentiated towards an osteogenic lineage due to the lower magnitudes of compressive strain, and the area contained in the center of the scaffolds with the greatest core-shell dimensional ratios were directed towards chondrogenesis. Due to the maintenance of the strain gradients over the course of dynamic stimulation it can be conferred that the local mechanical properties can also be extrapolated to determine the evolution of the tissue development. It would be expected that the overall localized mechanical properties will correlate well with the differences in mechanical properties observed in physiological tissue, where the elastic modulus of bone is several order of magnitudes greater than that of cartilage. By dynamically culturing a single stem cell source in a gradient consisting of mechanical properties the generation of different cellular phenotypes is shown to be controlled in a manner consistent with our previous and predicted work. All of these results further suggest that stem cells are highly mechano-sensitive and respond accordingly to their immediate dynamic mechanical surroundings.

Ultimately, the all-inclusive analysis for both the biochemical and mechanical properties of the dynamically cultured linear and biphasic scaffolds provides an in-depth

look at how spatially controlled magnitudes of strain can influence the multi-phenotypic differentiation of stems cells towards interfacial musculoskeletal tissue. The results from this work indicate that stem cell differentiation can be modulated by dynamic strain gradients even in the presence of a biochemical cue. These results further provide a mechanistic idea for how localized mechanical cues override the directed biochemical cues to provide groundwork for osteochondral interface tissue engineering. The cohesive data has been able to address the limitations in regenerating tissue composed of multi-cell types, regulated by both the global biochemical factors and the local mechanical stimuli. This study therefore provides a new outlook on directing a single multipotent stem cell source into multi-phenotypic musculoskeletal tissues in a spatially controlled manner by combining both mechanical and biochemical cues.

5.6 – Conclusions

Dynamic compressive loading to scaffolds consisting of spatially controlled mechanical properties in a depth-dependent manner can vary the local magnitudes of strain. This approach of mechanical stimulation allows for a novel means to directing multi-phenotypic stem cell differentiation in contrast to providing specific biochemical cues. In this experiment, it has been shown that MSCs can differentiate in a spatially controlled and phenotype-specific manner in response to different magnitudes of localized dynamic compressive strain in monolithic scaffolds. Ultimately, these results

suggest that MSCs can be controlled by varying the strain regimens of 3D scaffolds by modulating the mechanical properties of scaffolds in a depth-dependent manner. Therefore, this work provides a novel strategy to address interfacial tissue engineering by modulation of phenotype-specific MSC differentiation due to mechanical property gradients and the resulting localized strain gradients by mechanical stimulation.

5.7 – Tables & Figures

Primer	Forward	Reverse
GAPDH	*5'*-GCAAATTCCATGGCACCGT-*3'*	*5'*-TCGCCCCACTTGATTTTGG-*3'*
Osteogenic		
COL1A1	*5'*-CAACCTGGATGCCATCAAAG-*3'*	*5'*-TGCTGATGTACCAGTTCTTCTGG-*3'*
SPARC (ON)	*5'*-TGGACTCTGAGCTGACCGAATT-*3'*	*5'*-AGAAGGTTGTTGTCCTCATCCC-*3'*
Chondrogenic		
ACAN	*5'*-GTGATCCTTACCGTAAAGCCCAT-*3'*	*5'*-TCTCATTCTCAACCTCAGCGA-*3'*
COL2A1	*5'*-GGCAATAGCAGGTTCACGTACA-*3'*	*5'*-CGATAACAGTCTTGCCCCACTT-*3'*

TABLE 5.1. CUSTOM REAL-TIME POLYMERASE CHAIN REACTION (PCR) PRIMERS.

Sequences of forward and reverse primers for osteogenic and chondrogenic genes.

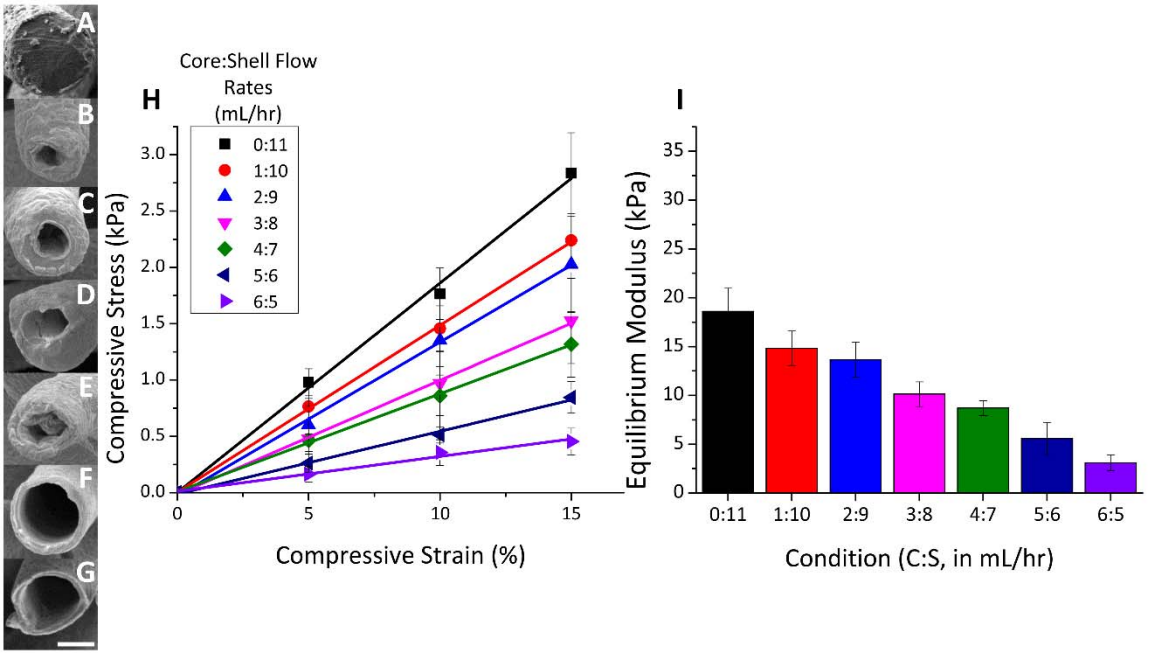

FIGURE 5.1. MECHANICAL PROPERTIES OF CORE-SHELL MICROFIBER SCAFFOLDS WITH DIFFERENT CORE/SHELL DIAMETER RATIOS RESULTED FROM ALTERING CORE:SHELL FLOW RATE DURING ELECTROSPINNING.

Representative cross-sectional images of electrospun core-shell microfibers with the following core:shell flow rate ratios (in mL/hr) during electrospinning. (A) 0:11, (B) 1:10, (C) 2:9, (D) 3:8, (E) 4:7, (F) 5:6 & (G) 6:5. (H) Representative compressive stress-strain graphs of three-dimensional electrospun scaffolds resulted from different core:shell flow rates. (I) Equilibrium moduli of electrospun scaffolds exhibiting decreased mechanical properties with increasing core:shell flow rate ratios (core diameter). Scale bar = 5 µm

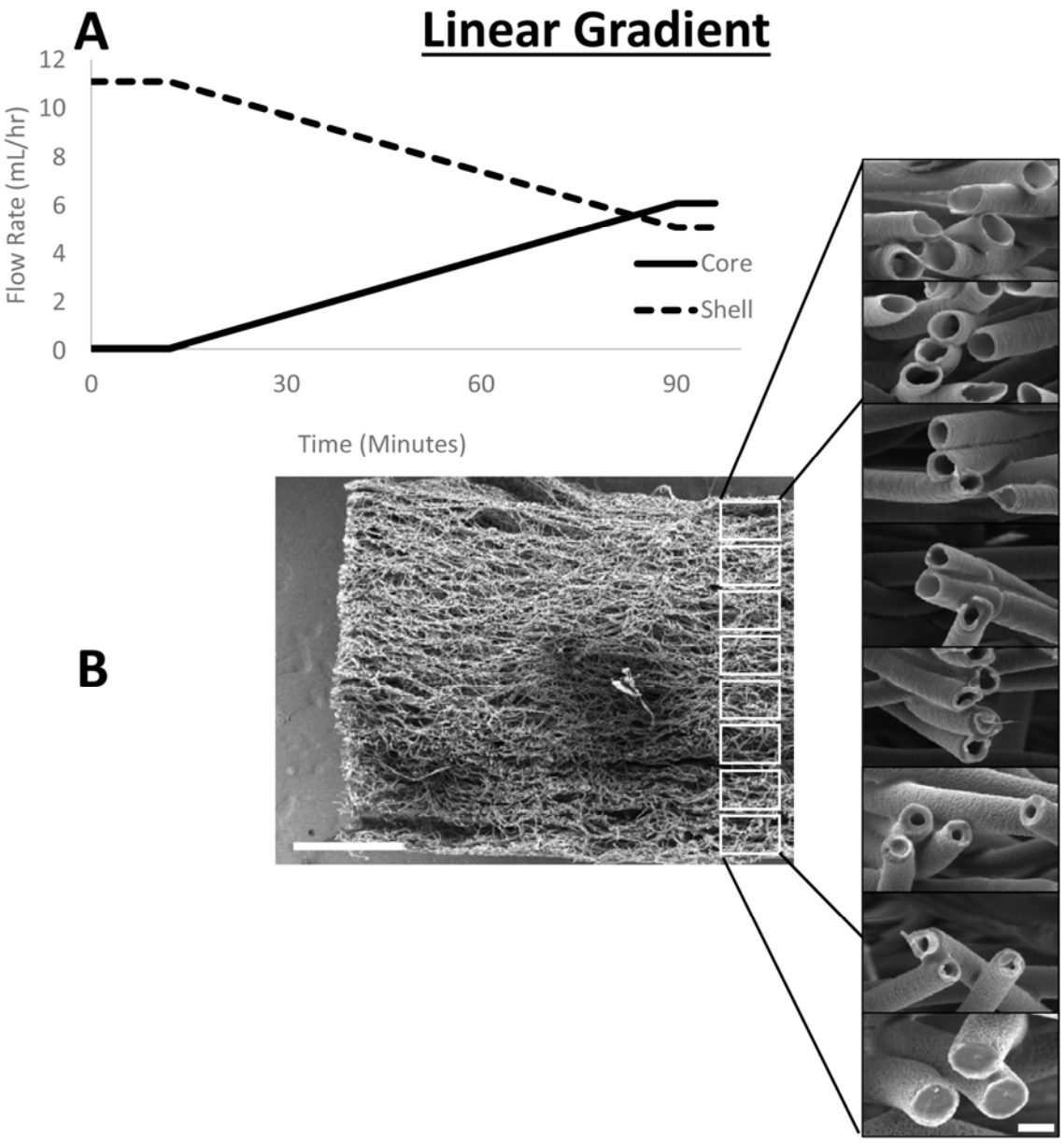

FIGURE 5.2. GENERATION AND CHARACTERIZATION OF A LINEAR GRADIENT IN THE HOLLOW CORE DIAMTER WITH RESPECT TO THE THICKNESS OF THE SCAFFOLD UNDER RECIPROCAL CORE:SHELL FLOW RATE CONTROL.

Monolithic scaffolds composed of varying core-shell dimensional ratios are fabricated by dynamically altering the core and shell polymeric flow rates. (A) Core and shell flow rates were reciprocally controlled while maintaining a total combined flow rate of 11 mL/hr. (B) A cross-sectional SEM image of the electrospun scaffold shows a continuous change

in the hollow core size in a depth-dependent manner (insets) with a relatively homogenous overall fiber diameter. Scale bars – 1mm, 10µm

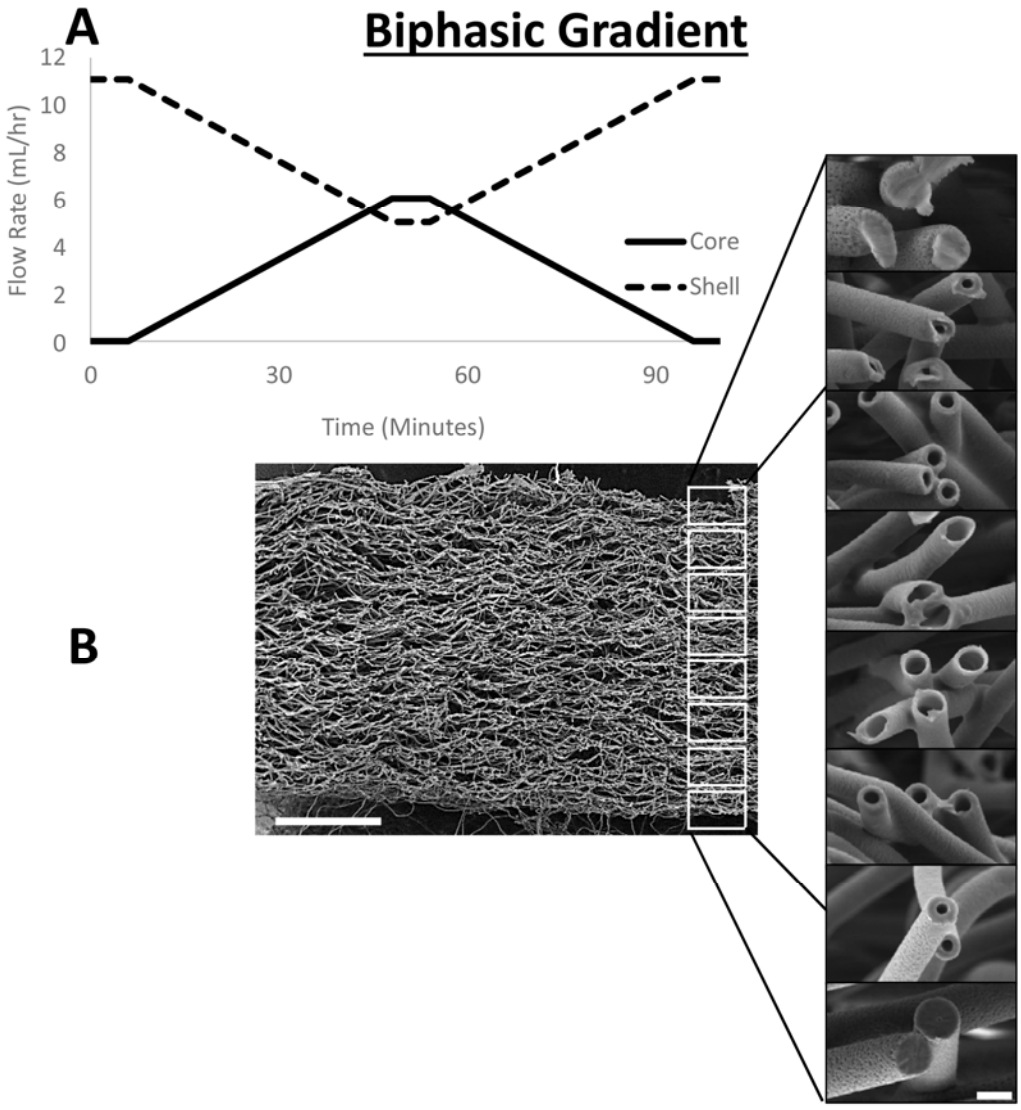

FIGURE 5.3. GENERATION AND CHARACTERIZATION OF A BIPHASIC GRADIENT IN THE HOLLOW CORE DIAMTER WITH RESPECT TO THE THICKNESS OF THE SCAFFOLD UNDER RECIPROCAL CORE:SHELL FLOW RATE CONTROL.

Monolithic scaffolds composed of varying core-shell dimensional ratios are fabricated by dynamically altering the core and shell polymeric flow rates. (A) Core and shell flow rates were reciprocally controlled while maintaining a total combined flow rate of 11 mL/hr. (B) A cross-sectional SEM image of the electrospun scaffold shows a biphasic change in the hollow core size in a depth-dependent manner (insets) with a relatively homogenous overall fiber diameter. Scale bars – 1mm, 10µm

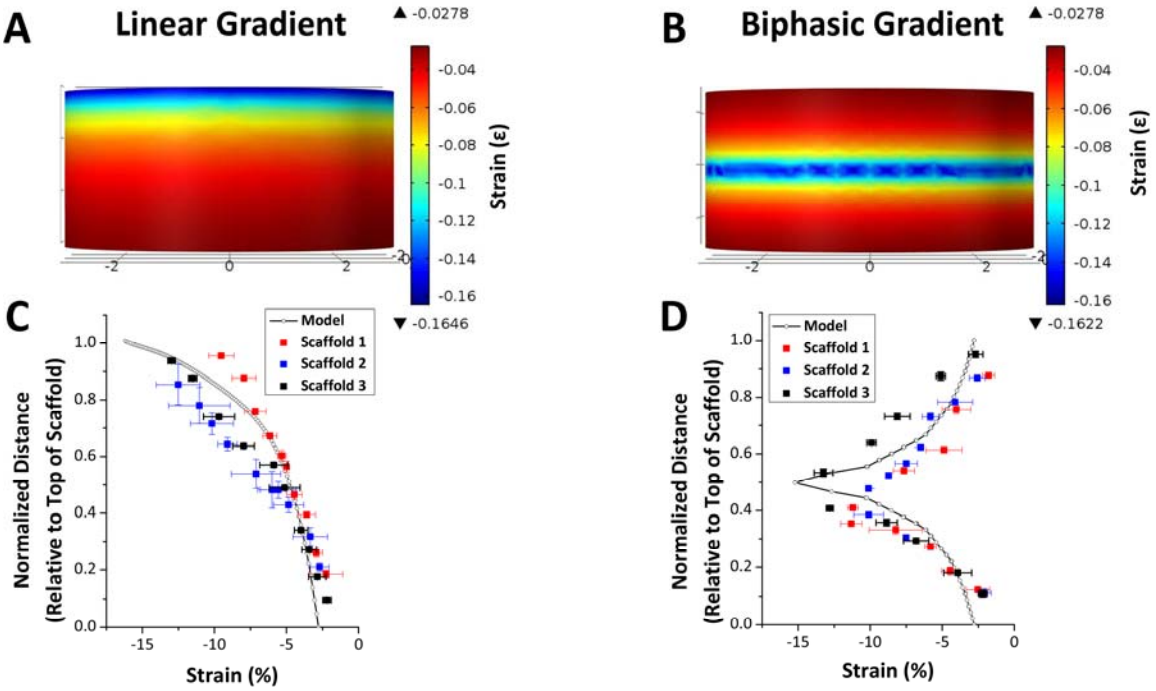

FIGURE 5.4. A COMSOL MODELING OF LINEAR AND BIPHASIC STRAIN GRADIENTS AND THEIR EXPERIMENTAL VALIDATION.

A COMSOL modeling was utilized to predict strain gradients generated by the scaffolds with (A) a linear or (B) biphasic core size gradient under compressive loading. The model predictions were compared to experimental measurements by a digital image correlation (DIC) technique to track local changes of compressive strain for both (C) linear and (D) biphasic gradients.

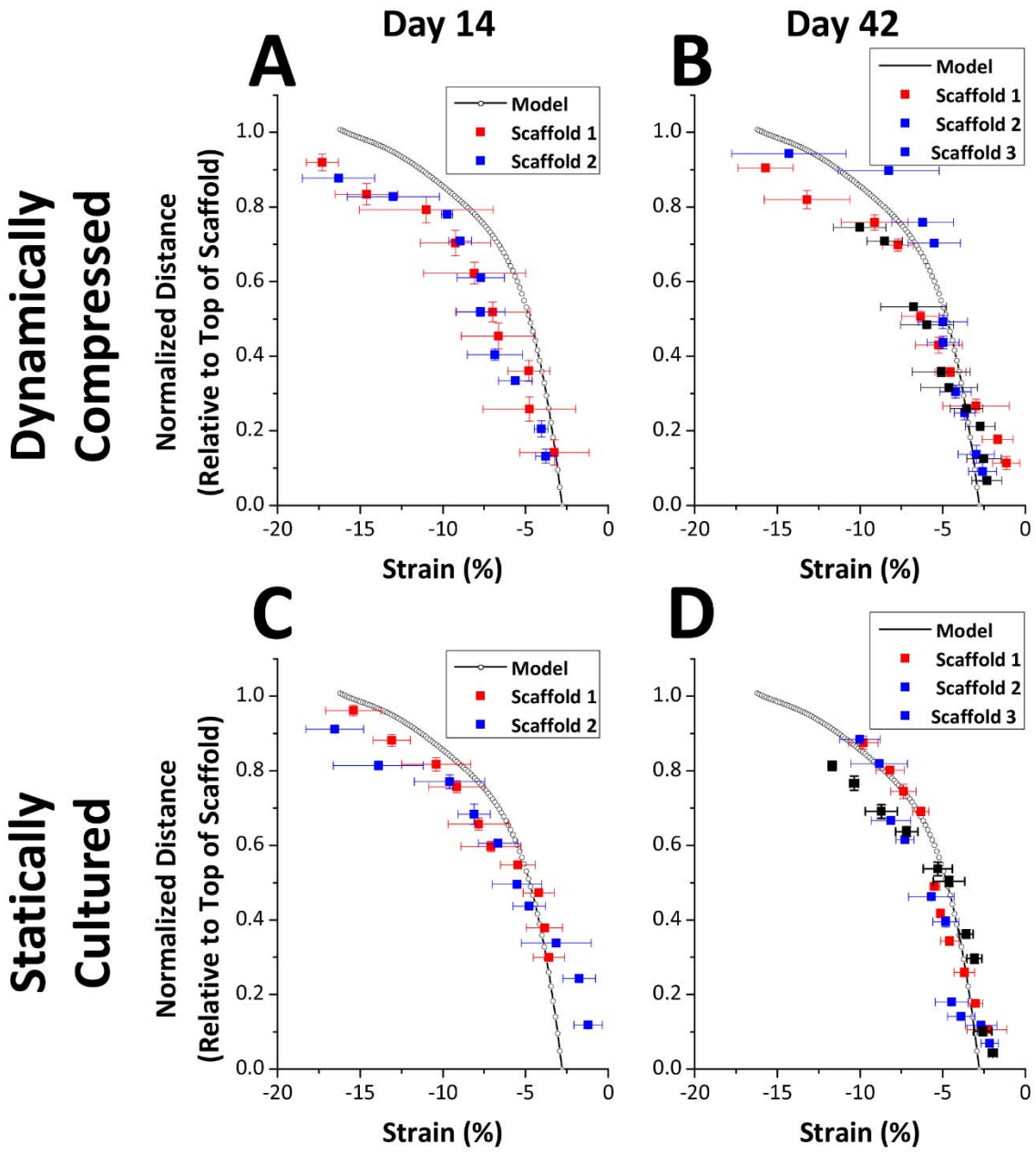

FIGURE 5.5. MAINTAINANCE OF LINEAR STRAIN GRADIENTS DURING CELL CULTURE.

The material designed strain gradient was maintained during either (A, B) dynamic or (C, D) static cell culture at (A, C) Day 14 or (B, D) Day 42.

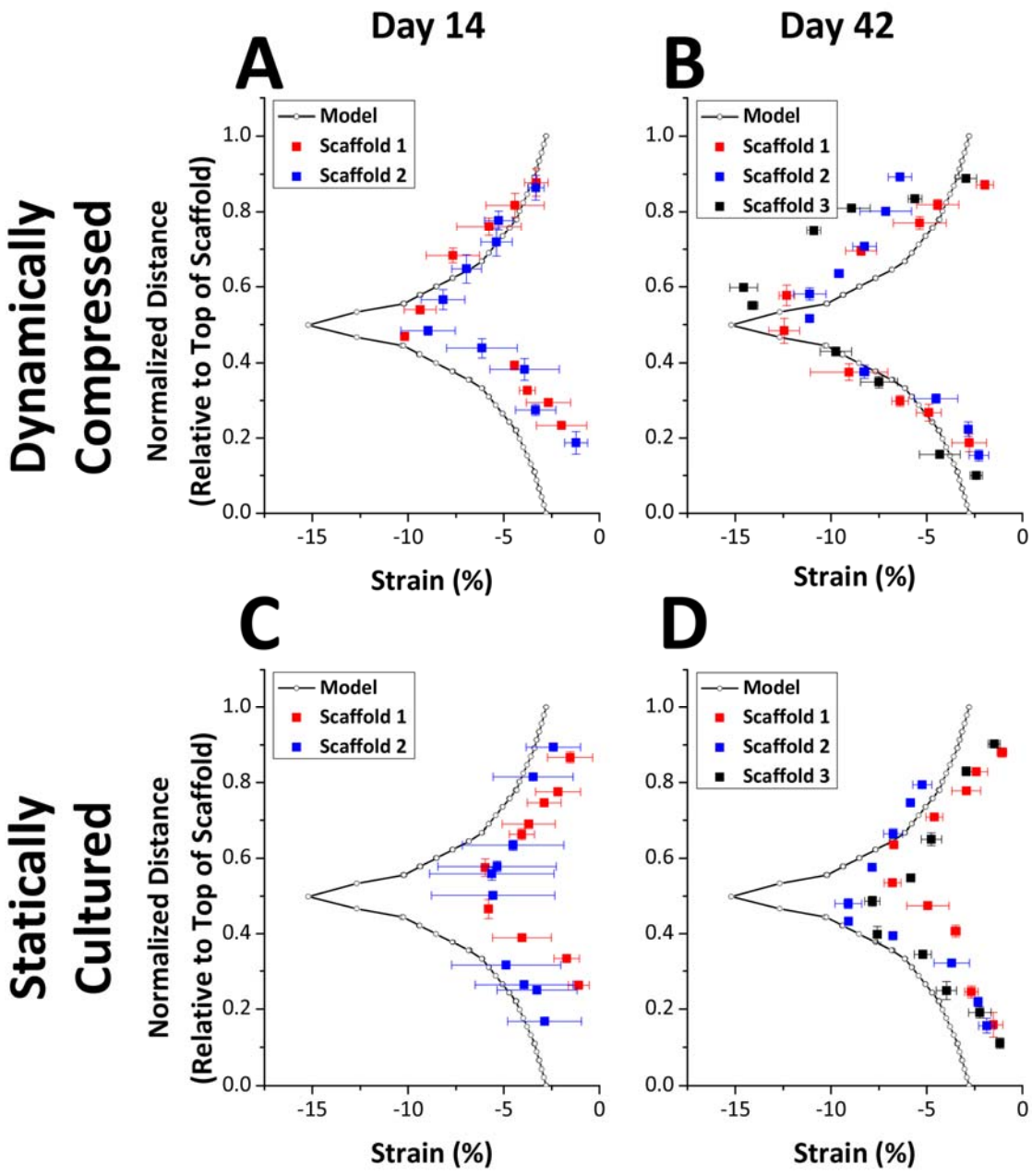

FIGURE 5.6. MAINTAINANCE OF BIPHASIC STRAIN GRADIENTS DURING CELL CULTURE.

The material designed strain gradient was maintained during either (A, B) dynamic or (C, D) static cell culture at (A, C) Day 14 or (B, D) Day 42.

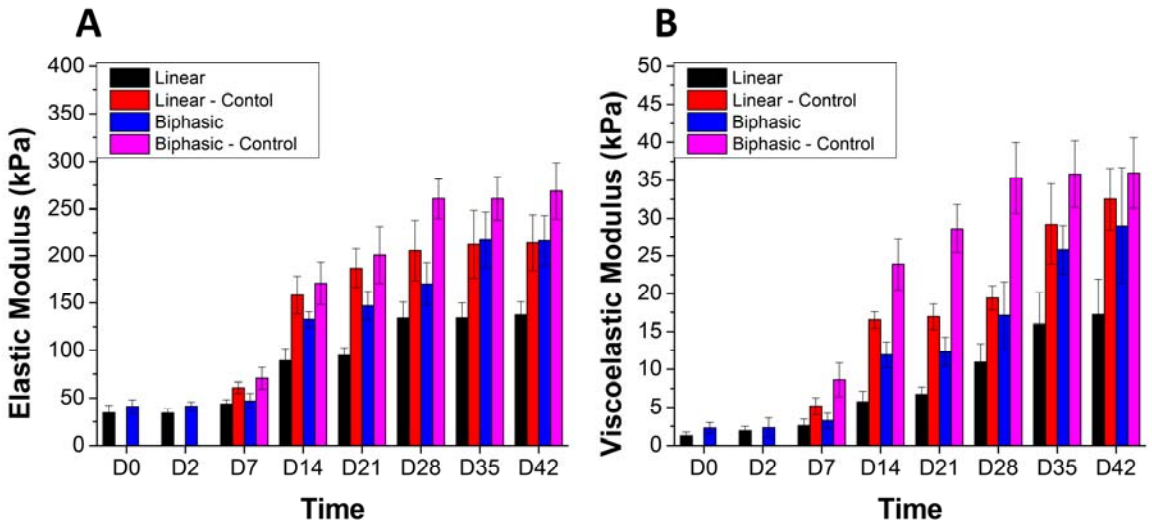

FIGURE 5.7. DYNAMIC MECHANICAL ANALYSIS OF CELL/SCAFFOLD CONSTRUCTS WITH VARIOUS ENGINEERED GRADIENT CONFIGURATIONS AND CULTURE DURATIONS.

Mechanical properties of the cell/scaffold gradient constructs was assessed by the deconvolution of (A) elastic and (B) viscoelastic moduli and analyzed at different time points up to 42 days (n=6).

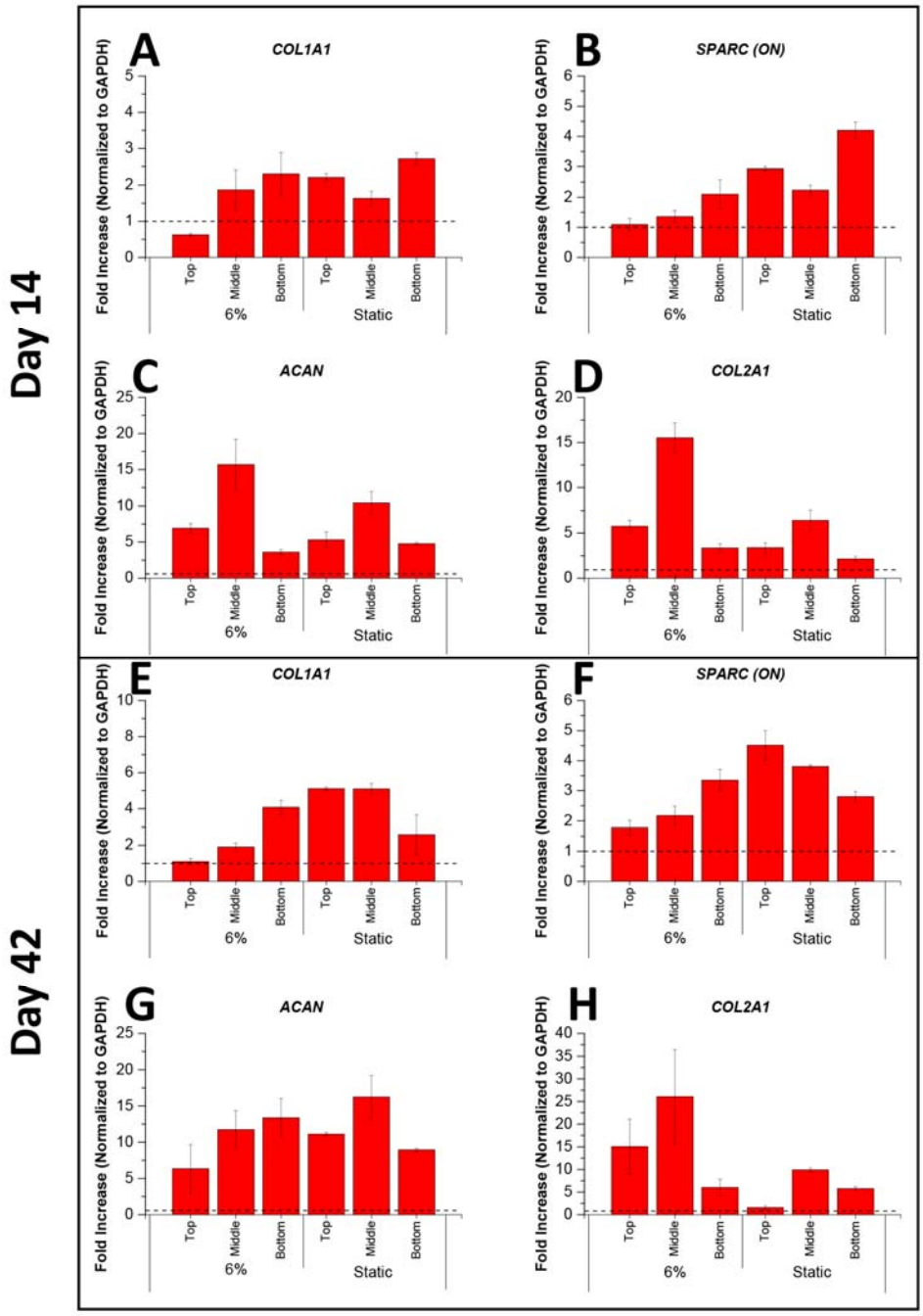

FIGURE 5.8. THE OSTEOGENIC OR CHONDROGENIC DIFFERENTIATION OF HMSCS IN AN ENGINEERED LINEAR STRAIN GRADIENT SCAFFOLD AS DETERMINED BY RELATIVE GENE EXPRESSION.

The relative gene expression of hMSCs in electrospun linear gradient scaffolds either under dynamic compressive or static culture conditions for (A-D) 14 and (E-H) 42 days

determined by qRT-PCR for osteogenic markers, (A, E) *COL1A1* and (B, F) *SPARC (ON)*, and chondrogenic markers, (C, G) *ACAN* and (D, H) *COL2A1*. Each gene expression was normalized to that of the cells before being cultured in the scaffold (dashed lines).

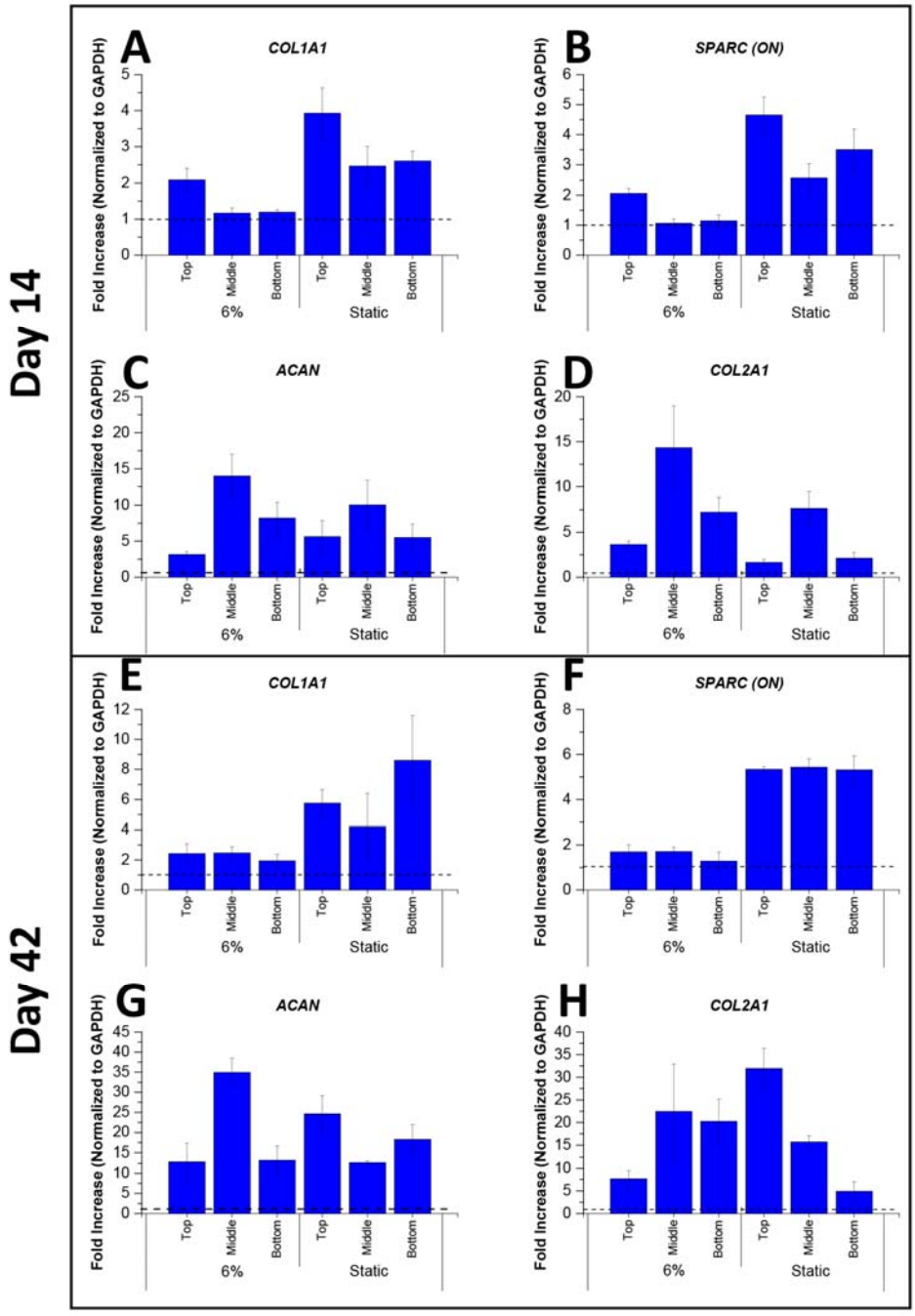

FIGURE 5.9. THE OSTEOGENIC OR CHONDROGENIC DIFFERENTIATION OF HMSCS IN AN ENGINEERED BIPHASIC STRAIN GRADIENT SCAFFOLD AS DETERMINED BY RELATIVE GENE EXPRESSION.

The relative gene expression of hMSCs in electrospun biphasic gradient scaffolds either under dynamic compressive or static culture conditions for (A-D) 14 and (E-H) 42 days

determined by qRT-PCR for osteogenic markers, (A, E) *COL1A1* and (B, F) *SPARC (ON)*, and chondrogenic markers, (C, G) *ACAN* and (D, H) *COL2A1*. Each gene expression was normalized to that of the cells before being cultured in the scaffold (dashed lines).

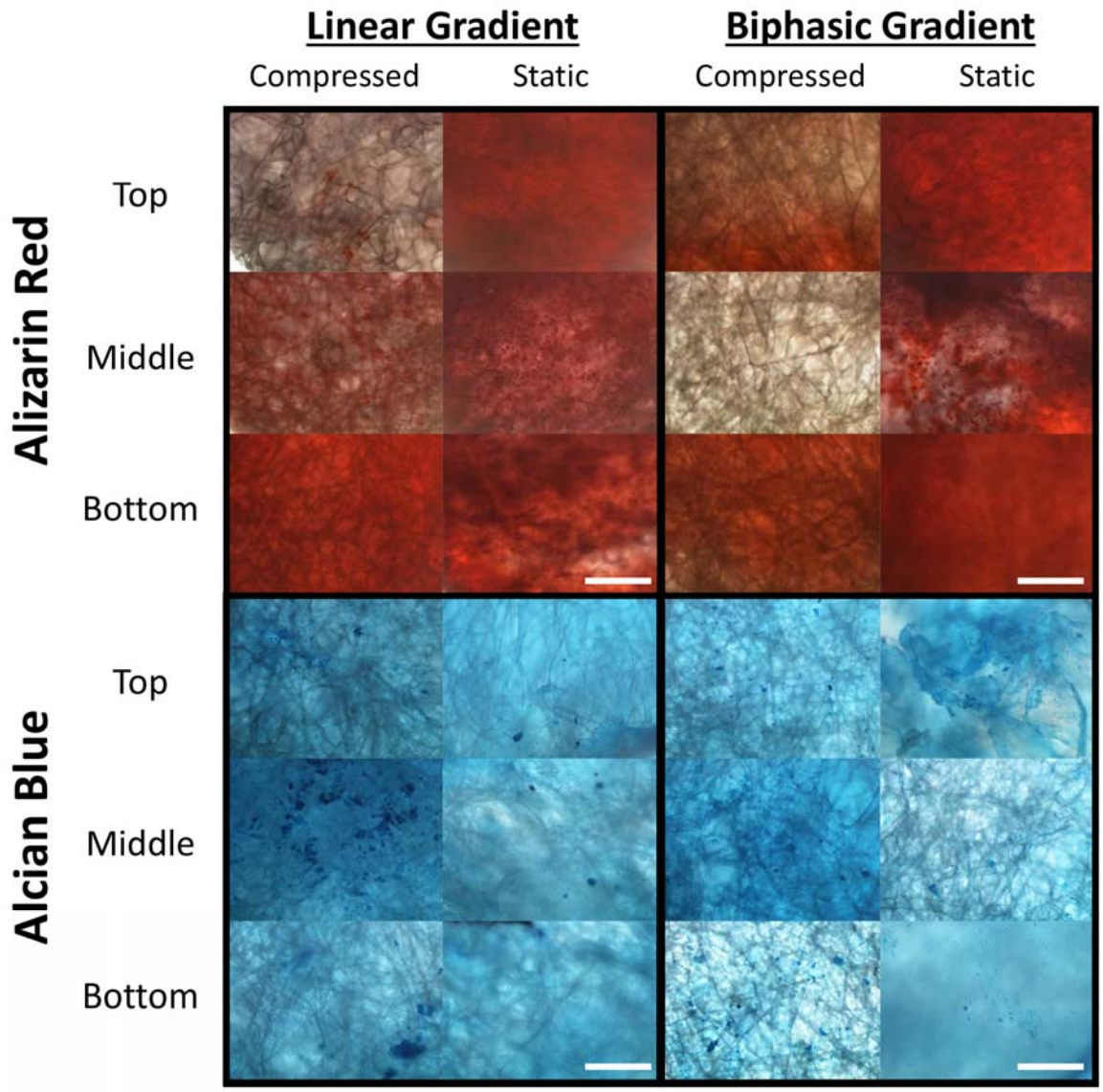

FIGURE 5.10. REPRESENTATIVE HISTOLOGY IMAGES OF CELL/SCAFFOLD CONSTRUCTS CULTURED UNDER VARIOUS GRADIENT CONDITIONS EXHIBITING DIFFERENT ECM COMPOSITIONS.

The cell/scaffold constructs with a linear or biphasic gradient, cultured under dynamic compressive stimulation for up to 42 days were subjected to histology imaging (alizarin red for calcium and alcian blue for glycosaminoglycan) to assess spatially controlled ECM deposition. Scale bars – 250 µm

CHAPTER 6 – CONCLUSIONS

6.1 – Summary

The work presented in this dissertation used combinatorial methodologies for directing stem cell differentiation by modulating magnitudes of compressive strain with mechanical stimulation, controlling micro- and macro-electrospun fiber scaffolds mechanics, and spatially controlling the mechanical properties of scaffold in a depth-dependent manner. It was demonstrated that MSCs differentiate in a magnitude-dependent and phenotype-specific manner in response to different magnitudes of dynamic compressive strain suggesting that MSCs are mechano-responsive and their multi-phenotypic differentiation can be controlled by varying the strain regimens. Additionally, it was shown that the mechanical properties of core-shell electrospun fibers can be modulated by controlling the composition and the dimension of core, decoupled from the cell-interfacing surface chemistry. More importantly, it was shown that mechanical properties of such fibers/scaffolds at the micro- and macroscale can be independently regulated by modulating micro- and macro-structure. Finally, spatial control of the mechanical properties of individual core-shell fibers in a monolithic scaffold was able to modulate the preferential multi-phenotypic differentiation of MSCs when subjected to dynamic compressive strain.

Overall, the aim of the work was to analyze the influence of mechanical stimulation on spatially controlled multi-phenotypic MSC differentiation. Indeed it was shown that MSC differentiation is highly regulated in response to mechanical loading. Taken all together these findings show that we can control stem cell differentiation by way of mechanical stimulation pertaining to the magnitudes of compressive strain they experience in lieu of biochemical cues commonly used for osteochondral tissue regeneration. Thus, this work provides an insight into additional avenues for regulating the morphogenesis of the osteochondral interfacial tissue via spatially controlled differentiation of a single stem cell source besides the commonly used biochemical directives.

6.2 – Future Directions

There are several additional avenues by which this work can further be enhanced to recapitulate the osteochondral interface for suitable use as a tissue replacement alternative. While electrospun microfibers provide a facile technique to generate 3D scaffolds that allow for complete cellular infiltration, they are orders of magnitude greater than native ECM found within physiological tissue. The inherently large pore size in the microfibrous scaffolds delays tissue maturation, especially on anchorage-dependent cells (*i.e.*, MSCs), requiring prolonged cell culture durations. Therefore, the feasibility of incorporating the advantages of a hydrogel that fills voids in the microfibrous structure to

provide adhesion sites to the seeded cells after hydro-gelation by cell culture media during cell seeding would alleviate these concerns. If one were to incorporate a third polymeric layer on the outside of the core-shell mechanical gradient consisting of a thermosensitive hydrogel, the stem cells can then be suspended within the large pores rather than directly anchored to the microfiber surface. Not only will this provide a more physiologic-like culture environment, but should further develop mature tissue morphogenesis.

Additionally, to further enhance the spatial differentiation of a single multi-potent stem cell source into a seamless transition of cartilage to bone one can utilize the principles of additional biochemical cues. The engineered core-shell dimensional ratio gradient provides a means by which phenotype-specific drugs for differentiation, such as small molecules or growth factors, can be incorporated into the monolithic scaffolds at the time of synthesis and be used to further direct stem cell differentiation. Furthermore, while the work presented in this dissertation primarily focused on using osteogenic differentiation media as the main biochemical cue for differentiation, one can explore the use of osteochondral cocktail media such as the addition of TFG-β.

Following the completion of the proposed studies it would be suggested to test the effects of the biochemical and/or dynamic mechanical gradients in conjunction with one another to determine the efficacy of recapitulating the structure and function of the

osteochondral interface. It would be emphatically suggested to test the engineered tissue constructs *in vivo* to determine the long-term stability and performance in animal models with the aim to eventually be looked at as suitable tissue replacement strategies to treat osteochondral defects for clinical applications.

CHAPTER 7 – REFERENCES

[1] Moutos FT, Freed LE, Guilak F. A biomimetic three-dimensional woven composite scaffold for functional tissue engineering of cartilage. Nat Mater 2007;6:162-7.

[2] Temenoff JS, Mikos AG. Review: tissue engineering for regeneration of articular cartilage. Biomaterials 2000;21:431-40.

[3] Bitton R. The economic burden of osteoarthritis. Am J Manag Care 2009;15:S230-5.

[4] Yelin E, Cisternas M, Foreman A, Pasta D, Murphy L, Helmick C. National and state medical expenditures and lost earnings attributable to arthritis and other rheumatic conditions—United States, 2003. MMWR Morbidity and mortality weekly report 2007;56:4.

[5] Birnbaum H, Pike C, Kaufman R, Marynchenko M, Kidolezi Y, Cifaldi M. Societal cost of rheumatoid arthritis patients in the US. Current medical research and opinion 2010;26:77-90.

[6] Jackson RW, Dieterichs C. The results of arthroscopic lavage and debridement of osteoarthritic knees based on the severity of degeneration: a 4- to 6-year symptomatic follow-up. Arthroscopy 2003;19:13-20.

[7] Shannon FJ, Devitt AT, Poynton AR, Fitzpatrick P, Walsh MG. Short-term benefit of arthroscopic washout in degenerative arthritis of the knee. Int Orthop 2001;25:242-5.

[8] Kreuz PC, Steinwachs MR, Erggelet C, Krause SJ, Konrad G, Uhl M, et al. Results after microfracture of full-thickness chondral defects in different compartments in the knee. Osteoarthritis and cartilage / OARS, Osteoarthritis Research Society 2006;14:1119-25.

[9] Vasiliadis HS, Wasiak J. Autologous chondrocyte implantation for full thickness articular cartilage defects of the knee. Cochrane Database Syst Rev 2010;10:CD003323.

[10] Kon E, Verdonk P, Condello V, Delcogliano M, Dhollander A, Filardo G, et al. Matrix-assisted autologous chondrocyte transplantation for the repair of cartilage defects of the knee: systematic clinical data review and study quality analysis. Am J Sports Med 2009;37 Suppl 1:156S-66S.

[11] Panseri S, Russo A, Cunha C, Bondi A, Di Martino A, Patella S, et al. Osteochondral tissue engineering approaches for articular cartilage and subchondral bone regeneration. Knee surgery, sports traumatology, arthroscopy : official journal of the ESSKA 2012;20:1182-91.

[12] Lipman JM, McDevitt CA, Sokoloff L. Xenografts of articular chondrocytes in the nude mouse. Calcified tissue international 1983;35:767-72.

[13] Oliveira JM, Rodrigues MT, Silva SS, Malafaya PB, Gomes ME, Viegas CA, et al. Novel hydroxyapatite/chitosan bilayered scaffold for osteochondral tissue-engineering applications: Scaffold design and its performance when seeded with goat bone marrow stromal cells. Biomaterials 2006;27:6123-37.

[14] Erisken C, Kalyon DM, Wang HJ, Ornek-Ballanco C, Xu JH. Osteochondral Tissue Formation Through Adipose-Derived Stromal Cell Differentiation on Biomimetic Polycaprolactone Nanofibrous Scaffolds with Graded Insulin and Beta-Glycerophosphate Concentrations. Tissue Engineering Part A 2011;17:1239-52.

[15] Wang L, Zhao L, Detamore MS. Human umbilical cord mesenchymal stromal cells in a sandwich approach for osteochondral tissue engineering. J Tissue Eng Regen Med 2011;5:712-21.

[16] Rodrigues MT, Lee SJ, Gomes ME, Reis RL, Atala A, Yoo JJ. Bilayered constructs aimed at osteochondral strategies: The influence of medium supplements in the osteogenic and chondrogenic differentiation of amniotic fluid-derived stem cells. Acta Biomaterialia 2012;8:2795-806.

[17] Martin I, Miot S, Barbero A, Jakob M, Wendt D. Osteochondral tissue engineering. Journal of biomechanics 2007;40:750-65.

[18] Agrawal C, Athanasiou K, Heckman J. Biodegradable PLA-PGA polymers for tissue engineering in orthopaedics. Materials Science Forum: Trans Tech Publ; 1997. p. 115-28.

[19] Gomes ME, Ribeiro AS, Malafaya PB, Reis RL, Cunha AM. A new approach based on injection moulding to produce biodegradable starch-based polymeric scaffolds: morphology, mechanical and degradation behaviour. Biomaterials 2001;22:883-9.

[20] Guidoin MF, Marois Y, Bejui J, Poddevin N, King MW, Guidoin R. Analysis of retrieved polymer fiber based replacements for the ACL. Biomaterials 2000;21:2461-74.

[21] Holy CE, Shoichet MS, Davies JE. Engineering three-dimensional bone tissue in vitro using biodegradable scaffolds: investigating initial cell-seeding density and culture period. Journal of biomedical materials research 2000;51:376-82.

[22] Hutmacher DW, Sittinger M, Risbud MV. Scaffold-based tissue engineering: rationale for computer-aided design and solid free-form fabrication systems. Trends in biotechnology 2004;22:354-62.

[23] Mikos AG, Thorsen AJ, Czerwonka LA, Bao Y, Langer R, Winslow DN, et al. Preparation and characterization of poly (L-lactic acid) foams. Polymer 1994;35:1068-77.

[24] Mooney DJ, Baldwin DF, Suh NP, Vacanti JP, Langer R. Novel approach to fabricate porous sponges of poly (D, L-lactic-co-glycolic acid) without the use of organic solvents. Biomaterials 1996;17:1417-22.

[25] Quirk RA, France RM, Shakesheff KM, Howdle SM. Supercritical fluid technologies and tissue engineering scaffolds. Current Opinion in Solid State and Materials Science 2004;8:313-21.

[26] Shea LD, Wang D, Franceschi RT, Mooney DJ. Engineered bone development from a pre-osteoblast cell line on three-dimensional scaffolds. Tissue engineering 2000;6:605-17.

[27] Washburn NR, Simon CG, Jr., Tona A, Elgendy HM, Karim A, Amis EJ. Co-extrusion of biocompatible polymers for scaffolds with co-continuous morphology. J Biomed Mater Res 2002;60:20-9.

[28] Woodfield TB, Malda J, De Wijn J, Peters F, Riesle J, van Blitterswijk CA. Design of porous scaffolds for cartilage tissue engineering using a three-dimensional fiber-deposition technique. Biomaterials 2004;25:4149-61.

[29] Malafaya P, Pedro A, Peterbauer A, Gabriel C, Redl H, Reis R. Chitosan particles agglomerated scaffolds for cartilage and osteochondral tissue engineering approaches with adipose tissue derived stem cells. Journal of Materials Science: Materials in Medicine 2005;16:1077-85.

[30] Guo X, Park H, Liu G, Liu W, Cao Y, Tabata Y, et al. In vitro generation of an osteochondral construct using injectable hydrogel composites encapsulating rabbit marrow mesenchymal stem cells. Biomaterials 2009;30:2741-52.

[31] Augst A, Marolt D, Freed LE, Vepari C, Meinel L, Farley M, et al. Effects of chondrogenic and osteogenic regulatory factors on composite constructs grown

using human mesenchymal stem cells, silk scaffolds and bioreactors. Journal of The Royal Society Interface 2008;5:929-39.

[32] Galois L, Freyria A, Grossin L, Hubert P, Mainard D, Herbage D, et al. Cartilage repair: surgical techniques and tissue engineering using polysaccharide- and collagen-based biomaterials. Biorheology 2004;41:433-43.

[33] Langer R. Selected advances in drug delivery and tissue engineering. Journal of controlled release : official journal of the Controlled Release Society 1999;62:7-11.

[34] Mano J, Silva G, Azevedo HS, Malafaya P, Sousa R, Silva S, et al. Natural origin biodegradable systems in tissue engineering and regenerative medicine: present status and some moving trends. Journal of The Royal Society Interface 2007;4:999-1030.

[35] Thomson R, Wake M, Yaszemski MJ, Mikos A. Biodegradable polymer scaffolds to regenerate organs. Biopolymers Ii: Springer; 1995. p. 245-74.

[36] Oliveira AL, Mano JF, Reis RL. Nature-inspired calcium phosphate coatings: present status and novel advances in the science of mimicry. Curr Opin Solid St M 2003;7:309-18.

[37] Huang J, Di Silvio L, Wang M, Tanner KE, Bonfield W. In vitro mechanical and biological assessment of hydroxyapatite-reinforced polyethylene composite. Journal of materials science Materials in medicine 1997;8:775-9.

[38] Schaefer D, Martin I, Shastri P, Padera RF, Langer R, Freed LE, et al. In vitro generation of osteochondral composites. Biomaterials 2000;21:2599-606.

[39] Guo X, Wang C, Duan C, Descamps M, Zhao Q, Dong L, et al. Repair of osteochondral defects with autologous chondrocytes seeded onto bioceramic scaffold in sheep. Tissue engineering 2004;10:1830-40.

[40] Solchaga LA, Temenoff JS, Gao J, Mikos AG, Caplan AI, Goldberg VM. Repair of osteochondral defects with hyaluronan-and polyester-based scaffolds. Osteoarthritis and cartilage 2005;13:297-309.

[41] van Susante JL, Buma P, Homminga GN, van den Berg WB, Veth RP. Chondrocyte-seeded hydroxyapatite for repair of large articular cartilage defects. A pilot study in the goat. Biomaterials 1998;19:2367-74.

[42] Wang X, Grogan SP, Rieser F, Winkelmann V, Maquet V, La Berge M, et al. Tissue engineering of biphasic cartilage constructs using various biodegradable scaffolds: an in vitro study. Biomaterials 2004;25:3681-8.

[43] Rose T, Craatz S, Hepp P, Raczynski C, Weiss J, Josten C, et al. The autologous osteochondral transplantation of the knee: clinical results, radiographic findings and histological aspects. Arch Orthop Trauma Surg 2005;125:628-37.

[44] Brittberg M. Autologous chondrocyte implantation--technique and long-term follow-up. Injury 2008;39 Suppl 1:S40-9.

[45] Lane JG, Massie JB, Ball ST, Amiel ME, Chen AC, Bae WC, et al. Follow-up of osteochondral plug transfers in a goat model: a 6-month study. Am J Sports Med 2004;32:1440-50.

[46] Ahn JH, Lee TH, Oh JS, Kim SY, Kim HJ, Park IK, et al. Novel hyaluronate-atelocollagen/beta-TCP-hydroxyapatite biphasic scaffold for the repair of osteochondral defects in rabbits. Tissue engineering Part A 2009;15:2595-604.

[47] Chen J, Chen H, Li P, Diao H, Zhu S, Dong L, et al. Simultaneous regeneration of articular cartilage and subchondral bone in vivo using MSCs induced by a spatially controlled gene delivery system in bilayered integrated scaffolds. Biomaterials 2011;32:4793-805.

[48] Gao J, Dennis JE, Solchaga LA, Goldberg VM, Caplan AI. Repair of osteochondral defect with tissue-engineered two-phase composite material of injectable calcium phosphate and hyaluronan sponge. Tissue engineering 2002;8:827-37.

[49] Hung CT, Lima EG, Mauck RL, Takai E, LeRoux MA, Lu HH, et al. Anatomically shaped osteochondral constructs for articular cartilage repair. Journal of biomechanics 2003;36:1853-64.

[50] Kandel RA, Grynpas M, Pilliar R, Lee J, Wang J, Waldman S, et al. Repair of osteochondral defects with biphasic cartilage-calcium polyphosphate constructs in a sheep model. Biomaterials 2006;27:4120-31.

[51] O'Shea TM, Miao X. Bilayered scaffolds for osteochondral tissue engineering. Tissue engineering Part B, Reviews 2008;14:447-64.

[52] Sherwood JK, Riley SL, Palazzolo R, Brown SC, Monkhouse DC, Coates M, et al. A three-dimensional osteochondral composite scaffold for articular cartilage repair. Biomaterials 2002;23:4739-51.

[53] Shimomura K, Moriguchi Y, Murawski CD, Yoshikawa H, Nakamura N. Osteochondral tissue engineering with biphasic scaffold: current strategies and techniques. Tissue engineering Part B, Reviews 2014;20:468-76.

[54] Niederauer GG, Slivka MA, Leatherbury NC, Korvick DL, Harroff HH, Ehler WC, et al. Evaluation of multiphase implants for repair of focal osteochondral defects in goats. Biomaterials 2000;21:2561-74.

[55] Marquass B, Somerson JS, Hepp P, Aigner T, Schwan S, Bader A, et al. A novel MSC-seeded triphasic construct for the repair of osteochondral defects. J Orthop Res 2010;28:1586-99.

[56] Mohan N, Dormer NH, Caldwell KL, Key VH, Berkland CJ, Detamore MS. Continuous gradients of material composition and growth factors for effective regeneration of the osteochondral interface. Tissue engineering Part A 2011;17:2845-55.

[57] Dormer NH, Singh M, Zhao L, Mohan N, Berkland CJ, Detamore MS. Osteochondral interface regeneration of the rabbit knee with macroscopic gradients of bioactive signals. Journal of biomedical materials research Part A 2012;100:162-70.

[58] Wang X, Wenk E, Zhang X, Meinel L, Vunjak-Novakovic G, Kaplan DL. Growth factor gradients via microsphere delivery in biopolymer scaffolds for osteochondral tissue engineering. Journal of controlled release : official journal of the Controlled Release Society 2009;134:81-90.

[59] Di Luca A, Longoni A, Criscenti G, Lorenzo-Moldero I, Klein-Gunnewiek M, Vancso J, et al. Surface energy and stiffness discrete gradients in additive manufactured scaffolds for osteochondral regeneration. Biofabrication 2016;8:015014.

[60] Kearney E, Farrell E, Prendergast P, Campbell V. Tensile strain as a regulator of mesenchymal stem cell osteogenesis. Annals of biomedical engineering 2010;38:1767-79.

[61] Liu L, Yuan W, Wang J. Mechanisms for osteogenic differentiation of human mesenchymal stem cells induced by fluid shear stress. Biomechanics and modeling in mechanobiology 2010;9:659-70.

[62] Luu YK, Capilla E, Rosen CJ, Gilsanz V, Pessin JE, Judex S, et al. Mechanical stimulation of mesenchymal stem cell proliferation and differentiation promotes osteogenesis while preventing dietary-induced obesity. Journal of Bone and Mineral Research 2009;24:50-61.

[63] Mauney J, Sjostorm S, Blumberg J, Horan R, O'leary J, Vunjak-Novakovic G, et al. Mechanical stimulation promotes osteogenic differentiation of human bone marrow stromal cells on 3-D partially demineralized bone scaffolds in vitro. Calcified tissue international 2004;74:458-68.

[64] Qi M-C, Hu J, Zou S-J, Chen H-Q, Zhou H-X, Han L-C. Mechanical strain induces osteogenic differentiation: Cbfa1 and Ets-1 expression in stretched rat mesenchymal stem cells. International journal of oral and maxillofacial surgery 2008;37:453-8.

[65] Yourek G, McCormick SM, Mao JJ, Reilly GC. Shear stress induces osteogenic differentiation of human mesenchymal stem cells. Regenerative medicine 2010;5:713-24.

[66] Angele P. Cyclic, mechanical compression enhances chondrogenesis of mesenchymal progenitor cells in tissue engineering scaffolds. 2004.

[67] Campbell JJ, Lee DA, Bader DL. Dynamic compressive strain influences chondrogenic gene expression in human mesenchymal stem cells. 2006.

[68] Huang C, Charles Y, Hagar KL, Frost LE, Sun Y, Cheung HS. Effects of cyclic compressive loading on chondrogenesis of rabbit bone-marrow derived mesenchymal stem cells. Stem cells 2004;22:313-23.

[69] Huang CYC, Reuben PM, Cheung HS. Temporal expression patterns and corresponding protein inductions of early responsive genes in rabbit bone marrow–derived mesenchymal stem cells under cyclic compressive loading. Stem cells 2005;23:1113-21.

[70] Mauck R, Byers B, Yuan X, Tuan R. Regulation of cartilaginous ECM gene transcription by chondrocytes and MSCs in 3D culture in response to dynamic loading. Biomechanics and modeling in mechanobiology 2007;6:113-25.

[71] Michalopoulos E, Knight RL, Korossis S, Kearney JN, Fisher J, Ingham E. Development of methods for studying the differentiation of human mesenchymal stem cells under cyclic compressive strain. Tissue Engineering Part C: Methods 2011;18:252-62.

[72] Terraciano V, Hwang N, Moroni L, Park HB, Zhang Z, Mizrahi J, et al. Differential response of adult and embryonic mesenchymal progenitor cells to mechanical compression in hydrogels. Stem cells 2007;25:2730-8.

[73] Grayson WL, Bhumiratana S, Grace Chao PH, Hung CT, Vunjak-Novakovic G. Spatial regulation of human mesenchymal stem cell differentiation in engineered osteochondral constructs: effects of pre-differentiation, soluble factors and medium perfusion. Osteoarthritis and cartilage / OARS, Osteoarthritis Research Society 2010;18:714-23.

[74] Goldman SM, Barabino GA. Spatial Engineering of Osteochondral Tissue Constructs Through Microfluidically Directed Differentiation of Mesenchymal Stem Cells. BioResearch open access 2016;5:109-17.

[75] Haasper C, Zeichen J, Meister R, Krettek C, Jagodzinski M. Tissue engineering of osteochondral constructs in vitro using bioreactors. Injury-International Journal of the Care of the Injured 2008;39:S66-S76.

[76] Chang C, Lin C, Chou C, Lin F, Liu H. Novel Bioreactors for osteochondral tissue engineering. Biomedical Engineering: Applications, Basis and Communications 2005;17:38-43.

[77] Wendt D, Jakob M, Martin I. Bioreactor-based engineering of osteochondral grafts: from model systems to tissue manufacturing. J Biosci Bioeng 2005;100:489-94.

[78] Pei Y, Fan JJ, Zhang XQ, Zhang ZY, Yu M. Repairing the osteochondral defect in goat with the tissue-engineered osteochondral graft preconstructed in a double-chamber stirring bioreactor. Biomed Res Int 2014;2014:219203.

[79] Steinmetz NJ, Aisenbrey EA, Westbrook KK, Qi HJ, Bryant SJ. Mechanical loading regulates human MSC differentiation in a multi-layer hydrogel for osteochondral tissue engineering. Acta Biomater 2015;21:142-53.

[80] Buckwalter JA, Mankin HJ. Articular cartilage .1. Tissue design and chondrocyte-matrix interactions. J Bone Joint Surg Am 1997;79A:600-11.

[81] Wang Y, Ding C, Wluka AE, Davis S, Ebeling PR, Jones G, et al. Factors affecting progression of knee cartilage defects in normal subjects over 2 years. Rheumatology 2006;45:79-84.

[82] Smith GD, Knutsen G, Richardson JB. A clinical review of cartilage repair techniques. The Journal of bone and joint surgery British volume 2005;87:445-9.

[83] Iwasa J, Engebretsen L, Shima Y, Ochi M. Clinical application of scaffolds for cartilage tissue engineering. Knee surgery, sports traumatology, arthroscopy : official journal of the ESSKA 2009;17:561-77.

[84] Wilson W, van Burken C, van Donkelaar C, Buma P, van Rietbergen B, Huiskes R. Causes of mechanically induced collagen damage in articular cartilage. J Orthop Res 2006;24:220-8.

[85] Vinatier C, Mrugala D, Jorgensen C, Guicheux J, Noel D. Cartilage engineering: a crucial combination of cells, biomaterials and biofactors. Trends in biotechnology 2009;27:307-14.

[86] Hutmacher DW, Ng KW, Kaps C, Sittinger M, Klaring S. Elastic cartilage engineering using novel scaffold architectures in combination with a biomimetic cell carrier. Biomaterials 2003;24:4445-58.

[87] Palmer AK, Werner FW. The triangular fibrocartilage complex of the wrist—Anatomy and function. The Journal of Hand Surgery 1981;6:153-62.

[88] Eyre DR, Wu JJ. Collagen of fibrocartilage: a distinctive molecular phenotype in bovine meniscus. FEBS letters 1983;158:265-70.

[89] Poole AR, Kojima T, Yasuda T, Mwale F, Kobayashi M, Laverty S. Composition and structure of articular cartilage: a template for tissue repair. Clinical orthopaedics and related research 2001:S26-33.

[90] Francis Suh JK, Matthew HWT. Application of chitosan-based polysaccharide biomaterials in cartilage tissue engineering: a review. Biomaterials 2000;21:2589-98.

[91] Mauck RL, Yuan X, Tuan RS. Chondrogenic differentiation and functional maturation of bovine mesenchymal stem cells in long-term agarose culture. Osteoarthritis and cartilage / OARS, Osteoarthritis Research Society 2006;14:179-89.

[92] Eyrich D, Wiese H, Mailer G, Skodacek D, Appel B, Sarhan H, et al. In vitro and in vivo cartilage engineering using a combination of chondrocyte-seeded long-term stable fibrin gels and polycaprolactone-based polyurethane scaffolds. Tissue engineering 2007;13:2207-18.

[93] Sophia Fox AJ, Bedi A, Rodeo SA. The Basic Science of Articular Cartilage: Structure, Composition, and Function. Sports Health: A Multidisciplinary Approach 2009;1:461-8.

[94] Pearle AD, Warren RF, Rodeo SA. Basic science of articular cartilage and osteoarthritis. Clinics in sports medicine 2005;24:1-12.

[95] Bhosale AM, Richardson JB. Articular cartilage: structure, injuries and review of management. British medical bulletin 2008;87:77-95.

[96] Oegema TR, Jr., Carpenter RJ, Hofmeister F, Thompson RC, Jr. The interaction of the zone of calcified cartilage and subchondral bone in osteoarthritis. Microscopy research and technique 1997;37:324-32.

[97] Sharma B, Williams CG, Kim TK, Sun D, Malik A, Khan M, et al. Designing zonal organization into tissue-engineered cartilage. Tissue engineering 2007;13:405-14.

[98] Klein TJ, Malda J, Sah RL, Hutmacher DW. Tissue engineering of articular cartilage with biomimetic zones. Tissue engineering Part B, Reviews 2009;15:143-57.

[99] Kim IL, Mauck RL, Burdick JA. Hydrogel design for cartilage tissue engineering: a case study with hyaluronic acid. Biomaterials 2011;32:8771-82.

[100] Ma Z, Gao C, Gong Y, Shen J. Paraffin spheres as porogen to fabricate poly(L-lactic acid) scaffolds with improved cytocompatibility for cartilage tissue engineering. Journal of biomedical materials research Part B, Applied biomaterials 2003;67:610-7.

[101] Reiffel AJ, Kafka C, Hernandez KA, Popa S, Perez JL, Zhou S, et al. High-fidelity tissue engineering of patient-specific auricles for reconstruction of pediatric microtia and other auricular deformities. PloS one 2013;8:e56506.

[102] Park J-S. Electrospinning and its applications. Advances in Natural Sciences: Nanoscience and Nanotechnology 2010;1:043002.

[103] Geng X, Kwon OH, Jang J. Electrospinning of chitosan dissolved in concentrated acetic acid solution. Biomaterials 2005;26:5427-32.

[104] Matthews JA, Boland ED, Wnek GE, Simpson DG, Bowlin GL. Electrospinning of collagen type II: A feasibility study. J Bioact Compat Pol 2003;18:125-34.

[105] Huang Z-M, Zhang Y-Z, Kotaki M, Ramakrishna S. A review on polymer nanofibers by electrospinning and their applications in nanocomposites. Composites science and technology 2003;63:2223-53.

[106] Gunatillake PA, Adhikari R. Biodegradable synthetic polymers for tissue engineering. Eur Cell Mater 2003;5:1-16; discussion

[107] Marin E, Briceño MI, Caballero-George C. Critical evaluation of biodegradable polymers used in nanodrugs. International journal of nanomedicine 2013;8:3071.

[108] Wu L, Li H, Li S, Li X, Yuan X, Zhang Y. Composite fibrous membranes of PLGA and chitosan prepared by coelectrospinning and coaxial electrospinning. Journal of biomedical materials research Part A 2010;92:563-74.

[109] Francis L, Venugopal J, Prabhakaran MP, Thavasi V, Marsano E, Ramakrishna S. Simultaneous electrospin-electrosprayed biocomposite nanofibrous scaffolds for bone tissue regeneration. Acta Biomater 2010;6:4100-9.

[110] Ding B, Kimura E, Sato T, Fujita S, Shiratori S. Fabrication of blend biodegradable nanofibrous nonwoven mats via multi-jet electrospinning. Polymer 2004;45:1895-902.

[111] Bazilevsky AV, Yarin AL, Megaridis CM. Co-electrospinning of core-shell fibers using a single-nozzle technique. Langmuir 2007;23:2311-4.

[112] Han D, Boyce ST, Steckl AJ. Versatile core-sheath biofibers using coaxial electrospinning. MRS Proceedings: Cambridge Univ Press; 2008. p. 1094-DD06-02.

[113] Qu H, Wei S, Guo Z. Coaxial electrospun nanostructures and their applications. J Mater Chem A 2013;1:11513-28.

[114] Zhang YZ, Wang X, Feng Y, Li J, Lim CT, Ramakrishna S. Coaxial electrospinning of (fluorescein isothiocyanate-conjugated bovine serum albumin)-encapsulated poly(epsilon-caprolactone) nanofibers for sustained release. Biomacromolecules 2006;7:1049-57.

[115] Gupta P, Wilkes GL. Some investigations on the fiber formation by utilizing a side-by-side bicomponent electrospinning approach. Polymer 2003;44:6353-9.

[116] Luo CJ, Nangrejo M, Edirisinghe M. A novel method of selecting solvents for polymer electrospinning. Polymer 2010;51:1654-62.

[117] Greiner A, Wendorff JH. Electrospinning: a fascinating method for the preparation of ultrathin fibers. Angew Chem Int Ed Engl 2007;46:5670-703.

[118] Pillay V, Dott C, Choonara YE, Tyagi C, Tomar L, Kumar P, et al. A Review of the Effect of Processing Variables on the Fabrication of Electrospun Nanofibers for Drug Delivery Applications. J Nanomater 2013;2013.

[119] Xu W, He X, Sarvestani AS, Jabbari E. Effect of a low-molecular-weight cross-linkable macromer on electrospinning of poly(lactide-co-glycolide) fibers. Journal of biomaterials science Polymer edition 2007;18:1369-85.

[120] Angammana CJ, Jayaram SH. Analysis of the Effects of Solution Conductivity on Electrospinning Process and Fiber Morphology. Ieee T Ind Appl 2011;47:1109-17.

[121] Fong H, Chun I, Reneker DH. Beaded nanofibers formed during electrospinning. Polymer 1999;40:4585-92.

[122] Sun ZC, Deitzel JM, Knopf J, Chen X, Gillespie JW. The effect of solvent dielectric properties on the collection of oriented electrospun fibers. Journal of Applied Polymer Science 2012;125:2585-94.

[123] Zargham S, Bazgir S, Tavakoli A, Rashidi AS, Damerchely R. The Effect of Flow Rate on Morphology and Deposition Area of Electrospun Nylon 6 Nanofiber. J Eng Fiber Fabr 2012;7:42-9.

[124] Ganan-Calvo AM, Rebollo-Munoz N, Montanero JM. The minimum or natural rate of flow and droplet size ejected by Taylor cone-jets: physical symmetries and scaling laws. New J Phys 2013;15:033035.

[125] Milleret V, Simona B, Neuenschwander P, Hall H. Tuning electrospinning parameters for production of 3D-fiber-fleeces with increased porosity for soft tissue engineering applications. Eur Cell Mater 2011;21:286-303.

[126] Sener A, Altay AS, Altay F. Effect of voltage on morphology of electrospun nanofibers. Electrical and Electronics Engineering (ELECO), 2011 7th International Conference on: IEEE; 2011. p. I-324-I-8.

[127] Liu Y, Dong LA, Fan J, Wang R, Yu JY. Effect of Applied Voltage on Diameter and Morphology of Ultrafine Fibers in Bubble Electrospinning. Journal of Applied Polymer Science 2011;120:592-8.

[128] Kumar P. Effect of colletor on electrospinning to fabricate aligned nano fiber 2012.

[129] Pant HR, Neupane MP, Pant B, Panthi G, Oh HJ, Lee MH, et al. Fabrication of highly porous poly (varepsilon-caprolactone) fibers for novel tissue scaffold via water-bath electrospinning. Colloids and surfaces B, Biointerfaces 2011;88:587-92.

[130] Errico C, Detta N, Puppi D, Piras AM, Chiellini F, Chiellini E. Polymeric nanostructured items electrospun on a cylindrical template: a simple procedure for their removal. Polym Int 2011;60:1162-6.

[131] Neves NM, Campos R, Pedro A, Cunha J, Macedo F, Reis RL. Patterning of polymer nanofiber meshes by electrospinning for biomedical applications. Int J Nanomedicine 2007;2:433-48.

[132] Santos MI, Tuzlakoglu K, Fuchs S, Gomes ME, Peters K, Unger RE, et al. Endothelial cell colonization and angiogenic potential of combined nano- and micro-fibrous scaffolds for bone tissue engineering. Biomaterials 2008;29:4306-13.

[133] Telemeco TA, Ayres C, Bowlin GL, Wnek GE, Boland ED, Cohen N, et al. Regulation of cellular infiltration into tissue engineering scaffolds composed of submicron diameter fibrils produced by electrospinning. Acta Biomaterialia 2005;1:377-85.

[134] Su Y, Lu B, Xie Y, Ma Z, Liu L, Zhao H, et al. Temperature effect on electrospinning of nanobelts: the case of hafnium oxide. Nanotechnology 2011;22:285609.

[135] De Vrieze S, Van Camp T, Nelvig A, Hagström B, Westbroek P, De Clerck K. The effect of temperature and humidity on electrospinning. Journal of Materials Science 2009;44:1357-62.

[136] Casper CL, Stephens JS, Tassi NG, Chase DB, Rabolt JF. Controlling Surface Morphology of Electrospun Polystyrene Fibers: Effect of Humidity and Molecular Weight in the Electrospinning Process. Macromolecules 2004;37:573-8.

[137] Doshi J, Reneker DH. Electrospinning process and applications of electrospun fibers. Industry Applications Society Annual Meeting, 1993, Conference Record of the 1993 IEEE: IEEE; 1993. p. 1698-703.

[138] Hashimoto K, Noshiro M, Ohno S, Kawamoto T, Satakeda H, Akagawa Y, et al. Characterization of a cartilage-derived 66-kDa protein (RGD-CAP/< i> β</i> ig-h3) that binds to collagen. Biochimica et Biophysica Acta (BBA)-Molecular Cell Research 1997;1355:303-14.

[139] Matthews JA, Wnek GE, Simpson DG, Bowlin GL. Electrospinning of collagen nanofibers. Biomacromolecules 2002;3:232-8.

[140] Meng LH, Arnoult O, Smith M, Wnek GE. Electrospinning of in situ crosslinked collagen nanofibers. J Mater Chem 2012;22:19412-7.

[141] Buttafoco L, Kolkman NG, Engbers-Buijtenhuijs P, Poot AA, Dijkstra PJ, Vermes I, et al. Electrospinning of collagen and elastin for tissue engineering applications. Biomaterials 2006;27:724-34.

[142] Chen Z, Mo X, Qing F. Electrospinning of collagen–chitosan complex. Materials Letters 2007;61:3490-4.

[143] Zhou J, Cao C, Ma X, Lin J. Electrospinning of silk fibroin and collagen for vascular tissue engineering. International journal of biological macromolecules 2010;47:514-9.

[144] Chen JP, Su CH. Surface modification of electrospun PLLA nanofibers by plasma treatment and cationized gelatin immobilization for cartilage tissue engineering. Acta Biomater 2011;7:234-43.

[145] Zhang YZ, Venugopal J, Huang ZM, Lim CT, Ramakrishna S. Crosslinking of the electrospun gelatin nanofibers. Polymer 2006;47:2911-7.

[146] Li JX, He AH, Zheng JF, Han CC. Gelatin and gelatin-hyaluronic acid nanofibrous membranes produced by electrospinning of their aqueous solutions. Biomacromolecules 2006;7:2243-7.

[147] Ji Y, Ghosh K, Shu XZ, Li B, Sokolov JC, Prestwich GD, et al. Electrospun three-dimensional hyaluronic acid nanofibrous scaffolds. Biomaterials 2006;27:3782-92.

[148] Brenner EK, Schiffman JD, Thompson EA, Toth LJ, Schauer CL. Electrospinning of hyaluronic acid nanofibers from aqueous ammonium solutions. Carbohyd Polym 2012;87:926-9.

[149] Shim IK, Suh WH, Lee SY, Lee SH, Heo SJ, Lee MC, et al. Chitosan nano-/microfibrous double-layered membrane with rolled-up three-dimensional structures for chondrocyte cultivation. Journal of biomedical materials research Part A 2009;90:595-602.

[150] Subramanian A, Vu D, Larsen GF, Lin HY. Preparation and evaluation of the electrospun chitosan/PEO fibers for potential applications in cartilage tissue engineering. Journal of biomaterials science Polymer edition 2005;16:861-73.

[151] Bhattarai N, Edmondson D, Veiseh O, Matsen FA, Zhang MQ. Electrospun chitosan-based nanofibers and their cellular compatibility. Biomaterials 2005;26:6176-84.

[152] Hasan A, Memic A, Annabi N, Hossain M, Paul A, Dokmeci MR, et al. Electrospun scaffolds for tissue engineering of vascular grafts. Acta Biomater 2014;10:11-25.

[153] Jang JH, Castano O, Kim HW. Electrospun materials as potential platforms for bone tissue engineering. Adv Drug Deliver Rev 2009;61:1065-83.

[154] Lee JY, Bashur CA, Goldstein AS, Schmidt CE. Polypyrrole-coated electrospun PLGA nanofibers for neural tissue applications. Biomaterials 2009;30:4325-35.

[155] Ladd MR, Lee SJ, Stitzel JD, Atala A, Yoo JJ. Co-electrospun dual scaffolding system with potential for muscle-tendon junction tissue engineering. Biomaterials 2011;32:1549-59.

[156] Nam J, Johnson J, Lannutti JJ, Agarwal S. Modulation of embryonic mesenchymal progenitor cell differentiation via control over pure mechanical modulus in electrospun nanofibers. Acta Biomater 2011;7:1516-24.

[157] Li WJ, Danielson KG, Alexander PG, Tuan RS. Biological response of chondrocytes cultured in three-dimensional nanofibrous poly(epsilon-caprolactone) scaffolds. Journal of biomedical materials research Part A 2003;67:1105-14.

[158] Xu J, Zhang JH, Gao WQ, Liang HW, Wang HY, Li JF. Preparation of chitosan/PLA blend micro/nanofibers by electrospinning. Materials Letters 2009;63:658-60.

[159] Luu YK, Kim K, Hsiao BS, Chu B, Hadjiargyrou M. Development of a nanostructured DNA delivery scaffold via electrospinning of PLGA and PLA-PEG block copolymers. Journal of controlled release : official journal of the Controlled Release Society 2003;89:341-53.

[160] McCullen SD, Gittard SD, Miller PR, Pourdeyhimi B, Narayan RJ, Loboa EG. Laser ablation imparts controlled micro-scale pores in electrospun scaffolds for tissue engineering applications. Annals of biomedical engineering 2011;39:3021-30.

[161] Thorvaldsson A, Stenhamre H, Gatenholm P, Walkenstrom P. Electrospinning of highly porous scaffolds for cartilage regeneration. Biomacromolecules 2008;9:1044-9.

[162] Aghdam RM, Najarian S, Shakhesi S, Khanlari S, Shaabani K, Sharifi S. Investigating the effect of PGA on physical and mechanical properties of electrospun PCL/PGA blend nanofibers. Journal of Applied Polymer Science 2012;124:123-31.

[163] Freed LE, Vunjak-Novakovic G, Biron RJ, Eagles DB, Lesnoy DC, Barlow SK, et al. Biodegradable polymer scaffolds for tissue engineering. Biotechnology (N Y) 1994;12:689-93.

[164] Hajiali H, Shahgasempour S, Naimi-Jamal MR, Peirovi H. Electrospun PGA/gelatin nanofibrous scaffolds and their potential application in vascular tissue engineering. International journal of nanomedicine 2011;6:2133-41.

[165] Li WJ, Tuli R, Huang X, Laquerriere P, Tuan RS. Multilineage differentiation of human mesenchymal stem cells in a three-dimensional nanofibrous scaffold. Biomaterials 2005;26:5158-66.

[166] Cipitria A, Skelton A, Dargaville T, Dalton P, Hutmacher D. Design, fabrication and characterization of PCL electrospun scaffolds—a review. J Mater Chem 2011;21:9419-53.

[167] Zheng R, Duan H, Xue J, Liu Y, Feng B, Zhao S, et al. The influence of Gelatin/PCL ratio and 3-D construct shape of electrospun membranes on cartilage regeneration. Biomaterials 2014;35:152-64.

[168] Shin HJ, Lee CH, Cho IH, Kim YJ, Lee YJ, Kim IA, et al. Electrospun PLGA nanofiber scaffolds for articular cartilage reconstruction: mechanical stability, degradation and cellular responses under mechanical stimulation in vitro. Journal of biomaterials science Polymer edition 2006;17:103-19.

[169] Toyokawa N, Fujioka H, Kokubu T, Nagura I, Inui A, Sakata R, et al. Electrospun Synthetic Polymer Scaffold for Cartilage Repair Without Cultured Cells in an Animal Model. Arthroscopy 2010;26:375-83.

[170] Chung C, Burdick JA. Engineering cartilage tissue. Adv Drug Deliv Rev 2008;60:243-62.

[171] Schulze-Tanzil G, Mobasheri A, de Souza P, John T, Shakibaei M. Loss of chondrogenic potential in dedifferentiated chondrocytes correlates with deficient Shc-Erk interaction and apoptosis. Osteoarthritis and cartilage / OARS, Osteoarthritis Research Society 2004;12:448-58.

[172] Schulze-Tanzil G. Activation and dedifferentiation of chondrocytes: implications in cartilage injury and repair. Annals of anatomy = Anatomischer Anzeiger : official organ of the Anatomische Gesellschaft 2009;191:325-38.

[173] Caron MM, Emans PJ, Coolsen MM, Voss L, Surtel DA, Cremers A, et al. Redifferentiation of dedifferentiated human articular chondrocytes: comparison of 2D and 3D cultures. Osteoarthritis and cartilage / OARS, Osteoarthritis Research Society 2012;20:1170-8.

[174] Noriega SE, Hasanova GI, Schneider MJ, Larsen GF, Subramanian A. Effect of fiber diameter on the spreading, proliferation and differentiation of chondrocytes on electrospun chitosan matrices. Cells, tissues, organs 2012;195:207-21.

[175] Shyy JY, Chien S. Role of integrins in endothelial mechanosensing of shear stress. Circulation research 2002;91:769-75.

[176] Ahrens PB, Solursh M, Reiter RS. Stage-related capacity for limb chondrogenesis in cell culture. Developmental biology 1977;60:69-82.

[177] Johnstone B, Hering TM, Caplan AI, Goldberg VM, Yoo JU. < i> In Vitro</i> Chondrogenesis of Bone Marrow-Derived Mesenchymal Progenitor Cells. Experimental cell research 1998;238:265-72.

[178] Shafiee A, Seyedjafari E, Sadat Taherzadeh E, Dinarvand P, Soleimani M, Ai J. Enhanced chondrogenesis of human nasal septum derived progenitors on nanofibrous scaffolds. Materials science & engineering C, Materials for biological applications 2014;40:445-54.

[179] Zhong W, Zhang W, Wang S, Qin J. Regulation of fibrochondrogenesis of mesenchymal stem cells in an integrated microfluidic platform embedded with biomimetic nanofibrous scaffolds. PloS one 2013;8:e61283.

[180] Woods A, Beier F. RhoA/ROCK signaling regulates chondrogenesis in a context-dependent manner. The Journal of biological chemistry 2006;281:13134-40.

[181] Ghosh S, Laha M, Mondal S, Sengupta S, Kaplan DL. In vitro model of mesenchymal condensation during chondrogenic development. Biomaterials 2009;30:6530-40.

[182] Nam J, Huang Y, Agarwal S, Lannutti J. Improved cellular infiltration in electrospun fiber via engineered porosity. Tissue engineering 2007;13:2249-57.

[183] Ekaputra AK, Prestwich GD, Cool SM, Hutmacher DW. Combining electrospun scaffolds with electrosprayed hydrogels leads to three-dimensional cellularization of hybrid constructs. Biomacromolecules 2008;9:2097-103.

[184] Lee JB, Jeong SI, Bae MS, Yang DH, Heo DN, Kim CH, et al. Highly porous electrospun nanofibers enhanced by ultrasonication for improved cellular infiltration. Tissue engineering Part A 2011;17:2695-702.

[185] Guimaraes A, Martins A, Pinho ED, Faria S, Reis RL, Neves NM. Solving cell infiltration limitations of electrospun nanofiber meshes for tissue engineering applications. Nanomedicine (Lond) 2010;5:539-54.

[186] Nam J, Rath B, Knobloch TJ, Lannutti JJ, Agarwal S. Novel electrospun scaffolds for the molecular analysis of chondrocytes under dynamic compression. Tissue engineering Part A 2009;15:513-23.

[187] Levorson EJ, Raman Sreerekha P, Chennazhi KP, Kasper FK, Nair SV, Mikos AG. Fabrication and characterization of multiscale electrospun scaffolds for cartilage regeneration. Biomedical materials (Bristol, England) 2013;8:014103.

[188] McCullen SD, Autefage H, Callanan A, Gentleman E, Stevens MM. Anisotropic fibrous scaffolds for articular cartilage regeneration. Tissue engineering Part A 2012;18:2073-83.

[189] Li G, Zhang T, Li M, Fu N, Fu Y, Ba K, et al. Electrospun fibers for dental and craniofacial applications. Current stem cell research & therapy 2014;9:187-95.

[190] Pittenger MF, Mackay AM, Beck SC, Jaiswal RK, Douglas R, Mosca JD, et al. Multilineage potential of adult human mesenchymal stem cells. Science 1999;284:143-7.

[191] Jiang Y, Jahagirdar BN, Reinhardt RL, Schwartz RE, Keene CD, Ortiz-Gonzalez XR, et al. Pluripotency of mesenchymal stem cells derived from adult marrow. Nature 2002;418:41-9.

[192] Bianco P, Riminucci M, Gronthos S, Robey PG. Bone marrow stromal stem cells: nature, biology, and potential applications. Stem cells 2001;19:180-92.

[193] Griffin MD, Ryan AE, Alagesan S, Lohan P, Treacy O, Ritter T. Anti-donor immune responses elicited by allogeneic mesenchymal stem cells: what have we learned so far? Immunol Cell Biol 2013;91:40-51.

[194] Nauta AJ, Fibbe WE. Immunomodulatory properties of mesenchymal stromal cells. Blood 2007;110:3499-506.

[195] Jo CH, Lee YG, Shin WH, Kim H, Chai JW, Jeong EC, et al. Intra-articular injection of mesenchymal stem cells for the treatment of osteoarthritis of the knee: a proof-of-concept clinical trial. Stem cells 2014;32:1254-66.

[196] Evans CH, Kraus VB, Setton LA. Progress in intra-articular therapy. Nature reviews Rheumatology 2014;10:11-22.

[197] Arthur A, Zannettino A, Gronthos S. The therapeutic applications of multipotential mesenchymal/stromal stem cells in skeletal tissue repair. Journal of cellular physiology 2009;218:237-45.

[198] Wakitani S, Mitsuoka T, Nakamura N, Toritsuka Y, Nakamura Y, Horibe S. Autologous bone marrow stromal cell transplantation for repair of full-thickness articular cartilage defects in human patellae: two case reports. Cell transplantation 2004;13:595-600.

[199] van Buul GM, Siebelt M, Leijs MJ, Bos PK, Waarsing JH, Kops N, et al. Mesenchymal stem cells reduce pain but not degenerative changes in a mono-iodoacetate rat model of osteoarthritis. J Orthop Res 2014;32:1167-74.

[200] DuFort CC, Paszek MJ, Weaver VM. Balancing forces: architectural control of mechanotransduction. Nature reviews Molecular cell biology 2011;12:308-19.

[201] Jaalouk DE, Lammerding J. Mechanotransduction gone awry. Nature reviews Molecular cell biology 2009;10:63-73.

[202] Nam J, Perera P, Rath B, Agarwal S. Dynamic regulation of bone morphogenetic proteins in engineered osteochondral constructs by biomechanical stimulation. Tissue engineering Part A 2013;19:783-92.

[203] Nam J, Aguda BD, Rath B, Agarwal S. Biomechanical thresholds regulate inflammation through the NF-κB pathway: experiments and modeling. PLoS One 2009;4:e5262.

[204] Shea CA, Rolfe RA, Murphy P. The importance of foetal movement for co-ordinated cartilage and bone development in utero : clinical consequences and potential for therapy. Bone & joint research 2015;4:105-16.

[205] Palomares KT, Gleason RE, Mason ZD, Cullinane DM, Einhorn TA, Gerstenfeld LC, et al. Mechanical stimulation alters tissue differentiation and molecular expression during bone healing. J Orthop Res 2009;27:1123-32.

[206] Mauck RL, Soltz MA, Wang CCB, Wong DD, Chao PHG, Valhmu WB, et al. Functional tissue engineering of articular cartilage through dynamic loading of chondrocyte-seeded agarose gels. J Biomech Eng-T Asme 2000;122:252-60.

[207] Roelofsen J, Klein-Nulend J, Burger EH. Mechanical stimulation by intermittent hydrostatic compression promotes bone-specific gene expression in vitro. Journal of biomechanics 1995;28:1493-503.

[208] Mauck RL, Byers BA, Yuan X, Tuan RS. Regulation of cartilaginous ECM gene transcription by chondrocytes and MSCs in 3D culture in response to dynamic loading. Biomechanics and modeling in mechanobiology 2007;6:113-25.

[209] Rath B, Nam J, Knobloch TJ, Lannutti JJ, Agarwal S. Compressive forces induce osteogenic gene expression in calvarial osteoblasts. Journal of biomechanics 2008;41:1095-103.

[210] Nam J, Rath B, Knobloch TJ, Lannutti JJ, Agarwal S. Novel electrospun scaffolds for the molecular analysis of chondrocytes under dynamic compression. Tissue engineering Part A 2008;15:513-23.

[211] Michalopoulos E, Knight RL, Korossis S, Kearney JN, Fisher J, Ingham E. Development of methods for studying the differentiation of human mesenchymal stem cells under cyclic compressive strain. Tissue engineering Part C, Methods 2012;18:252-62.

[212] Pelaez D, Huang CY, Cheung HS. Cyclic compression maintains viability and induces chondrogenesis of human mesenchymal stem cells in fibrin gel scaffolds. Stem cells and development 2009;18:93-102.

[213] Huang CY, Hagar KL, Frost LE, Sun Y, Cheung HS. Effects of cyclic compressive loading on chondrogenesis of rabbit bone-marrow derived mesenchymal stem cells. Stem cells 2004;22:313-23.

[214] Huang AH, Farrell MJ, Kim M, Mauck RL. Long-Term Dynamic Loading Improves the Mechanical Properties of Chondrogenic Mesenchymal Stem Cell-Laden Hydrogels. Eur Cells Mater 2010;19:72-85.

[215] Mauney JR, Sjostorm S, Blumberg J, Horan R, O'Leary JP, Vunjak-Novakovic G, et al. Mechanical stimulation promotes osteogenic differentiation of human bone marrow stromal cells on 3-D partially demineralized bone scaffolds in vitro. Calcified tissue international 2004;74:458-68.

[216] Angele P, Schumann D, Angele M, Kinner B, Englert C, Hente R, et al. Cyclic, mechanical compression enhances chondrogenesis of mesenchymal progenitor cells in tissue engineering scaffolds. Biorheology 2004;41:335-46.

[217] Horner CB, Ico G, Johnson J, Zhao Y, Nam J. Microstructure-dependent mechanical properties of electrospun core-shell scaffolds at multi-scale levels. Journal of the mechanical behavior of biomedical materials 2016;59:207-19.

[218] Taylor G. Electrically driven jets. Proceedings of the Royal Society of London A: Mathematical, Physical and Engineering Sciences: The Royal Society; 1969. p. 453-75.

[219] Nam J, Rath B, Knobloch TJ, Lannutti JJ, Agarwal S. Novel electrospun scaffolds for the molecular analysis of chondrocytes under dynamic compression. Tissue Engineering Part A 2008;15:513-23.

[220] Vincent J. Structural biomaterials. Princeton, NJ, USA: Princeton University Press; 2012.

[221] Livak KJ, Schmittgen TD. Analysis of relative gene expression data using real-time quantitative PCR and the 2− ΔΔCT method. methods 2001;25:402-8.

[222] Wang Y, Oh CM, Oliveira MC, Islam MS, Ortega A, Park BH. GPU accelerated real-time multi-functional spectral-domain optical coherence tomography system at 1300nm. Opt Express 2012;20:14797-813.

[223] Jagodzinski M, Breitbart A, Wehmeier M, Hesse E, Haasper C, Krettek C, et al. Influence of perfusion and cyclic compression on proliferation and differentiation of bone marrow stromal cells in 3-dimensional culture. Journal of biomechanics 2008;41:1885-91.

[224] Delaine-Smith RM, Reilly GC. The effects of mechanical loading on mesenchymal stem cell differentiation and matrix production. Vitamins and hormones 2011;87:417-80.

[225] Kreke MR, Sharp LA, Lee YW, Goldstein AS. Effect of intermittent shear stress on mechanotransductive signaling and osteoblastic differentiation of bone marrow stromal cells. Tissue engineering Part A 2008;14:529-37.

[226] Howard J, Grill SW, Bois JS. Turing's next steps: the mechanochemical basis of morphogenesis. Nature reviews Molecular cell biology 2011;12:392-8.

[227] Pap T, Korb-Pap A. Cartilage damage in osteoarthritis and rheumatoid arthritis--two unequal siblings. Nature reviews Rheumatology 2015;11:606-15.

[228] Sharma B, Elisseeff JH. Engineering structurally organized cartilage and bone tissues. Annals of biomedical engineering 2004;32:148-59.

[229] Langer R, Vacanti JP. Tissue engineering. Science 1993;260:920-6.

[230] Fisher MB, Mauck RL. Tissue engineering and regenerative medicine: recent innovations and the transition to translation. Tissue Engineering Part B: Reviews 2013;19:1-13.

[231] Leach JK. Multifunctional cell-instructive materials for tissue regeneration. Regenerative medicine 2006;1:447-55.

[232] Stevens MM, George JH. Exploring and engineering the cell surface interface. Science 2005;310:1135-8.

[233] Xu HH, Simon CG. Fast setting calcium phosphate–chitosan scaffold: mechanical properties and biocompatibility. Biomaterials 2005;26:1337-48.

[234] Khademhosseini A, Langer R, Borenstein J, Vacanti JP. Microscale technologies for tissue engineering and biology. Proceedings of the National Academy of Sciences of the United States of America 2006;103:2480-7.

[235] Engler AJ, Sen S, Sweeney HL, Discher DE. Matrix Elasticity Directs Stem Cell Lineage Specification. Cell 2006;126:677-89.

[236] Park JS, Chu JS, Tsou AD, Diop R, Tang Z, Wang A, et al. The effect of matrix stiffness on the differentiation of mesenchymal stem cells in response to TGF-β. Biomaterials 2011;32:3921-30.

[237] Pek YS, Wan AC, Ying JY. The effect of matrix stiffness on mesenchymal stem cell differentiation in a 3D thixotropic gel. Biomaterials 2010;31:385-91.

[238] Huang ZM, Zhang Y, Ramakrishna S. Double-layered composite nanofibers and their mechanical performance. Journal of Polymer Science Part B: Polymer Physics 2005;43:2852-61.

[239] Nam J, Johnson J, Lannutti JJ, Agarwal S. Modulation of embryonic mesenchymal progenitor cell differentiation via control over pure mechanical modulus in electrospun nanofibers. Acta Biomaterialia 2011;7:1516-24.

[240] Nerurkar NL, Sen S, Baker BM, Elliott DM, Mauck RL. Dynamic culture enhances stem cell infiltration and modulates extracellular matrix production on aligned electrospun nanofibrous scaffolds. Acta Biomaterialia 2011;7:485-91.

[241] Binulal NS, Deepthy M, Selvamurugan N, Shalumon KT, Suja S, Mony U, et al. Role of nanofibrous poly(caprolactone) scaffolds in human mesenchymal stem cell attachment and spreading for in vitro bone tissue engineering--response to osteogenic regulators. Tissue engineering Part A 2010;16:393-404.

[242] Maldonado M, Wong LY, Echeverria C, Ico G, Low K, Fujimoto T, et al. The effects of electrospun substrate-mediated cell colony morphology on the self-renewal of human induced pluripotent stem cells. Biomaterials 2015;50:10-9.

[243] Mauck RL, Soltz MA, Wang CC, Wong DD, Chao P-HG, Valhmu WB, et al. Functional tissue engineering of articular cartilage through dynamic loading of chondrocyte-seeded agarose gels. Journal of biomechanical engineering 2000;122:252-60.

[244] Moroni L, De Wijn J, Van Blitterswijk C. 3D fiber-deposited scaffolds for tissue engineering: influence of pores geometry and architecture on dynamic mechanical properties. Biomaterials 2006;27:974-85.

[245] Lee J, Guarino V, Gloria A, Ambrosio L, Tae G, Kim YH, et al. Regeneration of Achilles' tendon: the role of dynamic stimulation for enhanced cell proliferation and mechanical properties. Journal of biomaterials science Polymer edition 2010;21:1173-90.

[246] Bosworth LA, Rathbone SR, Bradley RS, Cartmell SH. Dynamic loading of electrospun yarns guides mesenchymal stem cells towards a tendon lineage. Journal of the mechanical behavior of biomedical materials 2014;39:175-83.

[247] Gurjarpadhye AA, DeWitt MR, Xu Y, Wang G, Rylander MN, Rylander CG. Dynamic Assessment of the Endothelialization of Tissue-Engineered Blood Vessels Using an Optical Coherence Tomography Catheter-Based Fluorescence Imaging System. Tissue engineering Part C, Methods 2014.

[248] Seliktar D, Black RA, Vito RP, Nerem RM. Dynamic mechanical conditioning of collagen-gel blood vessel constructs induces remodeling in vitro. Annals of biomedical engineering 2000;28:351-62.

[249] Li WJ, Laurencin CT, Caterson EJ, Tuan RS, Ko FK. Electrospun nanofibrous structure: a novel scaffold for tissue engineering. Journal of biomedical materials research 2002;60:613-21.

[250] Blackstone BN, Drexler JW, Powell HM. Tunable Engineered Skin Mechanics via Coaxial Electrospun Fiber Core Diameter. Tissue Engineering Part A 2014;20:2746-55.

[251] Schenke-Layland K, Rofail F, Heydarkhan S, Gluck JM, Ingle NP, Angelis E, et al. The use of three-dimensional nanostructures to instruct cells to produce extracellular matrix for regenerative medicine strategies. Biomaterials 2009;30:4665-75.

[252] Jiang H, Hu Y, Li Y, Zhao P, Zhu K, Chen W. A facile technique to prepare biodegradable coaxial electrospun nanofibers for controlled release of bioactive agents. Journal of controlled release : official journal of the Controlled Release Society 2005;108:237-43.

[253] Jiang H, Hu Y, Zhao P, Li Y, Zhu K. Modulation of protein release from biodegradable core-shell structured fibers prepared by coaxial electrospinning. Journal of biomedical materials research Part B, Applied biomaterials 2006;79:50-7.

[254] Sun Z, Zussman E, Yarin AL, Wendorff JH, Greiner A. Compound core–shell polymer nanofibers by co-electrospinning. Advanced Materials 2003;15:1929-32.

[255] Zhang YZ, Huang ZM, Xu XJ, Lim CT, Ramakrishna S. Preparation of core-shell structured PCL-r-gelatin Bi-component nanofibers by coaxial electrospinning. Chem Mater 2004;16:3406-9.

[256] Zhang YZ, Venugopal J, Huang ZM, Lim CT, Ramakrishna S. Characterization of the surface biocompatibility of the electrospun PCL-collagen nanofibers using fibroblasts. Biomacromolecules 2005;6:2583-9.

[257] Guan J, Fujimoto KL, Sacks MS, Wagner WR. Preparation and characterization of highly porous, biodegradable polyurethane scaffolds for soft tissue applications. Biomaterials 2005;26:3961-71.

[258] Gere J, Timoshenko S. Mechanics of materials, vol. Fourth SI Edition Cheltenham: Stanley Thornes 1999.

[259] Ugural A. Stresses in beams. Mechanics of Materials Singapore: McGraw-Hill 1991:175-82.

[260] Korhonen R, Laasanen M, Töyräs J, Rieppo J, Hirvonen J, Helminen H, et al. Comparison of the equilibrium response of articular cartilage in unconfined compression, confined compression and indentation. Journal of biomechanics 2002;35:903-9.

[261] Eshraghi S, Das S. Mechanical and microstructural properties of polycaprolactone scaffolds with one-dimensional, two-dimensional, and three-dimensional orthogonally oriented porous architectures produced by selective laser sintering. Acta Biomaterialia 2010;6:2467-76.

[262] Fukae R, Midorikawa T. Preparation of gelatin fiber by gel spinning and its mechanical properties. Journal of applied polymer science 2008;110:4011-5.

[263] Midorikawa T, Lawal OS, Sasaki Y, Fukae R. Structure and physical properties of gelatin fibers prepared by gel-spinning in ethylene glycol. Journal of applied polymer science 2012;125:E332-E8.

[264] Zein I, Hutmacher DW, Tan KC, Teoh SH. Fused deposition modeling of novel scaffold architectures for tissue engineering applications. Biomaterials 2002;23:1169-85.

[265] Gibson LJ, Ashby MF. Cellular solids: structure and properties: Cambridge university press; 1997.

[266] Sonnenschein MF. Porosity-dependent Young's modulus of membranes from polyetherether ketone. Journal of Polymer Science Part B: Polymer Physics 2003;41:1168-74.

[267] Bland JM, Altman DG. Regression towards the mean. BMJ: British Medical Journal 1994;308:1499.

[268] Croisier F, Duwez AS, Jérôme C, Léonard AF, van der Werf KO, Dijkstra PJ, et al. Mechanical testing of electrospun PCL fibers. Acta Biomaterialia 2012;8:218-24.

[269] Drexler JW, Powell HM. Regulation of electrospun scaffold stiffness via coaxial core diameter. Acta Biomater 2011;7:1133-9.

[270] D'Amore A, Amoroso N, Gottardi R, Hobson C, Carruthers C, Watkins S, et al. From single fiber to macro-level mechanics: A structural finite-element model for elastomeric fibrous biomaterials. Journal of the mechanical behavior of biomedical materials 2014;39:146-61.

[271] Wong S-C, Baji A, Leng S. Effect of fiber diameter on tensile properties of electrospun poly(ε-caprolactone). Polymer 2008;49:4713-22.

[272] Woodfield TBF, Malda J, de Wijn J, Peters F, Riesle J, van Blitterswijk CA. Design of porous scaffolds for cartilage tissue engineering using a three-dimensional fiber-deposition technique. Biomaterials 2004;25:4149-61.

[273] Johnson J, Ghosh A, Lannutti J. Microstructure-property relationships in a tissue-engineering scaffold. Journal of applied polymer science 2007;104:2919-27.

[274] Johnson J, Niehaus A, Nichols S, Lee D, Koepsel J, Anderson D, et al. Electrospun PCL in vitro: a microstructural basis for mechanical property changes. Journal of biomaterials science Polymer edition 2009;20:467-81.

[275] Soliman S, Sant S, Nichol JW, Khabiry M, Traversa E, Khademhosseini A. Controlling the porosity of fibrous scaffolds by modulating the fiber diameter and packing density. Journal of Biomedical Materials Research Part A 2011;96:566-74.

[276] Nam J, Perera P, Rath B, Agarwal S. Dynamic regulation of bone morphogenetic proteins in engineered osteochondral constructs by biomechanical stimulation. Tissue Engineering Part A 2012;19:783-92.

[277] Tuli R, Nandi S, Li W-J, Tuli S, Huang X, Manner PA, et al. Human mesenchymal progenitor cell-based tissue engineering of a single-unit osteochondral construct. Tissue engineering 2004;10:1169-79.

[278] Gao J, Dennis JE, Solchaga LA, Awadallah AS, Goldberg VM, Caplan AI. Tissue-engineered fabrication of an osteochondral composite graft using rat bone marrow-derived mesenchymal stem cells. Tissue engineering 2001;7:363-71.

[279] Gotterbarm T, Richter W, Jung M, Berardi Vilei S, Mainil-Varlet P, Yamashita T, et al. An in vivo study of a growth-factor enhanced, cell free, two-layered collagen-tricalcium phosphate in deep osteochondral defects. Biomaterials 2006;27:3387-95.

[280] Im GI, Ahn JH, Kim SY, Choi BS, Lee SW. A hyaluronate-atelocollagen/beta-tricalcium phosphate-hydroxyapatite biphasic scaffold for the repair of osteochondral defects: a porcine study. Tissue engineering Part A 2010;16:1189-200.

[281] Cui W, Wang Q, Chen G, Zhou S, Chang Q, Zuo Q, et al. Repair of articular cartilage defects with tissue-engineered osteochondral composites in pigs. J Biosci Bioeng 2011;111:493-500.

[282] Schleicher I, Lips KS, Sommer U, Schappat I, Martin AP, Szalay G, et al. Biphasic scaffolds for repair of deep osteochondral defects in a sheep model. The Journal of surgical research 2013;183:184-92.

[283] Guilak F. The deformation behavior and viscoelastic properties of chondrocytes in articular cartilage. Biorheology 2000;37:27-44.

[284] Jurvelin J, Buschmann M, Hunziker E. Mechanical anisotropy of the human knee articular cartilage in compression. Proceedings of the Institution of Mechanical Engineers, Part H: Journal of Engineering in Medicine 2003;217:215-9.

[285] Mente P, Lewis J. Elastic modulus of calcified cartilage is an order of magnitude less than that of subchondral bone. Journal of Orthopaedic Research 1994;12:637-47.

[286] Bretcanu O, Samaille C, Boccaccini AR. Simple methods to fabricate Bioglass®-derived glass–ceramic scaffolds exhibiting porosity gradient. Journal of Materials Science 2008;43:4127-34.

[287] Liu C, Han Z, Czernuszka J. Gradient collagen/nanohydroxyapatite composite scaffold: development and characterization. Acta biomaterialia 2009;5:661-9.

[288] Mohan N, Dormer NH, Caldwell KL, Key VH, Berkland CJ, Detamore MS. Continuous gradients of material composition and growth factors for effective regeneration of the osteochondral interface. Tissue Engineering Part A 2011;17:2845-55.

[289] De Bari C, Kurth TB, Augello A. Mesenchymal stem cells from development to postnatal joint homeostasis, aging, and disease. Birth Defects Research Part C: Embryo Today: Reviews 2010;90:257-71.

[290] Heng BC, Haider HK, Sim EK-W, Cao T, Ng SC. Strategies for directing the differentiation of stem cells into the cardiomyogenic lineage in vitro. Cardiovascular research 2004;62:34-42.

[291] Kratchmarova I, Blagoev B, Haack-Sorensen M, Kassem M, Mann M. Mechanism of divergent growth factor effects in mesenchymal stem cell differentiation. Science 2005;308:1472-7.

[292] Morrison SJ, Shah NM, Anderson DJ. Regulatory mechanisms in stem cell biology. Cell 1997;88:287-98.

[293] Rando TA. Stem cells, ageing and the quest for immortality. Nature 2006;441:1080-6.